Master's Thesis

High Resolution Pure Rotational Raman spectra of Benzene in the Ground State

Dong Eun Lee

Department of Chemistry

Graduate School of UNIST

2019

High Resolution Pure Rotational Raman spectra of Benzene in the Ground State

Dong Eun Lee

Department of Chemistry

Graduate School of UNIST

High Resolution Pure Rotational Raman Spectra of Benzene in the Ground State

A thesis/dissertation
submitted to the Graduate School of UNIST
in partial fulfillment of the
requirements for the degree of
Master of Science

Dong Eun Lee

12/06/2018
Approved by

Advisor
Prof. Thomas Schultz

High Resolution Pure Rotational Raman Spectra of Benzene in the Ground State

Dong Eun Lee

This certifies that the thesis/dissertation of Dong Eun Lee is approved.

12/06/ 2018 of submission

Signature

Advisor: Prof. Thomas Schultz

Signature

Prof. Yung Sam Kim

Signature

Prof. Oh-Hoon Kwon

Abstract

We used mass-Correlated Rotational Alignment SpectroscopY (mass-CRASY) and obtained pure rotational Raman spectra for benzene in a broad spectral bandwidth of 500 GHz. The rotational spectra were calibrated against a GPS stabilized clock. With a combined optomechanical and electronical delay and randomly sparse sampling, we achieved single MHz resolution for frequency domain spectra of benzene in the ground state. A ground state rotational constant, B_0 = 5689.2671(52) MHz and centrifugal distortion constants D_J = 1178 (50) Hz and D_{JK} = -2300(120) Hz were obtained in 1 MHz resolution spectrum. 1 MHz resolution pure rotational Raman benzene spectrum partially resolved K-structures in two bands. The partially resolved K structure in 1 MHz resolution gave us ideas on the J, K quantum numbers and centrifugal distortion constants for benzene, degeneracy due to molecular symmetry. We reconsider the discrepancies between literature data and our works, and various discussed uncertainties and error sources in different spectroscopic methods.

Contents

Main text (Ⅰ, Ⅱ, Ⅲ, Ⅳ, Ⅴ)----------1~43
Ⅰ. Introduction ----------1

Ⅱ. Experiments and Method ----------4

Ⅲ. Result & Discussion ----------7

Ⅳ. Conclusion ----------24

Ⅴ. Figures and Tables----------26

Appendix ----------43~94

A. Supplementary Information of the High-Resolution Benzene Spectra --- 43

B. Fragmentation and Fragments Rotational Spectra ----------75

Reference ----------95

Figures List

Figure 1: Experimental scheme of Mass-CRASY spectroscopy.

Figure 2: Random sparse measurement and continuous measurement comparison in the time domain spectra

Figure 3: Ground state benzene rotational spectrum measured with a 2 ns delay range scan.

Figure 4: Ground state benzene rotational spectrum measured by a 16 ns delay range scan.

Figure 5: Ground state benzene rotational spectrum measured by a 100 ns delay range scan.

Figure 6: Ground state benzene rotational spectrum measured by a 240 ns delay range scan.

Figure 7: Ground state benzene rotational spectrum measured by a 600 ns delay range scan.

Figure 8: Ground state benzene rotational spectrum measured by a μs delay range scan.

Figure 9: Magnified sections of the rotational spectra obtained by 1 μs sparse sampling in Fig. 8.

Figure 10: The two figures, (A) and (B) compare a band in spectra measured over 1 μs and 600 ns.

Figure A.1.1: Frequency domain ground state benzene rotational spectrum measured over 2 ns continuous measurement with GPS clock calibration.

Figure A.1.2: Frequency domain ground state benzene rotational spectrum measured over 16 ns continuous measurement with in-situ carbon disulfide rotational constant calibration.

Figure A.1.3: Frequency domain ground state benzene rotational spectrum measured over 100 ns random sparse measurement with GPS clock calibration.

Figure A.1.4: Frequency domain ground state benzene rotational spectrum measured over 200 ns random sparse measurement with GPS clock calibration.

Figure A.1.5: Frequency domain ground state benzene rotational spectrum measured over 600 ns random sparse measurement with GPS clock calibration.

Figure A.1.6: Frequency domain ground state benzene rotational spectrum measured over 1 μs random sparse measurement with GPS clock calibration.

Figure A.1.7: Frequency domain ground state benzene rotational spectrum measured over 2 μs random sparse measurement with GPS clock calibration.

Figure A.2.1: Experimental pure rotational Raman spectra of benzene with a different resolution are plotted in a range from 22740 MHz to 22775 MHz.

Figure A.2.2: Experimental pure rotational Raman spectra of benzene with a different resolution are plotted in a range from 34115 MHz to 34155 MHz.

Figure A.2.3: Experimental pure rotational Raman spectra of benzene with a different resolution are plotted in a range from 45495 MHz to 45530 MHz.

Figure A.2.4: Experimental pure rotational Raman spectra of benzene with a different resolution are plotted in a range from 56860 MHz to 56920 MHz.

Figure A.2.5: Experimental pure rotational Raman spectra of benzene with a different resolution are plotted in a range from 68245 MHz to 68290 MHz.

Figure A.2.6: Experimental pure rotational Raman spectra of benzene with a different resolution are plotted in a range from 79620 MHz to 79680 MHz.

Figure A.2.7: Experimental pure rotational Raman spectra of benzene with a different resolution are plotted in a range from 125145 MHz to 125180 MHz.

Figure A.2.8: Experimental pure rotational Raman spectra of benzene with a different resolution are plotted in a range from 147900 MHz to 147940 MHz.

Figure A.2.9: Experimental pure rotational Raman spectra of benzene with a different resolution are plotted in a range from 170640 MHz to 170710 MHz.

Figure A.2.10: Experimental pure rotational Raman spectra of benzene with a different resolution are plotted in a range from 193380 MHz to 193480 MHz.

Figure A.2.11 : Resolution comparison in a range from 0 to 8.0 MHz in Pgopher simulations in a range from 45500 MHz to 45530 MHz.

Figure A.2.12 : Resolution comparison in a range from 0 to 8.0 MHz in Pgopher simulations in a range from 102380 MHz to 102430 MHz.

Figure A.2.13 : Resolution comparison in a range from 0 to 8.0 MHz in Pgopher simulations in a range from 170640 MHz to 170710 MHz.

Figure A.2.14 : Resolution comparison in a range from 0 to 8.0 MHz in Pgopher simulations in a range from 193400 MHz to 193450 MHz.

Figure A.3.1 : Pgopher simulated spectra with a different temperature from 1 K to 298 K.

Figure A.3.2 : An enlarged simulated spectrum in a range between 170.660 GHz and 170.675 GHz.

Figure A.3.3 : An enlarged simulated spectrum in a range between 193.41 GHz and 193.435 GHz.

Figure A.3.4 : An enlarged simulated spectrum in a range between 56.8920 GHz and 56.8927 GHz.

Figure A.3.5 : Calculated 1 MHz resolution bands of pure rotational Raman benzene spectra in a range between 193400 MHz (193.400 GHz) to 193460 MHz (193.460 GHz).

Figure A.3.6 : Calculated 5 MHz resolution bands of pure rotational Raman benzene spectrum in a range between 193400 MHz (193.400 GHz) to 193450 MHz (193.450 GHz).

Figure A.3.7 : Calculated 10 MHz resolution bands of pure rotational Raman benzene spectrum in a range between 193400 MHz(193.400 GHz) to 1934500 MHz(193.450 GHz).

Figure B.1.1 : The mass spectrum was obtained in the uncalibrated frequency domain rotational spectra in 16 ns continuous measurement.

Figure B.1.2 : Rotational spectrum of 32S of a fragment from 32S12C32S in the frequency domain.

Figure B.1.3 : Rotational spectrum of 34S of a fragment from 34S12C32S in the frequency domain.

Figure B.1.4 : Rotational spectrum of 32S12C of a fragment from 32S12C32S in the frequency domain.

Figure B.1.5 : Rotational spectrum of 34S12C of a fragment from 34S12C32S in the frequency domain.

Figure B.1.6 : Rotational spectrum of C4H4 from C6H6 (benzene) in the frequency domain.

Figure B.1.7 : Rotational spectrum of 32S12C32S (main carbon disulfide isotope) in the frequency domain at the selected mass 76 u.

Figure B.1.8 : Rotational spectrum of 32S13C32S and 33S12C32S in the frequency domain at the selected mass 77 u.

Figure B.1.9 : Rotational spectrum of C6H6 (benzene) and 34S12C32S in the frequency domain at the selected mass 78 u.

Figure B.1.10 : Rotational spectrum of 34S12C34S in the frequency domain at the selected mass 80 u.

Figure B.1.11 : Rotational spectrum of fragments of 32S12C32S and 32S12C32S in the frequency domain.

Figure B.1.12 : Rotational spectrum of fragments of 34S12C32S and 32S12C32S in the frequency domain.

Figure B.1.13 : Rotational spectrum main isotope of benzene and the fragment in the frequency domain.

Figure B.2.1 : Three rotational spectra, rotational spectrum of mass 52 u (One of fragments from Benzene) , 76 u (Main isotoplogue of carbon disulfide) and 78 u (Benzene (12C6H6)) spectrum .

Figure B.3.1 : Three rotational spectra, rotational spectrum of mass 44 u (one of fragments from carbon disulfide (32S12C32S)), 76u(32S12C32S), and benzene (12C6H6) spectrum.

Tables List

Table 1: List of rotational constant of benzene in the ground state in the literatures.

Table 2: Rotational constant and centrifugal distortion constants comparison over the different times. B, D_J, and D_{JK} were obtained by a pure rotational Raman spectrum over 16 ns with continuous measurement as well as 100 ns, 200 ns, 600 ns, 1000 ns (= 1\ \mu s) with random sparse scan.

Table 3 : Pgopher Fitting for the single MHz resolution benzene spectrum for B = 5689.2671(52) MHz and D_J = 1178(50) Hz and D_{JK} =.-2300 (120) Hz

Table 4 : Different value for the rotational constant and centrifugal distortion constants of the 8 MHz resolution spectrum (Fig. 5 measured over 100 ns time delay) were determined based on the assumption of different molecular beam temperature.

Table B.1.1 : Rotational constant of fragments of carbon disulfide isotopomers and benzene. The rotational constants were obtained in uncalibrated frequency domain rotational spectra in 16 ns continuous measurement

Table B.1.2 : Rotational constant of fragments of carbon disulfide isotopomers (32S12C32S) $at\ 76\ u$. The rotational constants were obtained in uncalibrated frequency domain rotational spectra in 16 ns continuous measurement.

Table B.1.3 : Rotational constant of fragments of carbon disulfide isotopomers (32S12C34S) and benzene at 78 u. The rotational constants were obtained in uncalibrated frequency domain rotational spectra in 16 ns continuous measurement.

Table B.1.4 : Rotational constant of fragments of carbon disulfide isotopomers (34S12C34S) at 78 u. The rotational constants were obtained in uncalibrated frequency domain rotational spectra in 16 ns continuous measurement.

Table B.2.1 : Rotational constant of fragments of benzene and carbon disulfide. The rotational constants were obtained in frequency domain rotational spectra in 100 ns random sparse sampling measurement with GPS clock calibration.

Table B.3.1 : Rotational constant of fragments of carbon disulfide isotopomers and benzene. The rotational constants were obtained in 1 μs random sparse sampling measurement with GPS clock calibration.

Explanation of terms and abbreviations

Mass -CRASY : Mass-Correlated Rotational Alignment SpectroscopY

IR :Infra-Red Spectroscopy

UV : Ultra -Violet

RCS : Rotational Coherent Spectroscopy

TRFD : Time-resolved fluorescence depletion

fs-DFWM RCS : femtosecond Degenerate-Four-Wave-Minxing

Introduction

Aromatic molecules have a low reactivity and a high stability from its planar structure and resonance structure. Structures of benzene have been investigated over 80 years by various spectroscopic methods as benzene is one of the most typical aromatic molecules with a high symmetry D_{6h}. For the determination of molecular structures, the rotational constants allow us to determine a molecular structure. One of the rotational constants, B_0 has been determined as B_0 is tightly related to other rotational constants in the oblate top.

As benzene has no permanent dipole moment, it cannot have any pure rotational microwave spectrum in the ground state. Raman spectroscopy is another powerful tool to determine the rotational constants and, can be used for non-polar molecules such as benzene. Stoicheff reported the first rotational constant of benzene as 5682.6(1.5) MHz from a photographed pure rotational Raman spectrum in 1953[1], and refined the rotational constant of 5684.1(1.5) MHz in 1954 [2]. Not only pure rotational Raman spectra, but also rovibronic Raman spectra were obtained to improve the rotational constant of benzene[3].

Rovibrational IR(Infrared spectroscopy) experiments also obtained benzene spectra and analyzed rotational constants and molecular structure. Early benzene investigation with rovibrational IR gave the rotational constants of benzene and distortion constants with a big uncertainty and inaccuracy [4-7]. Thereafter, the rotational constants with improved accuracy were attained by IR spectroscopy with interferometer and Fourier transform analyses of rovibronic bands.[8-11]. Also, IR spectroscopy with frequency difference mixing was used [12] and gained spectra with Doppler-limited resolution. Junttila et al.[13] and Domenech et al.[14] obtained a precise rotational constant within sub-Doppler resolved IR spectroscopy, which implemented an opto-thermal spectrometer at low-temperature molecular beam conditions based on bolometric detection.

The rotational constants of benzene in the electronically excited states have been determined from rotationally resolved spectra. Rotationally resolved spectra were resolved with sub-Doppler resolution spectroscopy. [15] The first Doppler-free rotationally resolved electronic spectrum of benzene was obtained by one-photon UV excitation using a pulsed amplified continuous wave laser system.[16] Okruss et al. improved a resolution of UV spectrum within a sub-Doppler range with a tunable UV laser and a collimated molecular beam.[17] By crossing a molecular beam and a laser beam, Doi et al. measured sub-Doppler excitation spectra of a specific transition and resolved 1158 lines. [18] Baba et al. measured rotational spectra by fluorescence excitation spectrum, and gained rotational constants from more than 1000 calibrated rotational lines.[19]

Furthermore, time-domain spectroscopic methods have been performed to investigate the benzene molecular structures. Rotational Coherence Spectroscopy (RCS) measures rotational recurrences as functions of molecules for a time delay. This spectroscopy is a recent tool for studying molecular structures of clusters and large polyatomic molecules. Riehn et al. measured time domain rotational spectra for the ground state and excited states with time-resolved fluorescence depletion (TRFD)[20]. Jarzeba et al.[21] firstly used femtosecond Degenerate-Four-Wave-Mixing RCS (fs-DFWM RCS) and measured their spectrum over 1.4 ns. Later , Matylitstky et al. carried out the longer time delay measurement over a time range of 3.9 ns[22]. However, the resolution of the RSC spectra is lower than 100 MHz resolution in frequency domain spectra

The table revealed discrepancies between the reported rotational constants that significantly exceeded the reported a 1-σ uncertainty or 2-σ uncertainties. Table.1 shows the discrepancies between the literature value of not only B_0 but also D_J and D_{JK}. The rotational constant discrepancies can originate from centrifugal distortion constants. The values of rotational constants obtained by different spectroscopinc methods have discrepancies between them. Neglecting the centrifugal distortion

constants of D_J and D_{JK} makes MHz range inaccuracies in the rotational constants even if the ranges of the experimental accuracy is kHz. [23]

Mass-CRASY is an RCS method that probes a rotational wave packet by photo-ionization in a mass spectrometer[24-26]**.** This method correlates rotational Raman spectra to ion masses and allowed to assign spectra for molecular isotopologues in CS_2 [24, 26] and butadiene [25]**.**Table.1 summarizes the rotational constant B_0in the works of literature. Here we applied the high-resolution mass-CRASY to obtain rotational structure of benzene with accurate rotational constant and two centrifugal distortion constant

Experiment and Methods

Mass correlated pure rotational Raman spectra were measured by observation of a coherent rotational wave packet in the time domain over a time scale of 1 microsecond. Fig.1 illustrates the Mass-CRASY experimental scheme. A first femto-second laser alignment pulse (pump) created a rotational wave packet by impulsive Raman excitation of a cold molecular beam, and excited rotational states were proved via resonant multi-photon ionization with a femtosecond pulse (probe, ionization) [24-26]

This experimental set-up is described in the high resolution mass-CRASY paper[26]. Helium gas (99.999% purity) at 10 to 20 bar pressure was seeded with a small amount of benzene (Alfa Aesar, HPLC Grade, 99.5% purity) by passing over a liquid sample at room temperature. The seeded gas was expanded via a pulse valve (Evan-Lavie, E.L-7-4-2007-HRR, 150 mm nozzle, operating at 500 Hz and 80 ℃) [27] and generated a cold molecular beam. The average pressure of the source chamber remained below $4 \cdot 10^{-5}$ mbar. The molecular beam was skimmed into a mass spectrometer region (Wiley-McLaren mass spectrometer [28]) with an average pressure in the 10^{-7}mbar range. In the spectrometer region, a linearly polarized strong 800 nm IR alignment pulse traversed the molecular beam and generated a rotational wave-packet by rotational Raman excitation. The evolving wave packet caused transient molecular alignment, which was probed by two-photon ionization with a delayed 200 nm UV ionization pulse. Ions were detected with a multichannel plate detector and the ion-time-of-flight was measured with 0.5 ns time resolution in a scaler card (Fast Comtech P7886). Fig.1 shows a brief experimental scheme. Femtosecond light pulses were generated in a femtosecond laser oscillator (Coherent, Vitara-T, 800 nm central wavelength, 80 MHz repetition rate, 45 fs pulse duration). An electronic delay generator (Stanford Delay Generator, DG 535) selected oscillator pulses for amplification in two separate regenerative chirped-pulse amplifiers (Coherent, Libra USP-

1K-HE-200, 1 kHz repetition rate). Pulses from amplifier-1 were compressed to a pulse duration of a few hundred femtoseconds (fs), attenuated to 50 - 150 μJ pulse energy, and used as alignment pulses. Pulses from amplifier-2 were compressed to 45 fs and upconverted into 200 nm ionization pulses with non-linear Beta Barium Borate (BBO) crystals. The time delay between alignment and ionization laser pulse was controlled by a combination of opto-mechanical and electronic time delays. The alignment pulse was routed via a folded optomechanical delay line (Physik Instrumente MD-531), adding up from 0 to 4.8 m path length, equivalent to an adijustable time delay of 16 ns. Larger delays were obtained by selecting different oscillator pulses for the alignment and ionization amplifiers, adding discrete 12.5 ns delays. The combined delay could be adjusted between zero and 1 μs with few-fs precision. Alignment and ionization pulses were combined in front of the spectrometer. The two pulses and were jointly focused by a spherical mirror with 37.5 cm focal length onto the molecular beam in the spectrometer region. The ions were mass-analyzed in a time-of-flight mass spectrometer.

Time delays up 16 ns were controlled by an opto-mechanical delay stage. Longer time delays were achieved by selecting subsequent pulses from the laser oscillator for the probing step. The oscillator repetition rate was referenced to a GPS-stabilized clock to obtain accurate delay times. A set of mass-correlated rotational spectra had a tremendous amount of data when it was obtained by a continuous sampling measurement. Therefore, random sparse sampling was adopted and reduced an experimental time and data quality without compromising any data information, but mildly affected signal-to-noise ratio.

The better resolution requires the longer delay time. The sub-MHz resolution would require at least a 1000 ns alignment-ionization time delay. It would spend impractical measurement time if mass-CRASY measured and saved data for all alignment-ionization time delay points. If there are the number of sampling points and step sizes between sampling points are random, all artifacts or systematic errors become random errors that do not compromise the original signals. Thus, randomly

sampled alignment-ionization time delay reproduces signals with additional random errors. As a result, Fourier transformed frequency spectra of random sparse sampling measurement have slightly decreased the signal to noise ratio (S/N) due to the appended random errors.

Fig.2 represents a comparison between a random sparse sampling measurement with 2% of sampling points over a 1 μs of time delay in Fig.2.(A) and a full continuous sampling measurement over 2 ns in Fig.2.(B). The 1 μs time delay spectrum in Fig.2.(A) has a factor of 500 better resolution than the 2 ns time delay spectrum in Fig.2.(B). The random sparse sampling step size ranged from 1 ps to 99 ps. Random step sizes were generated by Python program based pseudo-random number generator (Mersenne-Twister algorithm). Fig.2.(A) shows the alignment-ionization time delay trace with the 20000 randomly sparse sampled points. In a magnifier of Fig.2.(A), there is enlarged time delay spectrum in a range between 0.4018 μs and 0.4019 μs. Sampled points are sharp bands were unsampled points are zero. Fig.2.(B) shows the alignment-ionization time delay of the 2 ns full continuous measurement. A magnifier of Fig.2.(B) shows that all points were measured over 2 ns. Recurrences appear as oscillatory structure on a noisy base line in Fig.2.(B).

One of the advantages of random sparse sampling is the lower experimental cost for a better resolution than available from continuous measurements. The experimental cost is reflected in time for measuring signals and analyzing data, as well as, the data storage requirements for the experimental data. The random sparse sampling measurement time is much shorter than continuous measurement because it measures fewer points than the continuous measurement time. Therefore, random sparse measurement requires less storage size than the continuous measurement.

Result and Discussion

Mass-CRASY deploys pulse picking, optomechanical delay stage, and random sparse delay scan. It allows us to obtain a longer delay than 16 ns. We obtained 400 MHz, 50 MHz, 4 MHz, and 1.5 MHz, and single MHz resolution pure rotational Raman benzene spectra in the ground state, and their rotational constant of B_0 in the ground state. Using Pgopher[29], Literature values of D_J (1242.8 MHz)[13] and D_{JK} (-2059.1 MHz)[13] were used to fit B_0, as these spectra could not resolve K splitting or observe band splitting due to the quantum number of K and the distortion constant of D_{JK}. The starting value of B_0 = 5689.27809 MHz[13], D_J = 1242.8 Hz [13], and D_{JK} = -2059.1 Hz [13] were used. The obtained rotational constants were tabulated in table.2. The pure rotational Raman spectra of a planar molecule in the ground state would not give rotational constant of A and C because the two rotational constant tightly related to B. centrifugal distortion constant of D_K also cannot be revealed in pure rotational Raman spectra of the oblate tops due to its selection rules and assumptions on the zero momenta of inertia defects for planar molecules. Therefore, the rotational constants of A and C, and the centrifugal distortion constant of D_K were fixed to be zero in the fitting. Also sextet centrifugal distortion constants of H_J, H_{JK}, H_{KJ}, and H_K are zero because planar molecules have no momentum of inertia defects. Obtained spectra were individually fitted to obtain experimental rotational constant and centrifugal distortion constants. The obtained constants were tabulated in table 2.

Fig.3,4,5,6,7,8-(a) shows mass spectrum. An axis of the mass spectrum was calibrated against the mass of the main isotope of benzene at 78 u and carbon disulfide at 76 u. Fig.3,4,5,6,7,8- (b) represents a corresponding alignment-ionization delay spectrum in the time domain for benzene was obtained. The molecular alignment-ionization signals were obtained by excitation of a coherent wave

packet and the subsequent observation of temporal signal modulations created by the wave packet evolution. These signals brought time-dependent rotational structure information. The result of the time domain measurement is a broadband spectrum, as well as, spanning from zero frequency to a cut-off determined by either the delay step size or the duration of the laser pulse as the absolute upper limit. A step size of 1 ps corresponds to a spectral range of 500 GHz, which is enough to attain complete mass-correlated rotational spectra for the cold benzene in the ground state. Fig. 3,4,5,6,7,8-(c) show frequency domain spectra. The time domain spectrum of (b) was converted into a frequency domain spectrum of (c) by Fourier transform analysis. In Fig. (c), red dots indicate that the bands have lines from the S branch while black dots point out lines of the R branch. Time domain spectra and a Fourier transformed frequency domain spectra have identical information on the molecular structures.

Fig.3-(a) shows a mass spectrum. We resolved benzene and carbon disulfide ion, as well as, their fragments. Fig3-(a) shows mass 34 u and it is one of the fragments of carbon disulfide isotoplogue (12C32S). Fig.3-(a) also shows its most abundant 13C istopologue of benzene at 79 u as well as cationic fragments of benzene at 77 u, 64 u, 54 u, 53 u, 52 u, 40 u, and 39 u. Mass 78 u was selected to obtain the alignment-ionization time delay trace of benzene.

Fig3-(b) shows the alignment-ionization time delay trace over 2ns with 1 ps step size. The range of the time domain is from 0 to 2 ns. This spectrum was continuously measured. The alignment trace S_{align} was obtained in terms of a selected mass m_i from the signal (S) and the reference signal (R) via $\frac{S_{m_i}}{COS(S_{m_i})-1}$, where Cosine function of COS(S_{m_i}) denotes cosine wave function averaging signals of 100 adjacent data points. The alignment trace was multiplied without any window function for anodization, padded to 16,384 points.

Fig.3-(c) shows a Fourier transformed, 400 MHz resolution, frequency domain pure rotational Raman

spectrum measured over 2 ns with a continuous measurement. The temperature of the frequency spectrum was assumed to be 4 K. 13 rotational bands were resolved in the spectrum. 5 bands consist of lines from only the R branch. The resolution of the spectrum has approximately 400-500 MHz in a non-apodized spectrum. The literature values for the D_J and D_{JK} were used to fit the rotational constant of benzene. The rotational constant is 5687.45(13). The values agree with the literature value of ref. [3, 4, 6, 19-22] while it disagrees against the literature values of ref [1, 2, 5, 7, 8, 11-14, 16-18, 30, 31]

Fig.4 shows the 50 MHz resolution spectrum measured with a 16 ns continuous measurement. Fig.4-(a) shows a mass spectrum. We observed benzene and carbon disulfide, and their fragments. Herein, carbon disulfide istopologues were observed at mass 77 u, 78 u, 80 u and their fragments also shown at mass 32 u (mass fragment from 32S12C32S at 76 u), mass 34 u (mass fragment from 32S12C34S), mass 44 u (mass fragment from 32S12C32S), and mass 46 u (mass fragment from 32S12C34S).

The Fig.4-(a) also shows the most abundant 13C istopologue of benzene at 79 u, as well as, cationic fragments of benzene at 77 u, 64 u, 54 u, 53 u, 52 u, 41 u, and 40 u. The mass 78 u was selected to obtain alignment-ionization time delay trace of benzene.

Fig.4-(b) shows the alignment-ionization time delay trace for a 16 ns scan with 1 ps step size. shows the alignment-ionization time delay trace over 2ns. The range of the time domain is from 0 to 16 ns This spectrum was continuously measured. The alignment trace S_{align} was obtained in terms of a selected mass m_i from the signal (S) and the reference signal (R) via $\frac{S_{m_i}}{COS(S_{m_i})-1}$, . The alignment trace was multiplied without any window function for apodization, and padded to 1048576 points before Fourier transformation.

Fig. 4-(c) shows the rotational Raman spectrum of benzene in the ground state, which is obtained over

16 ns continuous measurement. Its frequency axis was calibrated against using the ratio between rotational constant of carbon disulfide (3272.2910 MHz) in the experiment and literature value (3271.5615 MHz)[32]. The resolution of the spectrum is approximately 60-70 MHz in a non-apodized spectrum. A molecular beam temperature was estimated to be 4 K. The literature values of centrifugal distortion constants were used to determine the rotational constant of benzene.[13] There are 17 resolved bands. 6 bands among them consist of transition lines of only the R branch. The rotational constant of benzene is 5689.176(12) MHz. The value of rotational constant agreed with ref. [3, 19-22], however, the value did not agree to the literature values in ref.[1, 2, 5, 7-14, 17, 18, 30, 31]

Fig. 5 shows an 8-9 MHz resolution spectrum measured by a 100 ns random sparse sampling measurement. Fig. 5-(a) represents a mass spectrum. An abscissa of the mass spectrum was calibrated against the mass of the main isotope of benzene at 78 u and carbon disulfide at 76 u. The Fig. 5-(a) also shows the most abundant 13C istopologue of benzene at 79 u, and cationic fragments of benzene at 77 u, 64 u, 63 u, 62 u, 54 u,53 u 52 u, and 41 u. The mass 78 u was selected to obtain an alignment-ionization time delay trace of benzene.

Fig.5-(b) shows an alignment-ionization time delay trace for the 100 ns time delay scan. The range of the time domain is from 0 to 100 ns. This spectrum was randomly sampled by measuring data for 9.432 points along the time axis. The alignment trace S_{align} was obtained in terms of a selected mass m_i from the signal (S) and the reference signal (R) via $\frac{S_{m_i}}{COS(S_{m_i})-1}$. The alignment trace was multiplied without any window function for anodization, padded to 1048576 points before Fourier transformation. This spectrum was randomly sampled in sparse. This spectrum was randomly sampled in sparse. The number of sampling points is 9,432 point, and sampling ratio is 8.79%.

Fig.5-(c) shows the Fourier transformed Raman spectrum with the approximately 8-9 MHz resolution

in frequency domain. A molecular beam temperature was estimated to be 5 K. 16 bands were resolved in the spectrum. 5 bands consisted of transition lines in only the R branch. The rotational constant of benzene is 5689.302(14) MHz. The value did agree to the literature value of ref [3, 10 16, 19-21] but did not not agree against the value of ref. [1, 2, 5, 7-9, 11-14, 18, 30, 31]. The obtained centrifugal distortion constant of D_J is 1604 (62) Hz, which is far from the literature values in the Table 1.

Fig.6 shows 4 MHz resolution spectrum measured over a delay range from 0 to 240 ns with the random sparse sampling. Fig.6-(a) shows a mass spectrum. An abscissa of the mass spectrum was calibrated against the mass of the main isotope of benzene at 78 u signal and carbon disulfide at 76 u. The Fig.6-(a) also shows its most abundant 13C istopologue of benzene at 79 u, as well as, cationic fragments of benzene at 77 u, 64 u, 63 u, 54 u, 53 u, 52 u and 40 u. The mass 78 u was selected to obtain alignment-ionization time delay trace of benzene

Fig.6-(b) shows alignment-ionization time delay trace. The range of the time domain spectrum is from 0 to 600 ns. This spectrum was randomly sampled in sparse. The alignment trace S_{align} was obtained in terms of a selected mass m_i from the signal (S) and the reference signal (R) via $\frac{S_{m_i}}{COS(S_{m_i})-1}$The alignment trace was multiplied without any window function for anodization, padded to 2097152 points before Fourier transformation from time domain to frequency domain. This spectrum was randomly sampled in sparse. This spectrum was randomly sampled in sparse. The number of random sparse sampling point is 13,879 and sampling ratio is 5.75%

Fig.6-(c) shows the 4 MHz resolution pure rotational Raman spectrum. A molecular beam temerapture were assumed to be 4 K. There are 13 bands. Among 13 bands, 4 bands with a black dot consist of only transition lines from only the R branch while 5 bands with a red dot consist of only transition lines of the S branch in the 13 bands. The fitted rotational constant of benzene is 5689.274(10) MHz,

and the centrifugal distortion constant of D_J is 1393(74) Hz. A literature value of other centrifugal distortion constant was used to determine the constants[13]. The rotational constant of the 4 MHz benzene spectrum agreed with the 12 literature value in ref. [3, 4, 6, 10, 11, 13, 16, 19-22] did not agree with 10 literature value in ref.[1, 2, 5, 7-9, 12, 14, 17, 18, 30, 31]. The centrifugal distortion constant of D_J agreed with 3 literature values in ref.[3, 14, 21]

Fig.7 shows a 1.5.-1.8 MHz resolution spectrum measured over 600 ns random sparse sampling measurement. Fig7-(a) shows an integrated mass spectrum. An abscissa of the mass spectrum was calibrated against the mass of the main isotope of benzene at 78 u and carbon disulfide at 76 u. The Fig.7-(a) also shows the most abundant 13C istopologue of benzene at 79 u, as well as, cationic fragments of benzene at 77 u, 64 u, 54 u, 53 u, 52 u, 40 u, and 39 u. Mass 78 u was selected to obtain an alignment-ionization time delay trace of benzene.

Fig.7-(b) shows the time domain spectrum in a range from 0 ns to 600 ns. This spectrum was measured with random sparse sampling. The alignment trace S_{align} was obtained in terms of a selected mass m_i from the signal (S) and the reference signal (R) via $\frac{S_{m_i}}{COS(S_{m_i})-1}$. The alignment trace was multiplied without any window function for apodization and padded to 8388608 points. The number of random sparse sampling points is 13,321 and sampling ratio is 2.24 %.

Fi.g7-(c) The resolution of the rotational Raman spectrum is approximately 1.5-1.8 MHz. There is 12 resolved rotational band in the spectrum. The molecular beam temperature in the frequency spectrum was estimated to be 4 K. Black dot marked 4 bands consisting of only transition lines from the R branch. Red dot marked 5 bands consisting of only transition lines from the S branch. The fitted rotational constant of benzene was 5689.2713(88) MHz. The centrifugal distortion constant of D_J was 1223(79) Hz. The value of rotational constant agreed with the literature value of ref[3, 4, 6, 10, 11, 13, 16,

[19-22]. However, the obtained value of B_0 did not agree with the literature values of ref. [1, 2, 5, 7-9, 12, 14, 17, 18, 30]. The values of D_J in the 1.5-1.8 MHz resolution did agree with the literature values of ref.[3, 9, 10, 14, 18, 21, 30, 31].

We obtained the more accurate and precise rotational constant when we achieved the longer delay time. The higher resolution, the rotational constant became more precise. The table.1 shows that we can obtain the more structure parameter in the higher resolution achieved by the longer delay time. We obtained the lower resolution than 1.5 MHz in Fig.3, Fig.4, Fig5, Fig,6 and Fig.7. However, we could not attain another centrifugal distortion constant of D_{JK} as the 1.6 MHz resolution spectrum did not resolve K splitting or partially resolve K-splitting.

Observed bands in the spectra would be sharp if it is merely a single transition line from only one transition and one branch. The term centrifugal distortion constants produce a small energy gap difference on different rotational energy transition with different quantum numbers of J and K [2, 21]. However, there are multiple lines in the single band and the lines have an individually different transition from the same J but different K number if the lines are in the same branch. The lines of the R branch with even J number lies in front of lines of S branch but all lines would seem to be overlapped in 8 MHz or higher resolution rotational spectra. S and R branch became partially resolved from 4 MHz and the higher resolution pure rotational Raman spectra, therefore, an uncertainty from unresolved R and S branch was decreased in 4 MHz resolution spectrum and 1.6 MHz resolution spectrum. The 4 MHz, 1.6 MHz, 1 MHz resolution rotational spectra have a higher accuracy and precision than 8 MHz, 50 MHz, and 400 MHz resolution pure rotational Raman benzene spectra as pure rotational Raman spectra whose resolution is higher than 4 MHz distinguish S branch from R branch. Hence, the value of B_0 and D_J from 4 MHz resolution spectrum and 1.6 MHz resolution spectrum agrees to each other.

We resolved K-splitting in the two highest bands of pure rotational Raman benzene spectrum in the frequency domain and obtain the experimental value of B_0, D_J, and D_{JK} at the same time. Fig.8 shows the single MHz resolution spectrum measured over 1 μs random sparse sampling measurement. Fig.8-(a) shows a mass spectrum. An axis of the mass spectrum was calibrated against the mass of the main isotope of benzene at 78 u and carbon disulfide at 76 u. The Fig.8-(a) also shows its most abundant 13C istopologue of benzene at 79 u, as well as, cationic fragments of benzene at 77 u, 63 u, 52 u, and 39 u. The mass 78 u was selected to obtain alignment-ionization time delay trace of benzene.

The Fig. 8-(b) represents a corresponding alignment-ionization delay spectrum in the time domain for benzene was obtained. The range of the time domain is from 0 to 1 μs This spectrum was randomly sampled in sparse. The alignment trace S_{align} was obtained in terms of a selected mass m_i from the signal (S) and the reference signal (R) via $\frac{S_{m_i}}{COS(S_{m_i})-1}$. The alignment trace was multiplied without any window function for apodization, padded to 167771216 points. This spectrum was randomly sampled in sparse. The number of sampling points is 20,000 and the sampling ratio is 2 %.

In the Fig. 8 -(c), the time domain spectrum was converted into a frequency domain spectrum by Fourier transform analysis. The plotted rotational spectrum is a power spectrum. FWHM(Full-width-at-Half-Width) of non-apodized bands in the spectrum is approximately 1.0 MHz. There are 12 resolved rotational lines in the benzene spectrum (78 u) including S branch and R branch transition in the ground state. 4 bands contains transition lines from only R branch. 3 bands superimposed with transitions from S and R branch in a range between 34 GHz and 80 GHz. The second, fourth and sixth band consisted of lines from both S and R branch). Above 100 GHz, only lines of S branch observed. The partially resolved K structure was observed in 1 MHz resolution pure rotational Raman benzene spectrum measured over 1 μs.

Fig. 9 shows partially resolved K-splitting sub bands from D_J and D_{JK} in the two highest frequency side bands of the single MHz resolution spectrum. This figure shows that split sub-bands in two high frequency bands. The high-resolution benzene spectrum resolved two split bands due to D_{JK} and the quantum number of K. The observed band patterns depended on K value. Bands look like a single band in low frequency due to low K number while there is band splitting in the high frequency due to partially resolved K numbers. These split sub-bands individually assigned to determine both D_J and D_{JK} within a small number of bands.

Fig. 9 shows K-splitting in the pure rotational Raman benzene spectrum with the cold temperature (approx. 4 K). The three bands lying on high frequencies showed the splitting due to benzene three-fold symmetry. $(J_f, K_i) \leftarrow (J_f, K_i)$ indicates the rotational Raman transition of benzene in Fig.9. The Fig.9-(A) plotted the rotational spectrum in a range between 193.40 GHz and 170.71 GHz. S branch five transitions were fitted in two bands. The lower frequency band had a higher intensity than the upper frequency band. (8,0) ← (6,0), (8,1) ← (6,1), (8,2) ←(6,2), (8,3) ← (6,3), and (8,6) ← (6,6). A second band of (8,0) ← (6,0), (8,1) ← (6,1), (8,2) ← (6,2), (8,3) ← (6,3) is separate from one band for the (8,6) ← (6,6) transition. Fig. 9- (B) represented another two split sub-bands between 193.40 GHz and 193.46 GHz. Due to the limited Signal to noise ratio, individual transition can not be easily assigned.

Fig. 10 shows the comparison between partially resolved K-splitting sub bands of the single MHz resolution spectrum, compared to the unresolved bands of the approximate 1.5-1.8 MHz resolution spectrum. The K-structure was partially resolved by sub-bands in the two bands in 1 MHz resolution spectrum but they were less resolved in 1.5-1.8 MHz resolution spectrum measured in 600 ns time delay. A temperature of the two spectra is approximate 4 K. The two highest transition is (9,n) ← (7,n) in the S branch. Fig. 10-(A) shows unresolved sub bands in a frequency range between 170.65 GHz

and 170.71 GHz from 1.5-1.8 MHz resolution spectrum. Fig.10-(B) shows that less resolved sub-bands of 1.6 MHz in a frequency domain range between 193.40 and 193.46 GHz The (9,6) ← (7,6), and (9,7) ← (7,7) transitions were resolved in the 1 MHz resolution spectrum but were not resolved in 1.5-1.8 MHz resolution spectrum. The partially resolved sub-bands contributed to the determination of a set of rotational constant and two centrifugal distortions for the pure rotational Raman benzene spectrum in the ground state. Table.3 summarized fitted line positions with Pgopher. Nuclear spin statistical weights of benzene explain the intensity alternation of pure rotational Raman benzene spectrum and other oblate top molecules[33 34]. Fig. 9 and Fig. 10 shows specific K structures can be partially resolved in the 1 MHz resolution spectrum. The bands were split into sub-bands in Fig. 9 and Fig. 10. The Fig. 9 and Fig. 10 shows two highest frequency of the 1 MHz resolution benzene spectrum and Pgopher simulation. The K of 6p$\pm$3 number can be the center of the split sub-bands in the high frequency. Degeneracy affects K-splitting sub-bands intensity patterns of pure rotational Raman benzene spectra in the ground state. Molecular symmetry determines nuclear spin statistical weights or degeneracy, as well as, an individual sub-band or line intensity. The intensity of individual lines is determined by the Boltzmann population. Boltzmann population includes the temperature, energy, and degeneracy. Temperature would be fixed in the equilibrium state. An intensity of individual transitions tells the molecular symmetry of oblate top molecules. If molecules have molecular symmetry is D_{3h} or D_{6h} even higher symmetry, the molecules have unique line intensity tendency due to their degeneracy. Benzene has 6 hydrogen atoms and D_{6h} symmetry, which is higher symmetry than XY_3 and C_{3v} or D_{3h} [33]. These K sub-structures originated from the quantum number of J and K and the centrifugal distortion of D_J and D_{JK}. Degeneracy of benzene had been calculated, [35] and used to analyze the band profile. A degeneracy of 6p : 6p$\pm$1: 6p$\pm$2: 6p$\pm$3 = 10: 11: 9: 14 when p is 0,1,2,3⋯.[11, 35] In low J and K number in the low frequency, the individual transition lines are too agglomerated to be one transition even in high resolution such as a single MHz resolution. Resolving individual transition lines requires at least 88 KHz resolution, which is a factor of 12 higher than the highest resolution spectrum in here. Therefore, the degeneracy

effect on intensity cannot be observed in low bands of the Fig.8 spectra Therefore, it is hard to figure out the effect of degeneracy on the line and band intensities yet in the single MHz resolution but K of 6p$\pm$3 lines were expected to have the highest intensity of the bands in the experimental spectrum and calculated spectra of the Fig.8-(c), Fig.9 and Fig.10.

In Fig. 8 The rotational constant of B and two centrifugal distortion constants of D_J, and, D_{JK} were fitted simultaneously to the line position in the comparison to a simulated spectrum in 1 MHz resolution spectrum over 1 μs time delay scan with Pgopher[36]. A temperature of a molecular beam in the frequency spectrum was estimated to be 4 K. The structural parameters including B, D_J, and, D_{JK} is fitted in $0 \leq J_i \leq 7$ and $0 \leq K_i \leq 7$ for both R and S branches in the Fig.8-(c) spectrum. The rotational constant (B_0) and two centrifugal distortion constants (D_J and D_{JK}) were fitted at the same time. The fit gave result of the rotational constant in the ground state and the centrifugal distortion constants. B is 5689.2671(52) MHz. D_J is 1178(50) Hz. D_{JK} is -2300(120) Hz. The value of B agreed with the literature values of ref.[3, 4, 6, 10, 11, 16, 19-22]. The fitted rotational constant of a single MHz resolution, however, did not agree against the literature value of ref.[1, 2, 5, 7-9, 12-14, 17, 18, 30, 31]. D_J value agreed with the literature value of ref. [3, 8, 10, 12, 18, 20, 21, 30, 31]but disagreed against the value of ref.[11, 13, 14, 17]. D_{JK} agreed with the literature value of ref. [3, 12, 14, 20, 21, 30]but did not agree with ref. [8, 10, 11, 13, 18, 22]. The rotational constant and the two centrifugal distortions of D_J and D_{JK} were obtained in the pure rotational spectrum measured over $1\mu s$. The rotational constant and centrifugal distortion constant were summarized in Table 2.

Mass-CRASY obtained a single MHz resolution pure rotational Raman benzene spectrum over 1 μs random sparse sampling measurement, and B_0, D_J, and D_{JK} in the ground state. However, the rotational spectra could not determine two centrifugal distortion constants at the same time except a single MHz resolution rotational spectrum. In fact, neglecting the two centrifugal distortion constants

or inaccurate values of D_J, and D_{JK} can determine the inaccurate rotational constant. [23]A single MHz resolution spectrum partially resolved K-splitting from D_J and D_{JK} in the oblate top molecules, which has a small value of D_J and D_{JK}, as well as, determine the value of B_0, D_J, and D_{JK} at the same time. The distortion constants are in the range of bounds of centrifugal distortion constants calculated by Aliev and Watson. [37] To determine the rotational constant and two centrifugal distortion constants, we check the ranges of the centrifugal distortions. The ranges are noted :

$$89\ \text{Hz} \leq \text{D}_\text{J} \leq 1528\ \text{Hz}$$

$$-2638\ \text{Hz} \leq \text{D}_\text{JK} \leq -120\ \text{Hz}$$

$$60\ \text{Hz} \leq \text{D}_\text{K} \leq 1230\ \text{Hz}$$

The relationships between B_0, D_J, D_{JK}, and D_K have been studied on D_{6h} symmetry and molecular planarity. Therefore, the relationships were used to determine the values of constants. According to Aliev et al.[38] and Dowling et al.[39], there are the relationships between centrifugal distortion constants of highly symmetric planar molecules such as benzene and planar molecules with D_{3h} or higher symmetry. (1) $D_{JK} = -\frac{15}{8} D_J = -1.875\, D_J$, and $D_J > 0$ for all oblate top [38]. (2) $2D_J + 3D_{JK} + 4D_K = 0$ [39] (3)$D_J + D_{JK} + D_K > 0$ [38]. (4) $D_K = \frac{29}{32} D_J$ from (1), (2). (5) $D_J + D_{JK} + D_K = \frac{1}{32} D_J > 0$ from (1),(2),(3), and (4) Aliev et al calculated centrifugal distortion constants relationship – (1) $D_{JK} \cong 2D_J[(\frac{C_0}{B_0})^4 - 1] = -1.875$ [38]. A ratio of centrifugal distortion constants of Mass-CRASY is -1.95, which is close to the theoretical value. Meanwhile, Dowling et al.[39] showed three centrifugal distortion constants have a simple relationship : (2) $2D_J + 3D_{JK} + 4D_K = 0$. These relationships of D_J, D_{JK}, and D_K were used to determined B_0, D_J, and D_{JK} to compare them with literature values of D_J and D_{JK} and their ratios.

There are two branches in the pure rotational Raman spectra. One is R branch, and the other is S branch. R branch energy term, S branch energy term.

(1) $\nu = E_{J+1,K} - E_{J,K} = 2B_0(J+1) - 4D_J(J+1)^3 - 4D_{JK}(J+1)K^2$ for R branch

($\Delta J = 1, \Delta K = 0$ J,K=0,1,2,3⋯)

(2) $\nu = E_{J+2,K} - E_{J,K} = (4B_0 - 6D_J)(J+\frac{3}{2}) - 4D_{JK}(J+\frac{3}{2})K^2$ for S branch

($\Delta J = 2, \Delta K = 0$ J,K=0,1,2,3⋯)

We observed an intensity alternation of pure rotational Raman benzene spectra. A distance between neighboring lines of the R branch is approximately $2B_0$ as well as that between two adjoining lines of S branch is around $4B_0$. These frequency domain spectra show an intensity of bands consisting of lines of only R branch is higher than that of bands from only S branch in a range between 20 GHz to 80 GHz. However, the intensity of bands consisting of lines in only R branch rapidly decreases in the cold spectra, as well as, the intensity of lines and bands in only S branch is far higher than in R branch.

Relevant uncertainties in the CRASY measurement are (1) Doppler effects including Doppler shift and Doppler broadening; (2) The air refractive index; (3) the opto-mechanical delay accuracy; (4) The oscillator frequency [26]; The standard deviation of the fitted rotational constant is $9.14 \cdot 10^{-7}$ of 5689.2671(52) MHz from 1 MHz resolution spectrum ($9.14 \cdot 10^{-7}$ = (0.0052/5689.2671)). (1) Doppler effect is less than $1 \cdot 10^{-7}$ in the experimental frame [26] (2) The air-refractive index of the beam (n) would be changed due to air temperature, pressure, and humidity in the laboratory. However, the air refractive index uncertainty ($\frac{\Delta n}{n}$) is less than $1 \cdot 10^{-7}$[26] as it was calibrated against NIST Shopper equation [40]. (3) Opto-mechanical delay uncertainty (C/N) is determined by the thermal-expansion coefficient of the delay stage (C) and the number of oscillator pulse jump (N). The thermo-

expansion delay stage coefficient (C) is $\frac{7 \cdot 10^{-7}}{℃}$ and the number of oscillator pulse jump is 80 (1000 ns delay scan / 12.5 ns oscillator pulse), as well, as the error was reset when oscillator pulse jump restarted. (4) The uncertainty of the oscillator frequency was measured by Allan deviation. The modified Allan deviation of the oscillator frequency is less than $1 \cdot 10^{-8}$, and its noise was characterized as random white noise. The stated fitted uncertainty of 5689.2671(52) obtained by mass-CRASY is therefore the larger error than the uncertainties. The fitted uncertainty gives the true numerical 1-σ uncertainty, and

There are discrepancies between benzene rotational constant and centrifugal distortion and values in the works of literature and the obtained values. Table 1. shows the literature values for the benzene rotational constant and centrifugal distortion constant compared with our value of B_0, D_J, and D_{JK}. Unresolved K structures in literature spectra may account for the discrepancies. [6-8, 11, 13, 14, 18, 30, 41]. The unresolved K-splitting causes difficulties to determine the rotational constant of B_0, and centrifugal distortion constants. The difficulties can be theoretically resolved by properly estimated values of the centrifugal distortion constants [42]. In addition, we might not be able to ignore D_{JK} and the K-splitting of pure rotational Raman bands. Neglected D_{JK} values and absence of K-splitting in the spectra would lead to errors in determining the value of the rotational constant and centrifugal distortion constants [43]. Furthermore, error sources can be low absorption intensity, which deteriorated the measurement accuracy [7], as well as, an unresolved Q branch [8], calibration errors [8, 11, 13, 14, 16, 17 20 18], mis-assignment of bands and lines due to overlapping hot band including hot vibrational bands [8 13 14] and perturbation from nearby states [8, 12, 14, 30]. These error sources did not exist in the present data, which were calibrated and referenced against an GPS-disciplined clock.[26]. As a result, the GPS-calibrated spectra allow us to properly assign bands and lines of pure rotational Raman spectra in the ground state. The rotational constants of the 1 MHz resolution spectrum in Fig. 8, Fig. 9, and Fig. 10.

Fitting assumptions for the fit of the rotational constant and centrifugal distortion constants in Pgopher may add other uncertainty. We used the literature constant values of Junttila et al. [13] as a starting value because the values are the most precise values in the literature of Table.1. However, the starting values for fitting the rotational constant and centrifugal distortion constants of D_J and D_{JK} could distort values of the rotational constant and distortion constants. Okruss et al [17]. explained the discrepancies with the rotational constants values of Riedle et al. [16] could be originated inappropriate starting value as Riedle et al. [16] fitted their data by ground state constant from Pliva et al values [30], which are considered to have a calibration error. However, If starting values are improper in nonlinear methods, they can estimate wrong parameters as fitted values may converge to a local minimum or maximum rather than to the global minimum or maximum .[44]

Estimating the temperature of the molecular beam in the experiment also adds uncertainty in fitting the rotational constant. The Boltzmann distribution envelope of the single MHz resolution rotational spectrum corresponds to a simulated spectrum with a temperature of 4 K or lower temperature. However, the two high frequency bands of single MHz resolution appear to have the higher temperature than 4 K in Pgopher simulation (e.g., 6 K or higher). Therefore, it seems to have two different temperatures or a certain range of molecular temperature. We set a single temperature of 4 K for the single MHz resolution rotational spectrum. However, the temperature of 4 K was estimated but could not be an exact temperature. Individually or partially resolved K structures can indicate the temperatures of a spectrum and bands as the intensity of sub-bands are determined by the temperature, and can be compared with simulated spectra. Unresolved K-splitting made a fitting when we determine the constants in Figs. 5,6,7. We observed partially resolved K structures in the two bands but could not observe individually resolved transition lines within the 1 MHz resolution data. Therefore, we could not perfectly estimate the molecular beam temperature of the spectra in Fig. 3,4,5,6,7, and 8. Especially Fig. 5 does not perfectly follow the Boltzmann distribution. Therefore, the rotational constants and centrifugal distortion constants of D_J, and D_{JK} were assumed a different

temperature as shown in Table.4. Note that the temperature dependent values of the rotational constant differ from each other in Table.4. The rotational constant was mildly affected since band shapes and center of bands are affected by the intensity of the individual lines, which are determined by the Boltzmann distribution at a given temperature [33]. (See Appendix A, Appendix A shows temperature dependent centers and shapes of bands.) Domenech et al.[14] also had a similar problem on molecular temperature. Their spectrum has a different intensity profile from the calculated spectrum. They suggested that the molecular beam cannot be characterized by a single rotational temperature, and that their spectra were be reflected by two different temperatures, such as 6 K for low J and 13 K for high J in the spectra. [14].

Effects of the estimated temperature of the molecular beam are different from those of Doppler effects in the calculation of uncertainties [45]. As matter of fact, a molecular beam can have two or multiple temperatures[45-47] and non-Boltzmann rotational distribution can be observed in the supersonic jet. [46, 48, 49]. The molecular beam can be ellipsoidal rather than a perfectly circular. The ellipsoidal shaped molecular beam has a perpendicular temperature and a parallel temperature [47] The two temperature have their own Boltzmann distribution. [47]. Molecular beam temperature spread out in a narrow range and cannot be a single temperature. Therefore, there is not a single Boltzmann distribution from one temperature. [45]. However, estimation of rotational temperature is hard when molecular beam temperature profile is not allowed during experiments [14]. Hence, estimating molecular beam temperature still has a limitation and add uncertainty in the determination of the rotational constant and centrifugal distortion constants. Non-Boltzmann distribution would occur because the rotational and vibrational energy levels are coupled due to a rapidly cooled down gas of supersonic jet or an extremely cold temperature below 1 K.[48, 49]. The non-equilibrium distribution of rotational energy levels occurs due to a small number of collisions between molecules and a low gas density ,and its distribution deviates from Boltzmann distribution with a single temperature [46] However, The estimating a temperature of the molecular beam have an effects in determination of the rotational

constant and centrifugal distortion constants, therefore, it is hard to predict true temperature. Fitting with a single temperature can add uncertainty in the higher resolution spectra with sub-MHz and KHz resolution.

Conclusion

The ground state rotational constant of benzene in the literatures shows significant discrepancies between different published results. Sources of the discrepancies may include unresolved K structures and, an insufficient resolution, calibration errors in different experimental methods, overlapped rovibronic transition lines of the high J, K values in a high temperature, and shifted lines from energy perturbations of hot rovibronic bands and lines (c.f., Coriolis interactions and Fermi interactions, $\ell -$ resonance). We used Mass-CRASY to reexamine the rotational constant of B_0, and centrifugal distortion constants of D_J and D_{JK} against the GPS disciplined clock calibration in a low temperature molecular beam. We performed Mass-CRASY experiments to obtain 400 MHz, 50 MHz, 8-9 MHz, 4-5 MHz, 1.6-1.8 MHz, and the single MHz resolution pure rotational Raman spectra of benzene, and obtained accurate rotational constants. The pure rotational Raman spectra with 4 MHz,1.6-1.8 MHz and the single MHz showed that position of lines in two different branches can be distinguished at even low temperature of 4 K-6 K. The single MHz resolution rotational Raman benzene spectrum was measured over $1\ \mu s$ delay time and partially resolved pure rotational sub-bands due to K-splitting in $(J+2) \leftarrow (J)$. The partially resolved K-splitting originated from a term including the quantum number K and the centrifugal distortion constant of D_{JK}. We obtained the experimental ground state rotational constant of B_0 and two centrifugal distortion constants of D_J and D_{JK} in the benzene spectrum with K-splitting. Pure rotational Raman spectra on the planar molecule do not give us D_K, but we could estimate ground state D_K value from the relationships between two centrifugal distortion constants of D_J and D_{JK}. Benzene might be not still simple within the resolution on pure rotational Raman spectra that we achieved hitherto. It requires at least a 10-folded better resolution (0.1 MHz) to resolve individual transition lines with a given J and K value. However, we expect that the resolution of mass-CRASY experiment will further improve based on the

combined opto-electronical delay and the random sparse measurement method. For achievement for individual K-splitting and investigating even more accurate molecular structures and more accurately, the following improvements should be included: (1)Better resolution with the longer delay time range, better data processing to deal with burdensome mass-correlated data set. (2) the better S/N ratio, (3) the better temperature estimation for the molecular beam. They are required to perform upcoming high-resolution spectra with sub-MHz resolution to sub-KHz resolution to investigate spectral details that we and you have never been before.

Figures and Tables

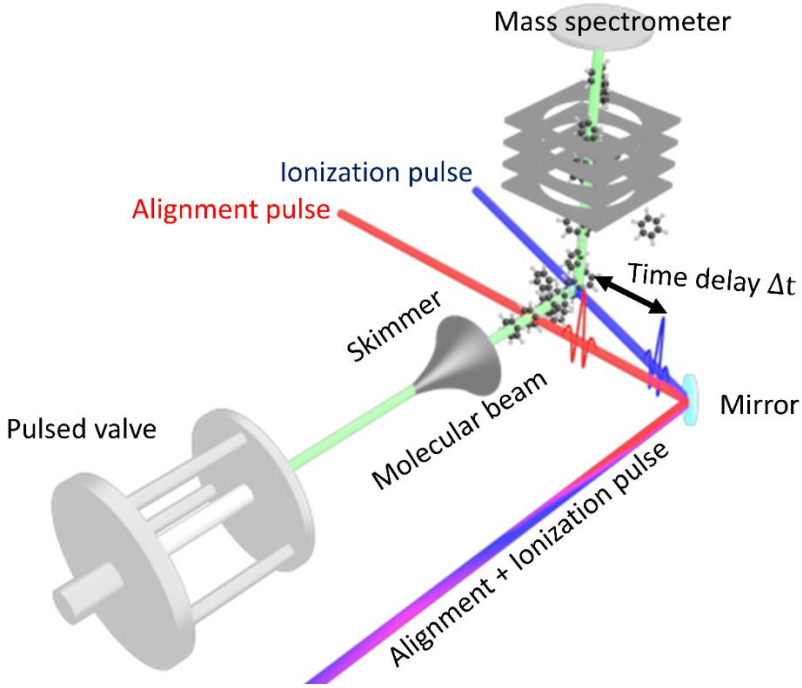

Figure 1 : Experimental scheme : This scheme representation of the CRASY experiment [26] : A pulse valve generated a cold supersonic molecular beam with a low temperature. A red beam is alignment pulse (pulse width = 1 ps, $\lambda_{Alignment}$ = 800 nm) and aligns benzene molecules. A blue beam describes the probe pulse (pulse width = 45 fs, $\lambda_{Ionization}$ = 200 nm) and ionizes molecules after a time delay (Δt = 12.5 ns). Time-dependent signal modulation were observed in a Wiley-McLauren TOF(Time of Flight)-mass spectrometer[28] The angle between alignment beam and ionization beam became increased along with the opto-mechanical delay even the two beams coincidently had started at the beginning. The time delay was reference against a GPS stabilized clock for calibration during the measurement

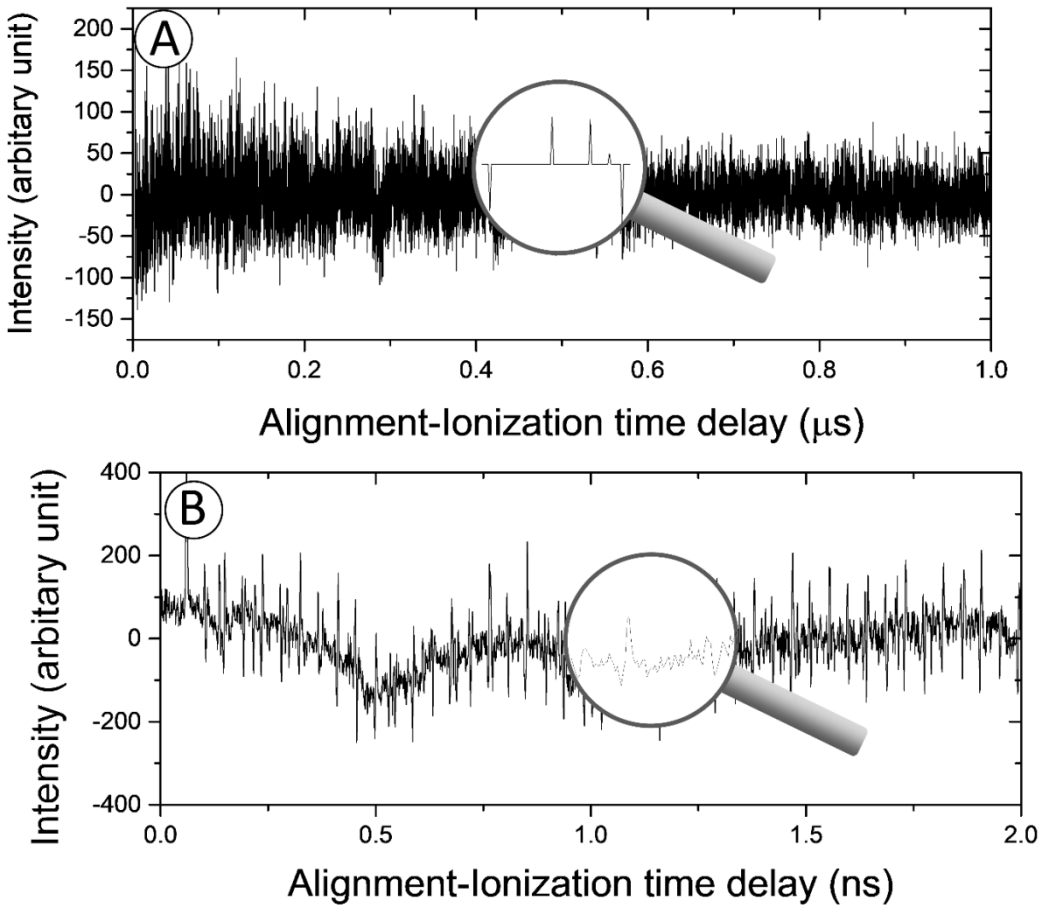

Figure 2 : Random sparse measurement and continuous measurement comparison. (A) is a time delay trace from random sparse measurement over 1 μs. An enlarged figure shows the random sparse sampled points in a range from 0.4018 to 0.4019 μs. (B) is a time delay trace from a continuous measurement over 2ns.

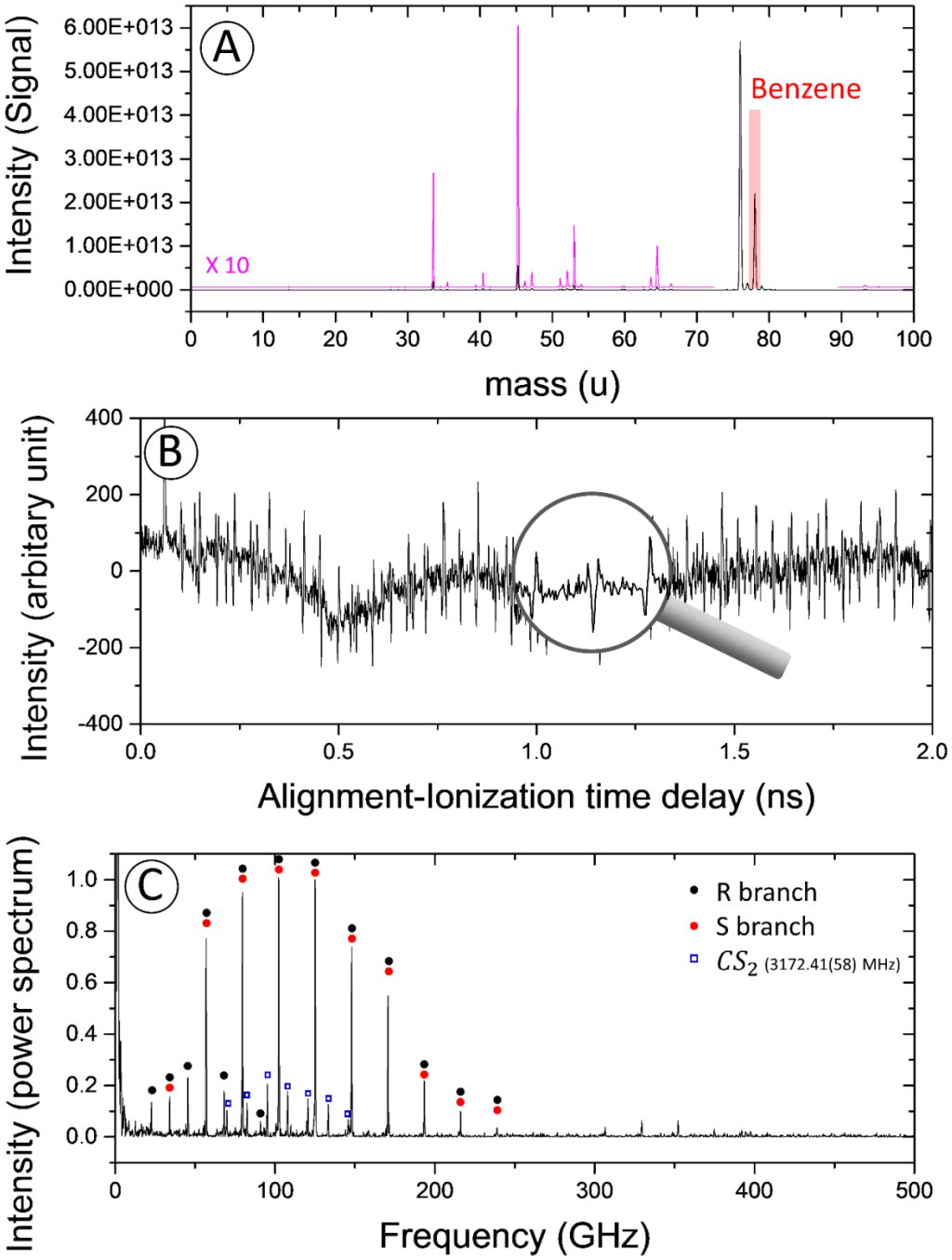

Figure 3 : Ground state benzene (C_6H_6, 78 u) rotational spectrum measured with a 2 ns delay range. (a) Mass spectrum integrated of 2 ns continuous delay scanning. (b) Time delay trace of benzene at mass 78 u. The enlarged time trace shows a range from 1.1 ns to 1.25 ns. (c) Rotational spectrum of benzene (mass 78 u).

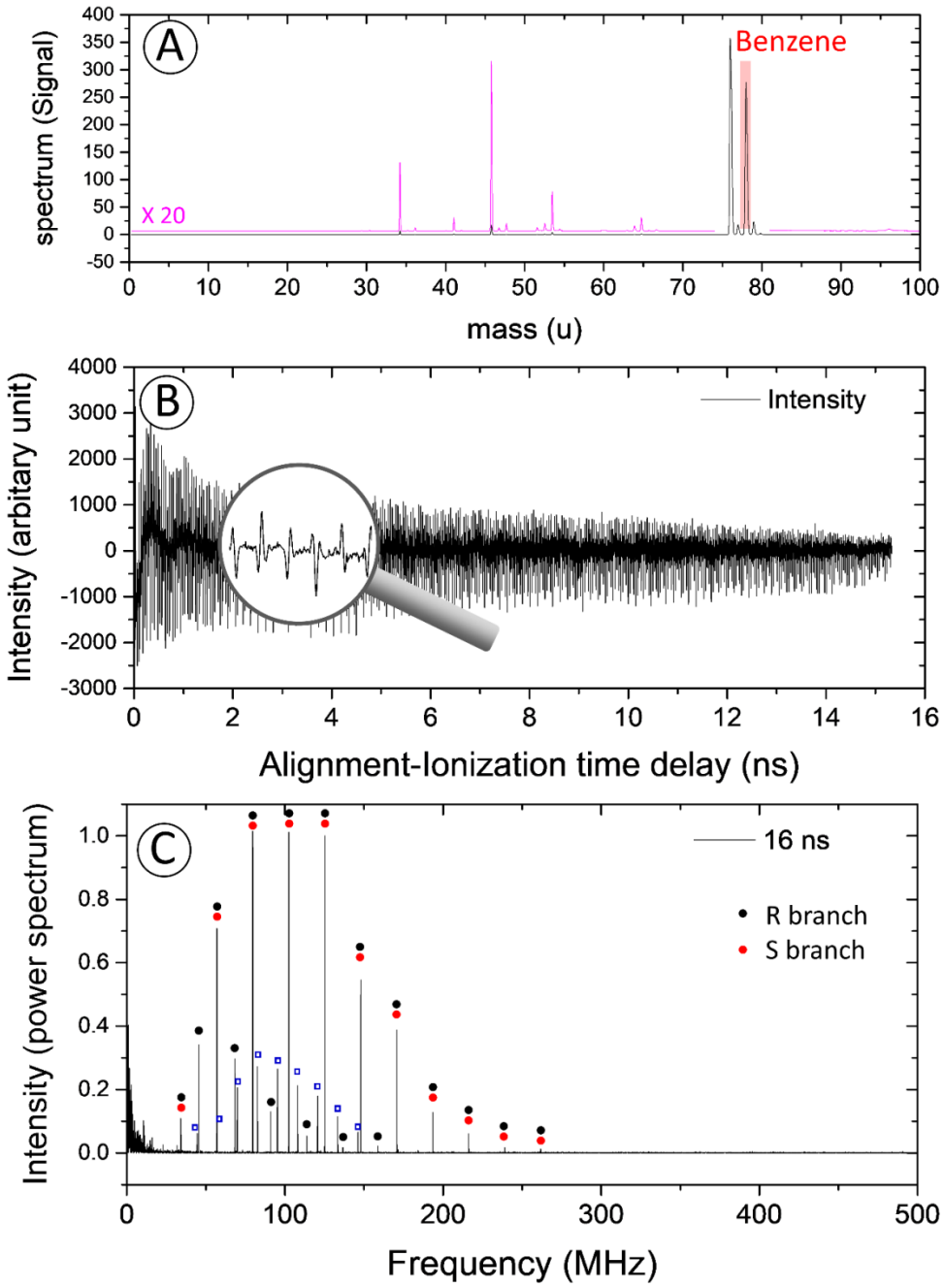

Figure 4 : Ground state benzene (C_6H_6, 78 u) rotational spectrum measured by a 16 ns delay range. (a) Mass spectrum of 16 ns continuous delay scan. Signals for carbon disulfide (76 u) were also observed and were used to calibrate the rotational frequency axis in the (c). (b) Time delay trace of benzene at mass 78 u. The enlarged time trace of a magnifier shows a range from 3.0 ns to 3.2 ns. (c) Rotational spectrum of benzene in mass 78 u.

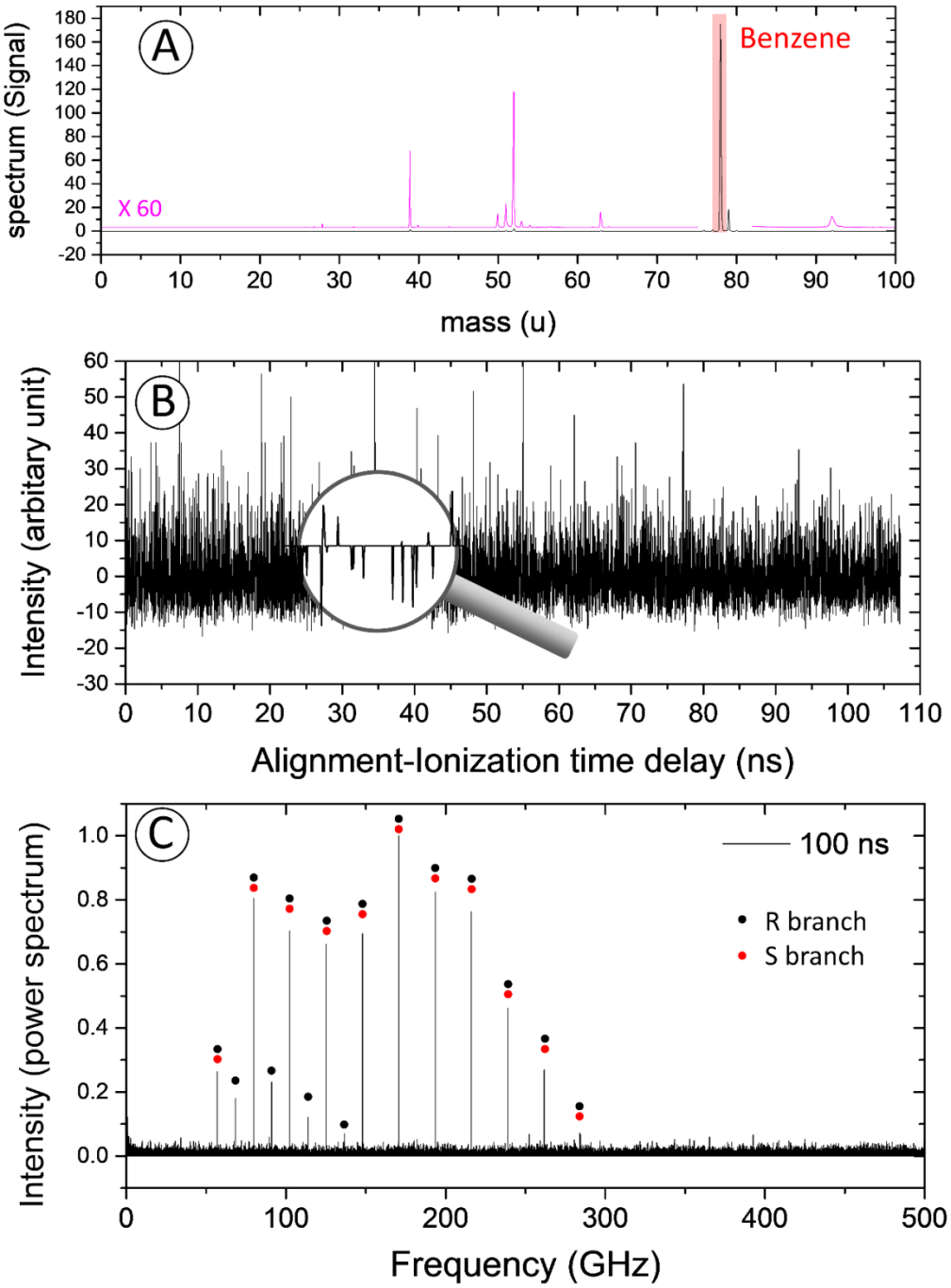

Figure 5 : Ground state benzene (C_6H_6, 78 u) rotational spectrum measured by a 100 ns delay range. (a) An integrated mass spectrum for 100 ns random sparse delay scan. (b) Time delay trace of benzene at mass 78 u. The enlarged time trace of a magnifier is a range from 30.05 ns to 30.25 ns (c) Rotational spectrum of benzene (mass 78 u)

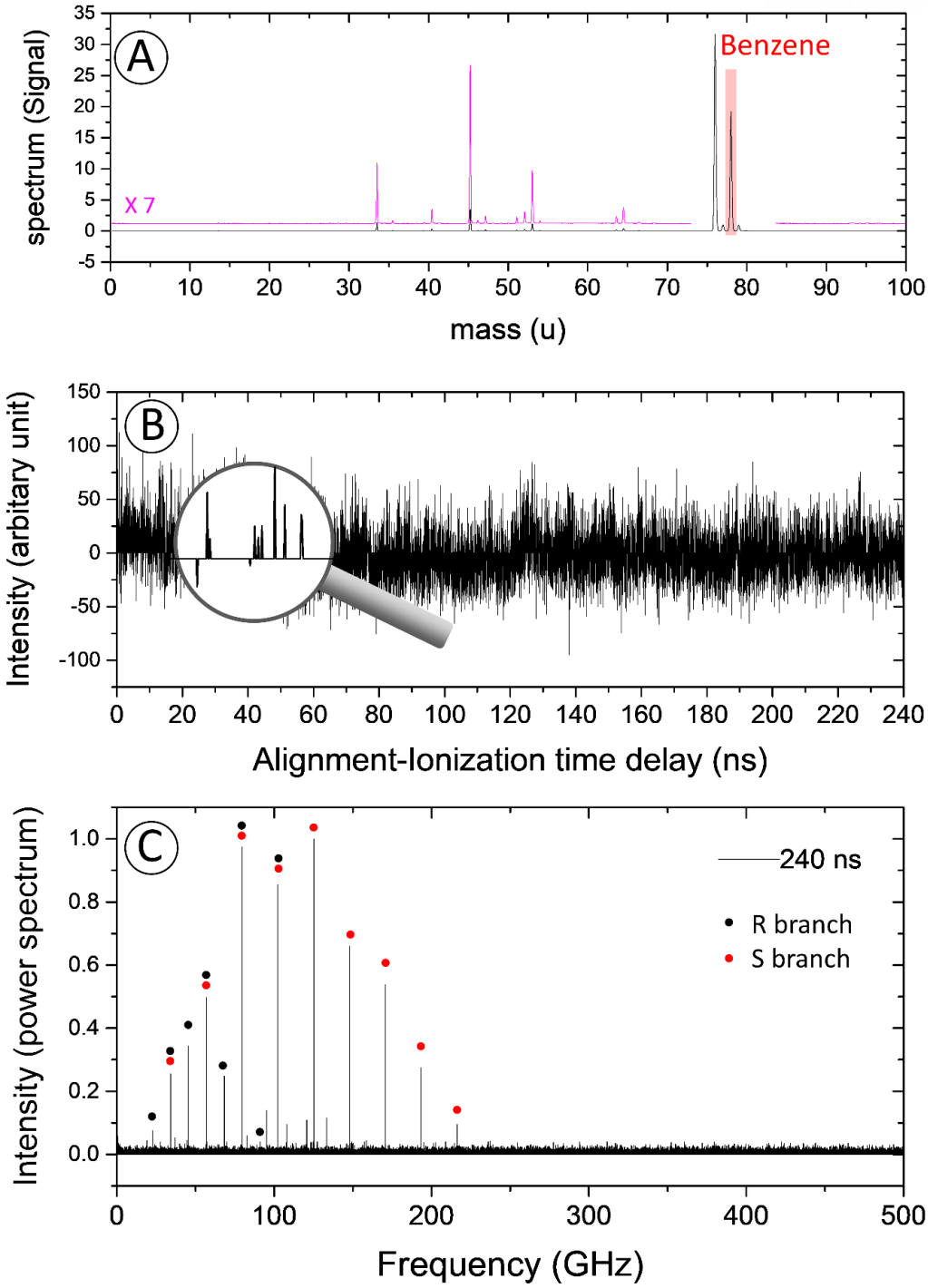

Figure 6 : Ground state benzene (C_6H_6, 78 u) rotational spectrum measured by 240 ns delay range. (a) Mass spectrum of 240 ns random sparse delay scan. (b) Time delay trace of benzene in mass 78 u. . The enlarged time trace of a magnifier shows a range from 30.05 ns to 30.25 ns (c) Rotational spectrum of benzene (mass 78 u).

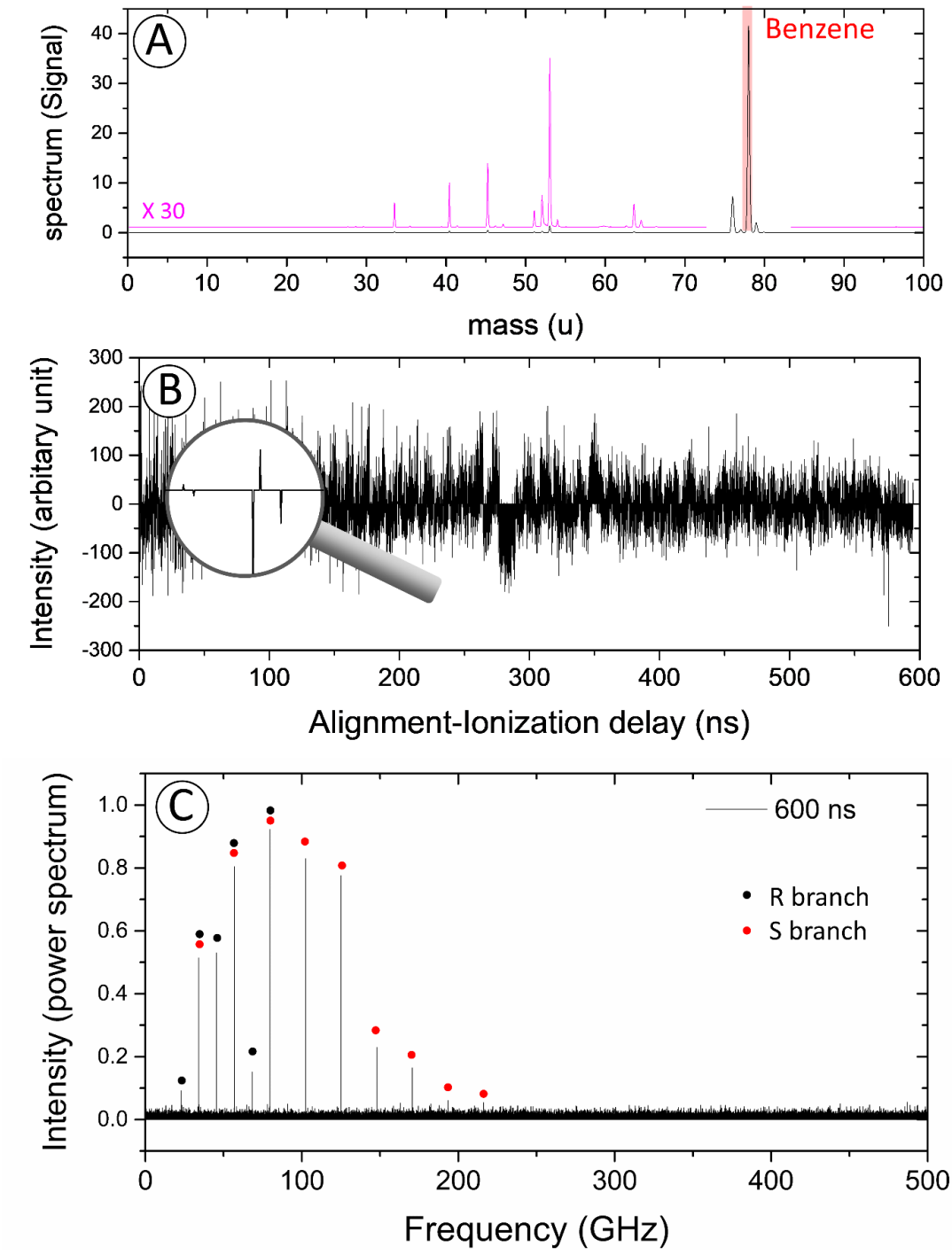

Figure 7: Ground state benzene (C_6H_6, 78 u) rotational spectrum measured by a 600 ns delay scan. (a) Integrated mass spectrum of 600 ns random sparse delay scan. (b) Time delay trace of benzene at mass 78 u. The enlarged time trace in a magnifier shows a range from 30.05 ns to 30.25 ns. (c) Rotational spectrum of benzene (mass 78 u).

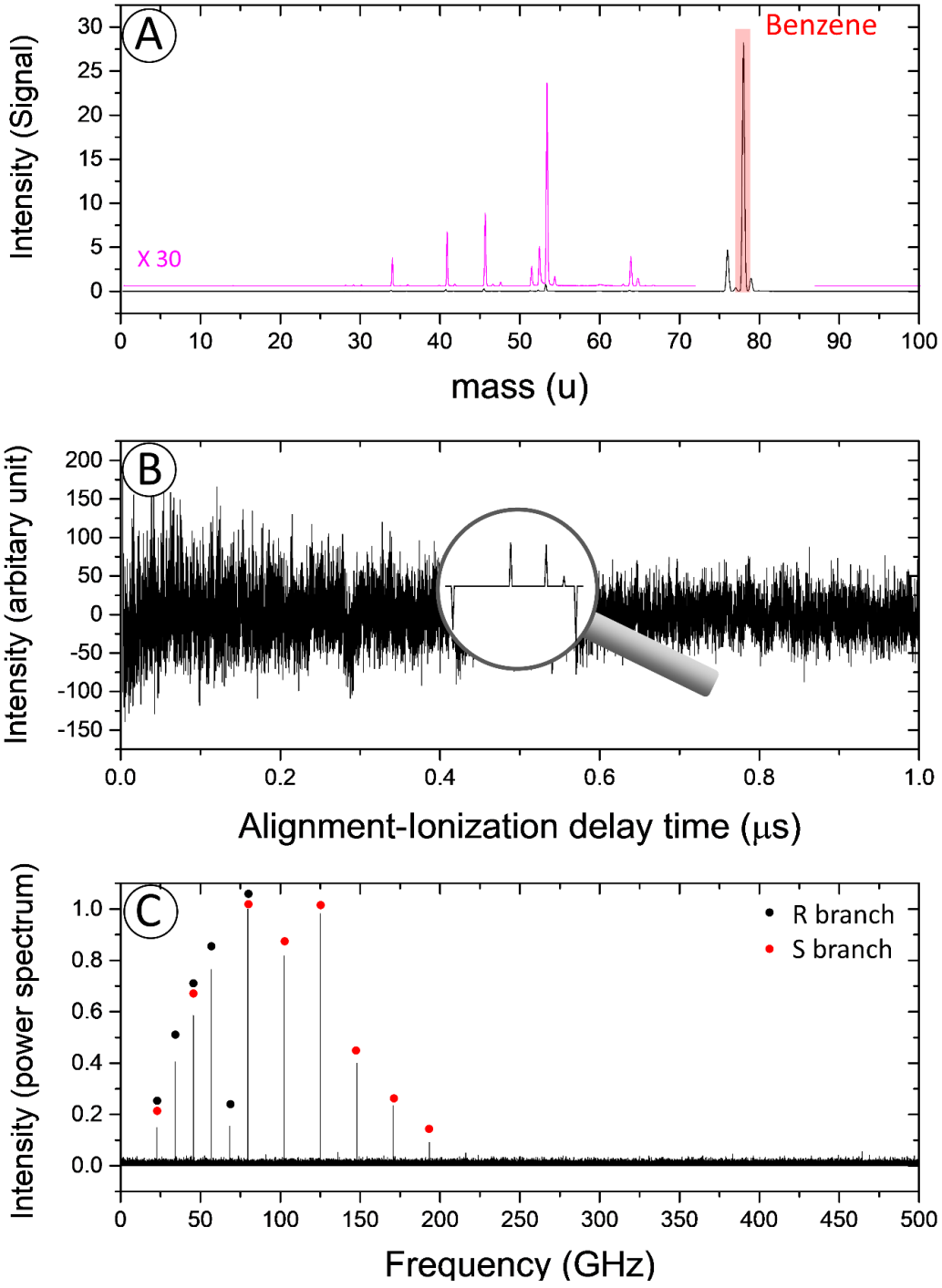

Figure 8 : Ground state benzene (C_6H_6, 78 u) rotational spectrum measured by a 1 μs delay range scan. (a) Integrated mass spectrum of 1 μs random sparse delay scan. (b) Time delay trace of benzene at mass 78 u. The enlarged time trace shows a range from 0.4018 μs to 0.4019 μs. (c) Rotational spectrum of benzene (mass 78 u).

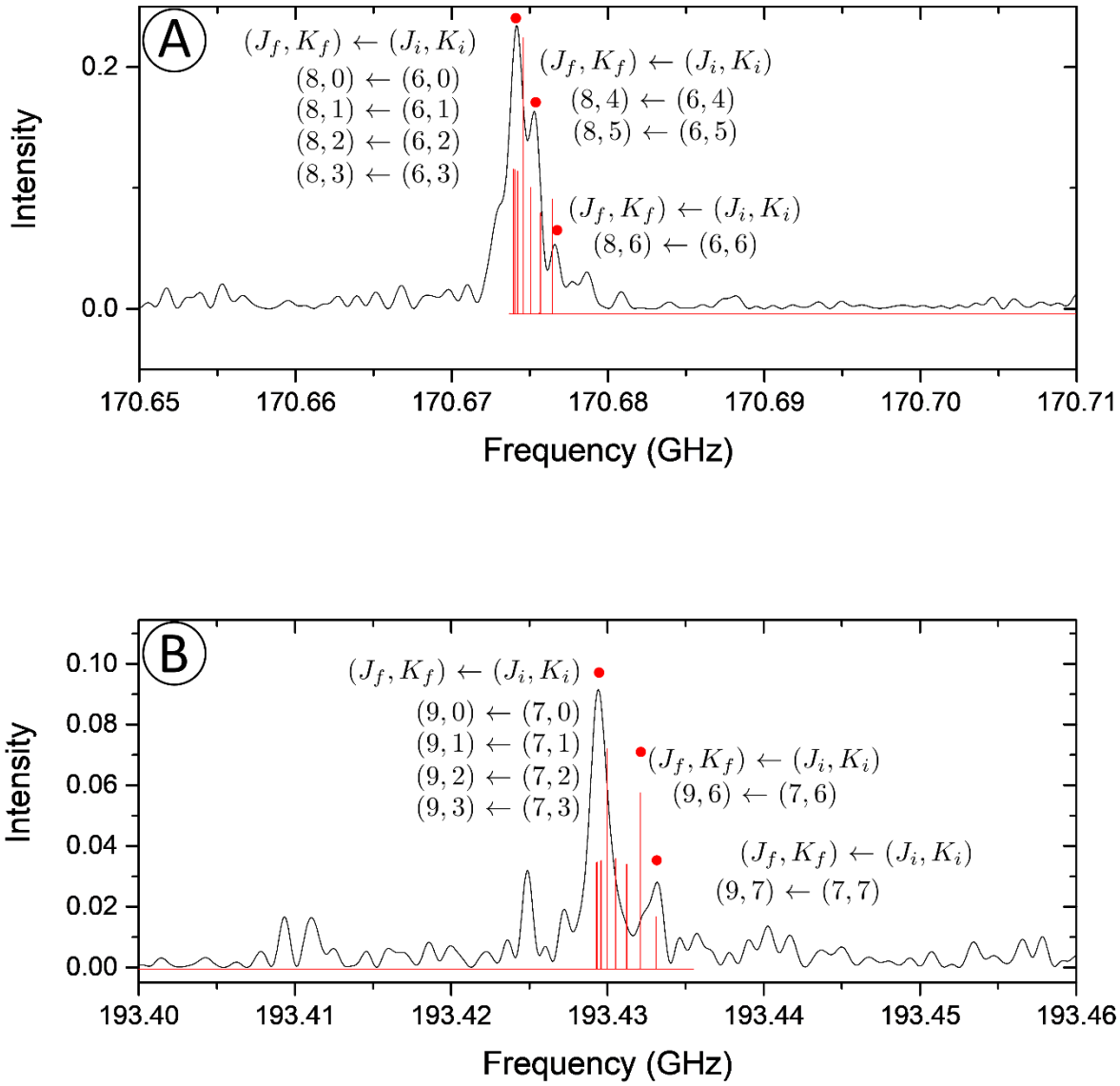

Figure 9 : Magnified sections of the rotational spectra obtained by 1 μs sparse sampling in Fig. 8. Red lines represent a simulated spectrum based on B = 5689.2671 MHz, D_J =1178 Hz, and D_{JK} = -2300 Hz from 1 MHz resolution Pgopher fitting. Black bands show partially resolved sub-bands due to the quantum number K and centrifugal distortion constant D_{JK}. (A) is plotted in a range from 170.65 to 170.71 GHz. (B) is plotted between 193.40 and 193.46 GHz.

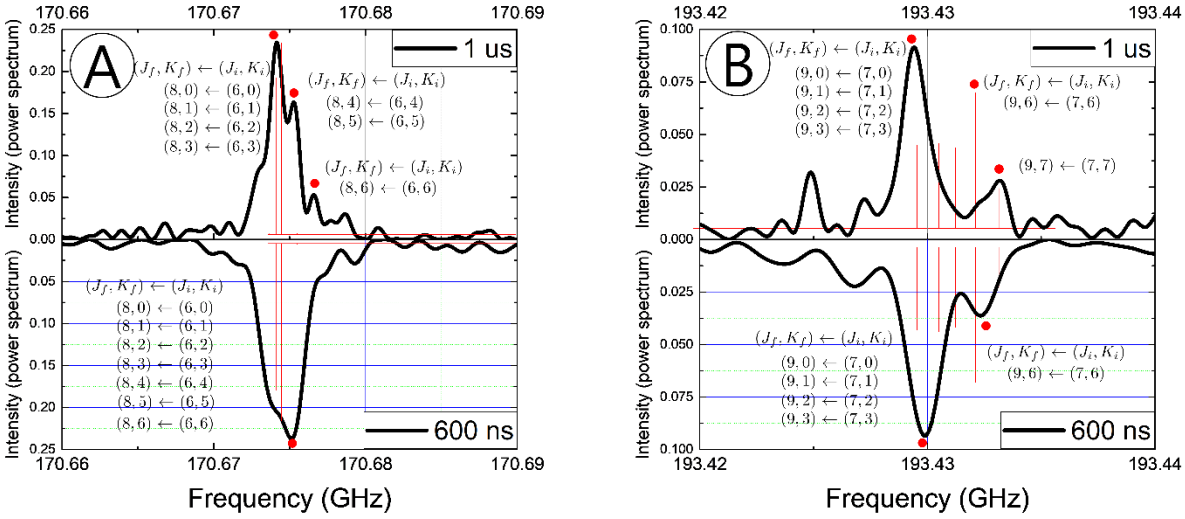

Figure 10 : The two figures, (A) and (B) compare a band in the 1 MHz resolution of spectrum measured over 1 μs and 600 ns. (A) is plotted in a range from 170.65 to 170.71 GHz. (B) is plotted between 193.40 and 193.46 GHz. Red lines represent a Pgopher [36] simulated spectrum based on B (5689.2671 MHz), D_J (1178 Hz), and D_{JK} (-2300 Hz) from Pgopher fitting. Black bands show partially resolved sub-bands due to the quantum number of K and centrifugal distortion constant D_{JK}.

B_0 (MHz)	D_J (Hz)	D_{JK} (Hz)	Method	Year
$5682.6\ (1.4)^a$	360^c	-	Pure rotational Raman (vis)	1953 [1]
$5684.1\ (1.5)^a$	-	-	Pure rotational Raman (vis)	1954 [2]
$5688.6\ (4.6)^a$	-	-	Rovibronic IR $(v_{11})^f$	1957 [4]
$5685.5\ (3.0)^a$	360^c	-	Rovibronic IR $(v_7 + v_{16})^f$	1958 [5]
$5688.6\ (1.0)^a$	-	-	Rovibronic IR $(v_{11})^f$	1968 [6]
$5692.40\ (39)^a$	$1620\ (10)^a$	-	Rovibronic IR $(v_4)^f$	1974 [7]
$5688.59\ (75)^a$	$1300(200)^a$	$-3600(2000)^a$	Rovibronic Raman$(v_1)^f$	1979 [3]
$5688.69\ (18)^a$	$1100(40)^a$	-2068^c	Rovibronic IR $(v_{11})^f$	1980 [8]
$5688.916\ (42)^b$	$1179(23)^b$	$-2100(100)^b$	Rovibronic IR $(v_{20})^f$	1982 [30]
5688.910(2)	-	-	Rovibronic IR $(v_{13})^f$	1983 [31]
5688.915^c	1179^c	-2100^c	Rovibronic IR $(3-\mu m\ band)^f$	1987 [12]
$5689.248\ (45)^a$	$1191(11)^a$	$-2040(50)^a$	Rovibronic IR $(v_{11})^f$	1988 [10]
$5689.31(9)^a$	-	-	UV $(S_1 6_0^1 \leftarrow S_0\ \&\ S_1 6_0^1 1_0^1 \leftarrow S_0)^e$	1989 [16]
$5688.92\ (6)^a$	-	-	Rovibronic IR $(v_{20})^f$	1990 [9]
$5689.266\ (6)^a$	$1231(1)^a$	$-2065(3)^a$	Rovibronic IR $(v_{11})^f$	1990 [11]
$5689.27809\ (99)^a$	$1242.8(9.74)^c$	$-2059.1(22.3)^c$	Rovibronic IR $(v_{18})^f$	1991 [13]
$5689.2406\ (126)^a$	$1477(87.8)^a$	$-2530(202)^a$	Rovibronic IR $(v_{20})^f$	1991 [14]
5689.220 (26)	$960(7)^a$	$-1960(210)^a$	UV $(S_1 6_0^1 \leftarrow S_0)$	1999 [17]
$5689.10\ (28)^b$	-	-	RCS (Time Resolve Fluorescence Depletion) ,	2001 [20]
$5687.7\ (3.0)^a$	$1300(100)^a$	$-3000(1200)^a$	RCS (Degenerate Four Wave Mixing) 1.4 ns delay	2002 [21]

$5689.25\ (11)^a$	-	-	RCS (Degenerate Four Wave Mixing) 2.78 ns delay	2002 [22]
$5688.95\ (55)^a$	$1100(200)^a$	$-1400(400)^a$	RCS (Degenerate Four Wave Mixing) 0.44 ns delay	2002 [22]
$5689.212(9)^a$	$1220(1)^a$	$-1980(30)^a$	UV $(S_1 6_0^1 \leftarrow S_0)$	2004 [18]
$5689.22(45)^a$	-	-	Fluorescence excitation	2011 [19]
5689.49^c	-	-	$MP2/6-31+G^g$	2015 [50]

Table 1. List of rotational constant of benzene in the ground state in the literatures. (a):Values in brackets denote the 1-σ fit standard deviation for the last digits. (b):Values in brackets denote the 2-σ fit standard deviation for the last digits. (c)The authors did not give an uncertainty for values. (d) IR(v13) f ,IR (v_{13} +v_{16}) f , IR(v_2+v_{13}+v_{16}) f ,IR (v_3 +v_{10} +v_{13}) f were investigated within the range of 3-mm . (e) The transitions, $S_1 6_0^1 \leftarrow S_0$ at 259 nm and $S_1 6_0^1 1_0^1 \leftarrow S_0$ at 253 nm were respectively recorded.[2] (f) Wilson notation [3] (g): The calculated rotational constants of the zero vibrational level in the ground state obtained by ab initio calculation.

Delay time (temperature)	2 ns (4 K) [d]	16 ns (4 K) [d]	100 ns (5 K) [c]	240 ns (4 K) [c]	600 ns (4 K) [c]	1,000 ns (4 K) [c]
B_0 (MHz)	5687.45(13)	5689.176(12)	5689.302(14)	5689.274(10)	5689.2713(88)	5689.2671(52)
D_J (Hz)	1242.8 [a]	1242.8 [a]	1964(59)	1393(74)	1223(79)	1178(50)
D_{JK} (Hz)	−2059.1 [a]	−2059.1 [a]	-2059.1^a	-2059.1^a	-2059.1^a	-2300 (120)
Resolution [b]	Approx. 400 MHz	Approx. 50 MHz	Approx. 8-9 MHz	Approx. 4 MHz	Approx. 1.5-1.8 MHz	Approx. 1.0 MHz

Table 2 Rotational constant and centrifugal distortion constants comparison over the different times. B_0, D_J, and D_{JK} were obtained by a pure rotational Raman spectrum over 16 ns with continuous measurement as well as 100 ns, 200 ns, 600 ns, 1000 ns (= 1 μs) with random sparse scan. (a) : literature values from Junttila et al [13] (b) : FWHM of the spectral resolution with non-apodization. (c) : Random sparse measurement with an experimental calibration based on an external GPS disciplined clock with accuracy of 10^{-7}. (d) Continuous measurement with the experimental calibration based on the external GPS clock in (c).

Observed(MHz)	Calculated (MHz)	Obs-Calc (MHz)	J_f	K_f	J_i	K_i	Branch
193429.4	193429.8038	-0.3708	9	3	7	3	S
193429.4	193429.8038	-0.3708	9	3	7	3	S
193429.4	193429.3964	0.0366	9	2	7	2	S
193429.4	193429.1519	0.2811	9	1	7	1	S
193429.4	193429.0704	0.3626	9	0	7	0	S
193432.5	193432.0039	0.4571	9	6	7	6	S
193432.5	193432.0039	0.4571	9	6	7	6	S
193433.1	193433.0632	0.0478	9	7	7	7	S
170676.6	170676.4539	0.1361	8	6	6	6	S
170674.2	170674.5126	-0.3536	8	3	6	3	S
170674.2	170674.5126	-0.3536	8	3	6	3	S
170674.2	170674.1531	0.0059	8	2	6	2	S
170674.2	170673.9374	0.2216	8	1	6	1	S
170674.2	170673.8655	0.2935	8	0	6	0	S
170675.2	170675.0159	0.2001	8	4	6	4	S
170675.2	170675.663	-0.447	8	5	6	5	S
170676.6	170675.663	0.927	8	5	6	5	S
170676.6	170676.4539	0.1361	8	6	6	6	S
147918.8	147918.227	0.595	7	0	5	0	S
147918.8	147918.2893	0.5327	7	1	5	1	S
147918.8	147918.4762	0.3458	7	2	5	2	S
147918.8	147918.7878	0.0342	7	3	5	3	S
147918.8	147918.7878	0.0342	7	3	5	3	S

147918.8	147919.224	-0.402	7	4	5	4	S
125162.5	125162.2127	0.3243	6	0	4	0	S
125162.5	125162.2654	0.2716	6	1	4	1	S
125162.5	125162.4236	0.1134	6	2	4	2	S
125162.5	125162.6872	-0.1502	6	3	4	3	S
125162.5	125162.6872	-0.1502	6	3	4	3	S
125162.5	125163.0563	-0.5193	6	4	4	4	S
102406.1	102405.8803	0.1977	5	0	3	0	S
102406.1	102405.9235	0.1545	5	1	3	1	S
102406.1	102406.0529	0.0251	5	2	3	2	S
102406.1	102406.2686	-0.1906	5	3	3	3	S
102406.1	102406.2686	-0.1906	5	3	3	3	S
91026.96	91027.6708	-0.7138	8	7	7	7	R
91026.96	91027.1723	-0.2153	8	6	7	6	R
91026.96	91027.1723	-0.2153	8	6	7	6	R
91026.96	91026.7505	0.2065	8	5	7	5	R
79649.41	79649.2879	0.1221	4	0	2	0	S
79649.41	79649.3214	0.0886	4	1	2	1	S
79649.41	79649.4221	-0.0121	4	2	2	2	S
79649.41	79649.2816	0.1284	7	6	6	6	R
79649.41	79649.2816	0.1284	7	6	6	6	R
68270.73	68270.8723	-0.1423	6	5	5	5	R
68270.73	68270.6134	0.1166	6	4	5	4	R
68270.73	68270.4121	0.3179	6	3	5	3	R
68270.73	68270.4121	0.3179	6	3	5	3	R

56892.37	56892.493	-0.119	3	0	1	0	S
56892.37	56892.4428	-0.0688	5	4	4	4	R
56892.37	56892.517	-0.143	3	1	1	1	S
56892.37	56892.2751	0.0989	5	3	4	3	R
56892.37	56892.2751	0.0989	5	3	4	3	R
45513.93	45513.9935	-0.0675	4	3	3	3	R
45513.93	45513.9935	-0.0675	4	3	3	3	R
45513.93	45513.8976	0.0284	4	2	3	2	R
34135.42	34135.5244	-0.1074	3	2	2	2	R
34135.42	34135.5536	-0.1366	2	0	0	0	S
34135.42	34135.4813	-0.0643	3	1	2	1	R
22756.88	22757.0357	-0.1607	2	1	1	1	R

Table 3 : Pgopher Fitting for the single MHz resolution benzene spectrum.

Temperature	B_0 (MHz)	D_J (Hz)	D_{JK} (Hz)
2 K	5689.331(12)	1964(59)	-2059.1 [13]
5 K	5689.302(14)	1604(62)	-2059.1 [13]
8 K	5689.267(11)	1305(47)	-2059.1 [13]
9 K	5689.262(11)	1263(46)	-2059.1 [13]
10 K	5689.263(12)	1278(56)	-2059.1 [13]
15 K	5689.239(12)	1136(57)	-2170(170)
18 K	5689.232(13)	1111(63)	-2370(130)
20 K	5689.233(14)	1100(64)	-2220(150)
45 K	5689.231(16)	1028(73)	-2430(180)

Table 4 : Different value for the rotational constant and centrifugal distortion constants of the 8 MHz resolution spectrum (Fig. 5 measured over 100 ns time delay) were determined based on the assumption of different molecular beam temperature. Literature values of Junttila et al. were used as starting values (B is 5689.27809 MHz [13] , D_J =1242.8 Hz [13] D_{JK} = -2059.1 Hz [13]) For the low temperature, D_{JK} was fixed. Values in brackets denote the 1-σ fit standard deviation for the last digits.

Appendix

Appendix A. Supplementary information of the high-resolution benzene spectra

A.1 Benzene spectra with different resolutions

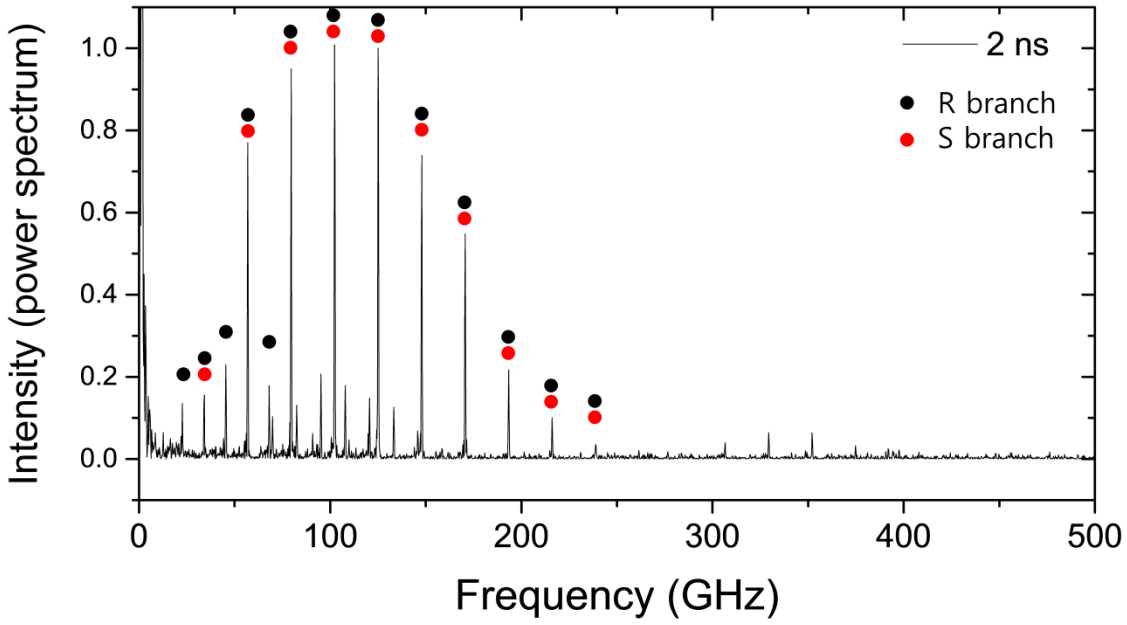

Figure A.1.1: Benzene (C_6H_6, 78 u) rotational spectrum measured over 2 ns continuous measurement with GPS clock calibration

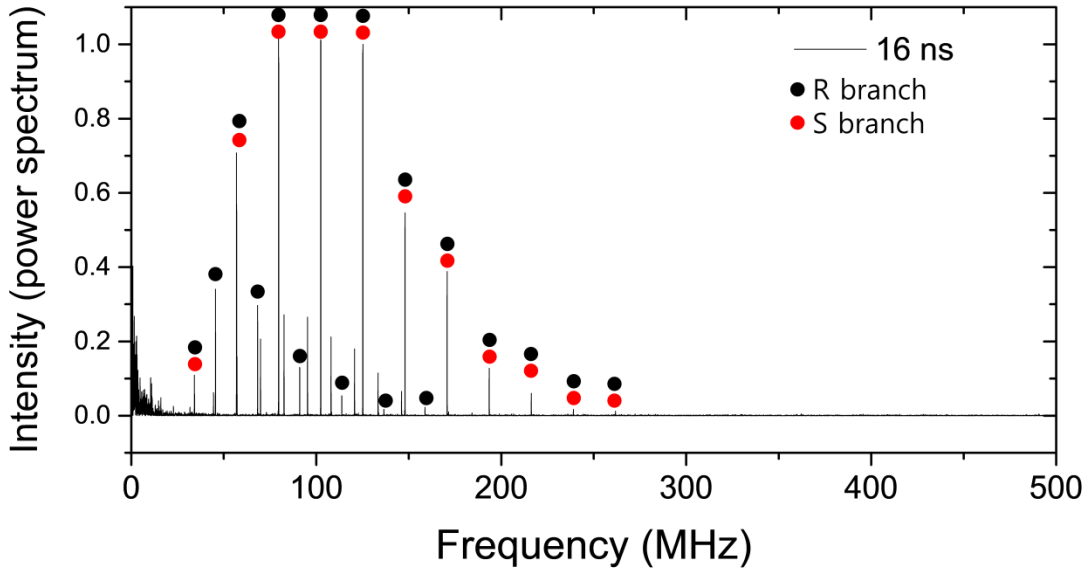

Figure A.1.2: Benzene (C_6H_6, 78 u) rotational spectrum measured over 16 ns continuous measurement with in-situ carbon disulfide rotational constant calibration.

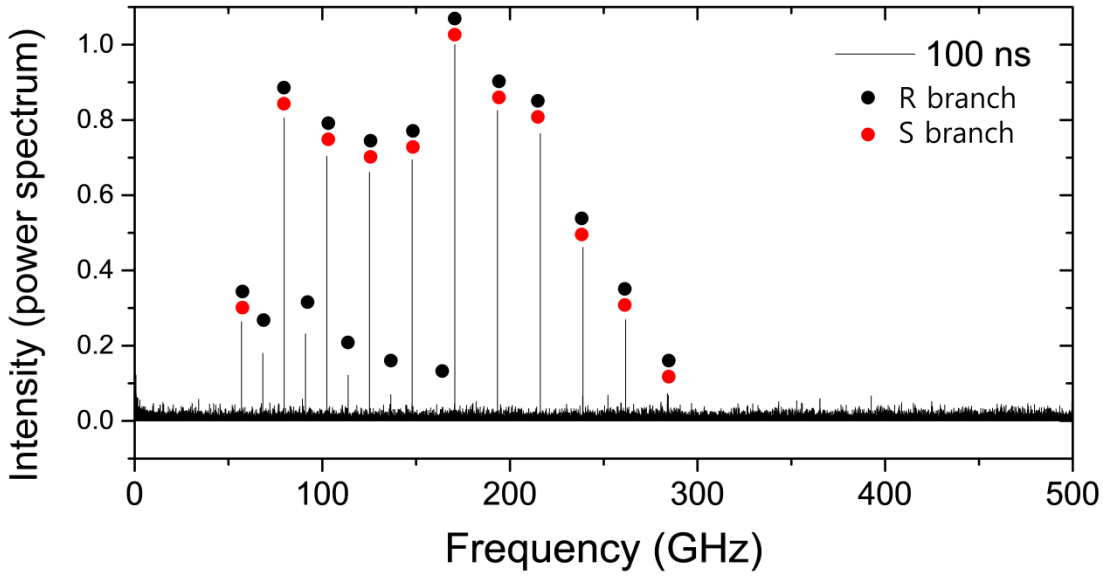

Figure A.1.3: Benzene (C_6H_6, 78 u) rotational spectrum measured over 100 ns random sparse measurement with GPS clock calibration

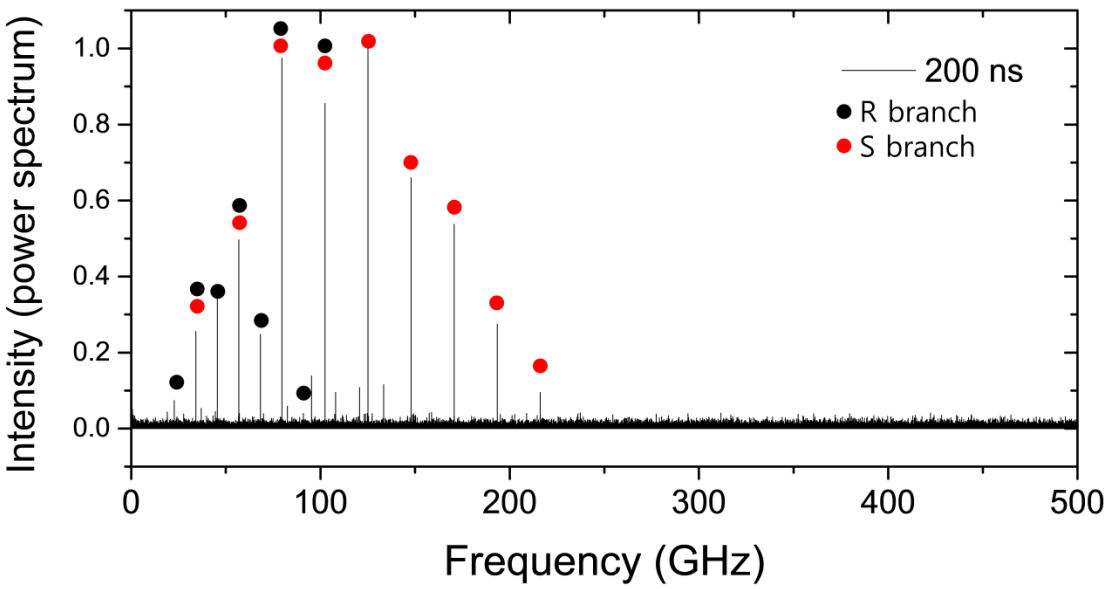

Figure A.1.4: Benzene (C_6H_6, 78 u) rotational spectrum measured over 200 ns random sparse measurement with GPS clock calibration

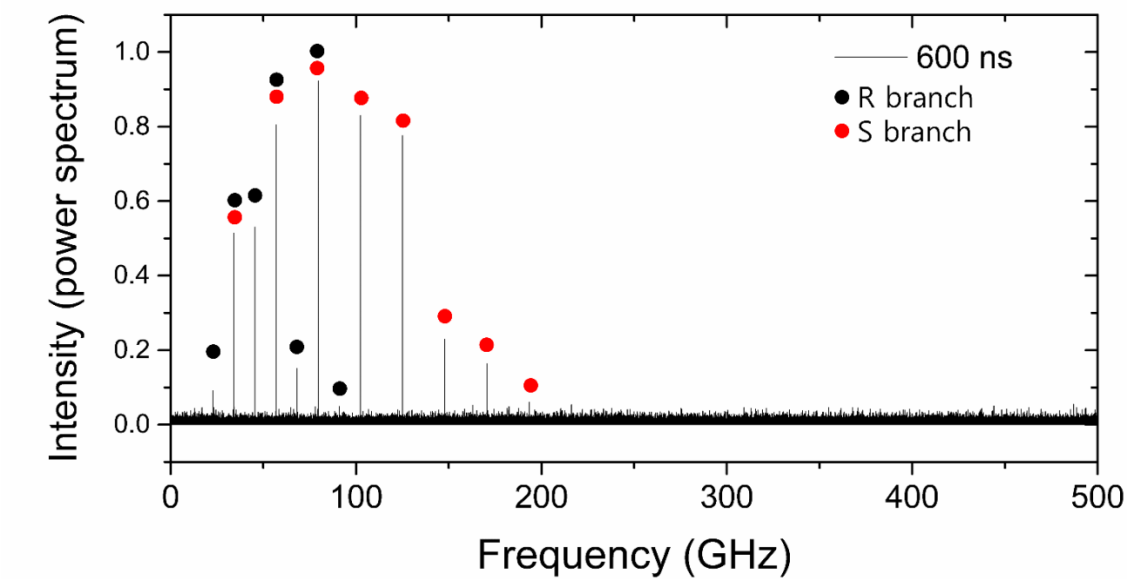

Figure A.1.5: Benzene (C_6H_6, 78 u) rotational spectrum measured over 600 ns random sparse measurement with GPS clock calibration

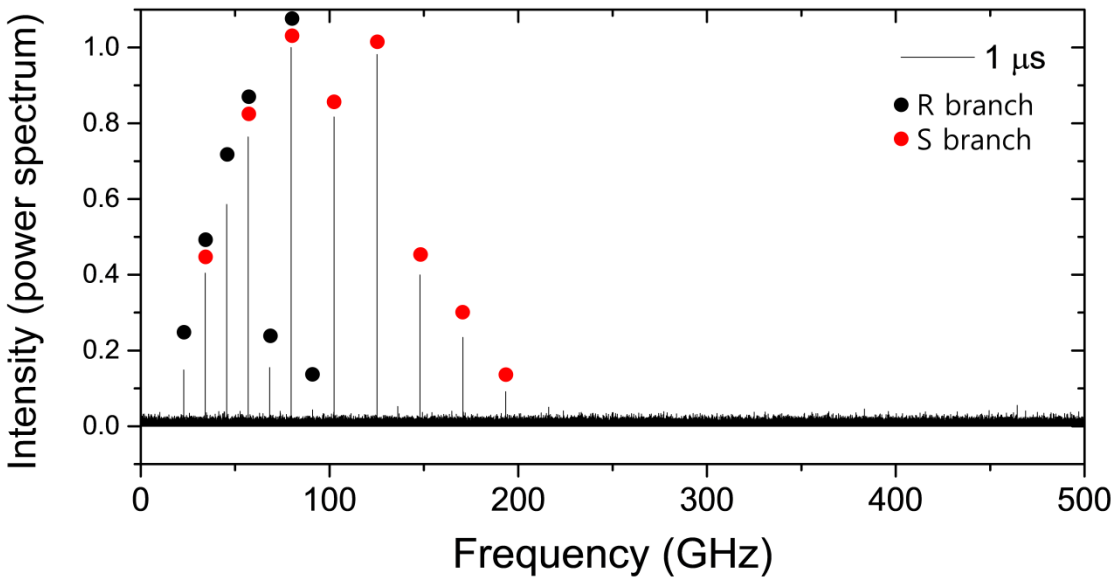

Figure A.1.6 : Benzene (C_6H_6, 78 u) rotational spectrum measured over 1 μs random sparse measurement with GPS clock calibration

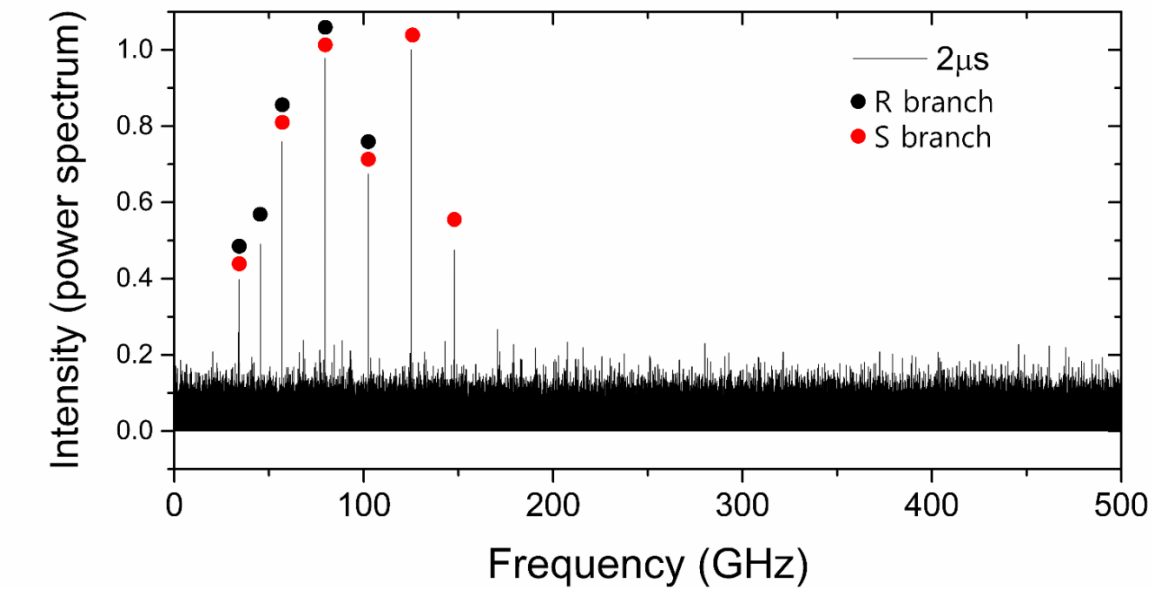

Figure A.1.7: Benzene (C_6H_6, 78 u) rotational spectrum measured over 2 μs random sparse measurement with GPS clock calibration. The rotational constants were not determined due to bad S/N.

A.2 Position of bands in different resolution spectra.

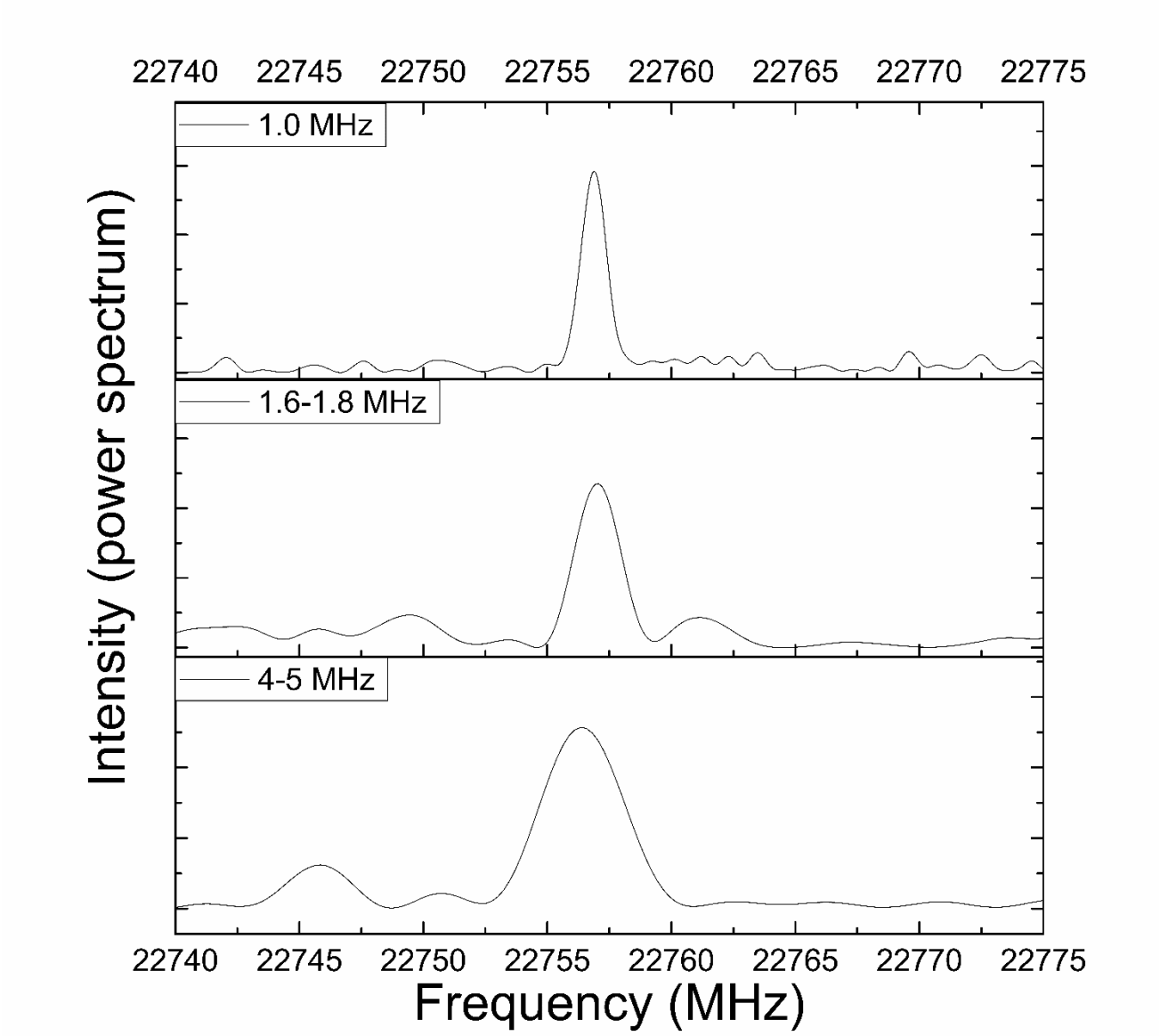

Figure A.2.1: Experimental pure rotational Raman spectra of benzene with a different resolution are plotted. Top : the 1 MHz resolution spectrum in a range from 22740 MHz to 22775 MHz There are only 1 transition Middle : the approximate 1.6 MHz resolution spectrum in the range. Bottom : the approximate 4-5 MHz resolution spectrum in the range. There is only one transition in the band. $(J_f, J_i) \leftarrow (J_i, K_i)$ is (2,1) ← (1,1). The rotational spectra are non-apodized spectra.

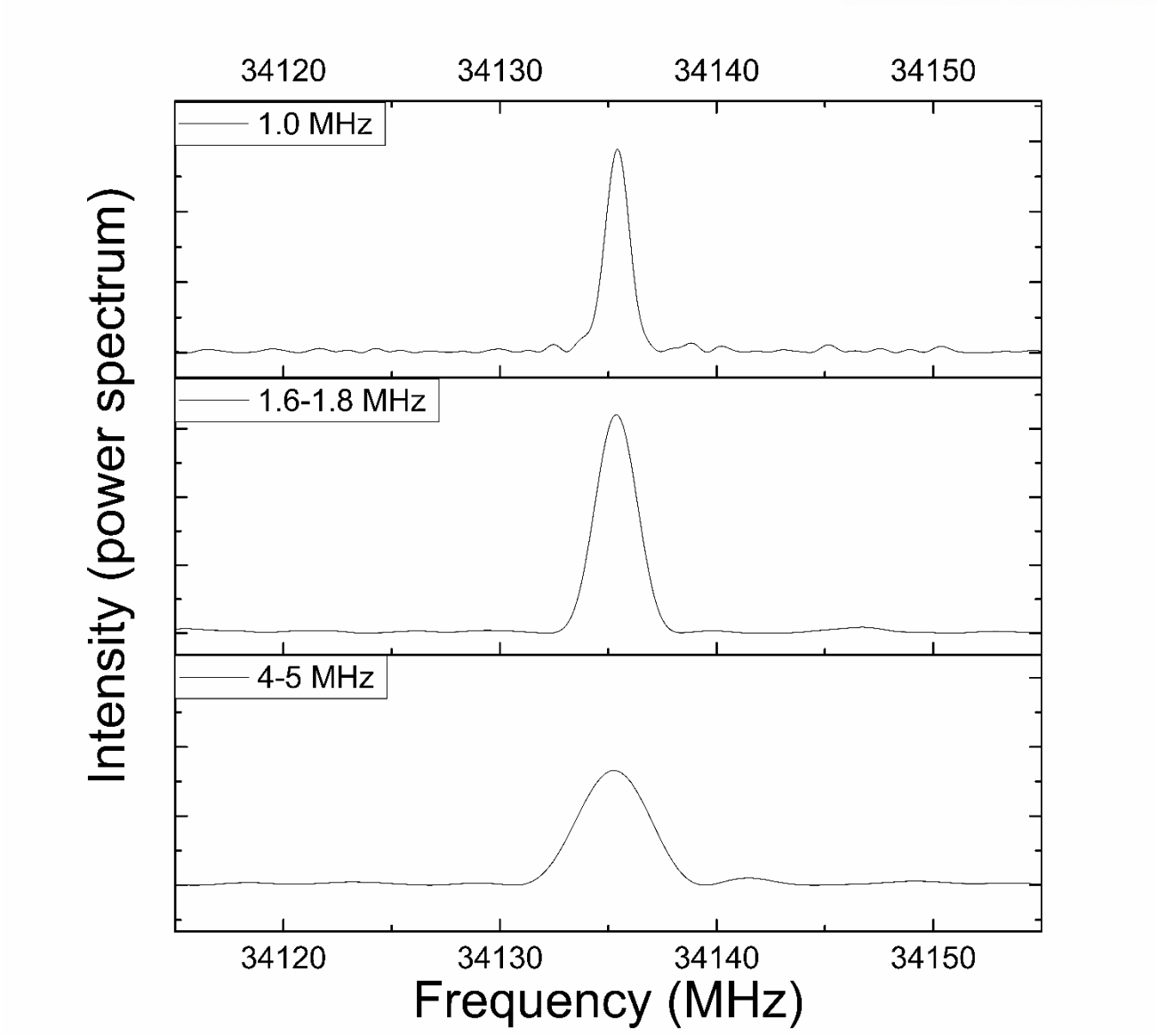

Figure A.2.2: Experimental pure rotational Raman spectra of benzene with a different resolution are plotted. Top : the 1 MHz resolution spectrum in a range from 34115 MHz to 34155 MHz There are only 1 transition Middle : the approximate 1.6 MHz resolution spectrum in the range. Bottom : the approximate 4-5 MHz resolution spectrum in the range. The rotational spectra are non-apodized spectra.

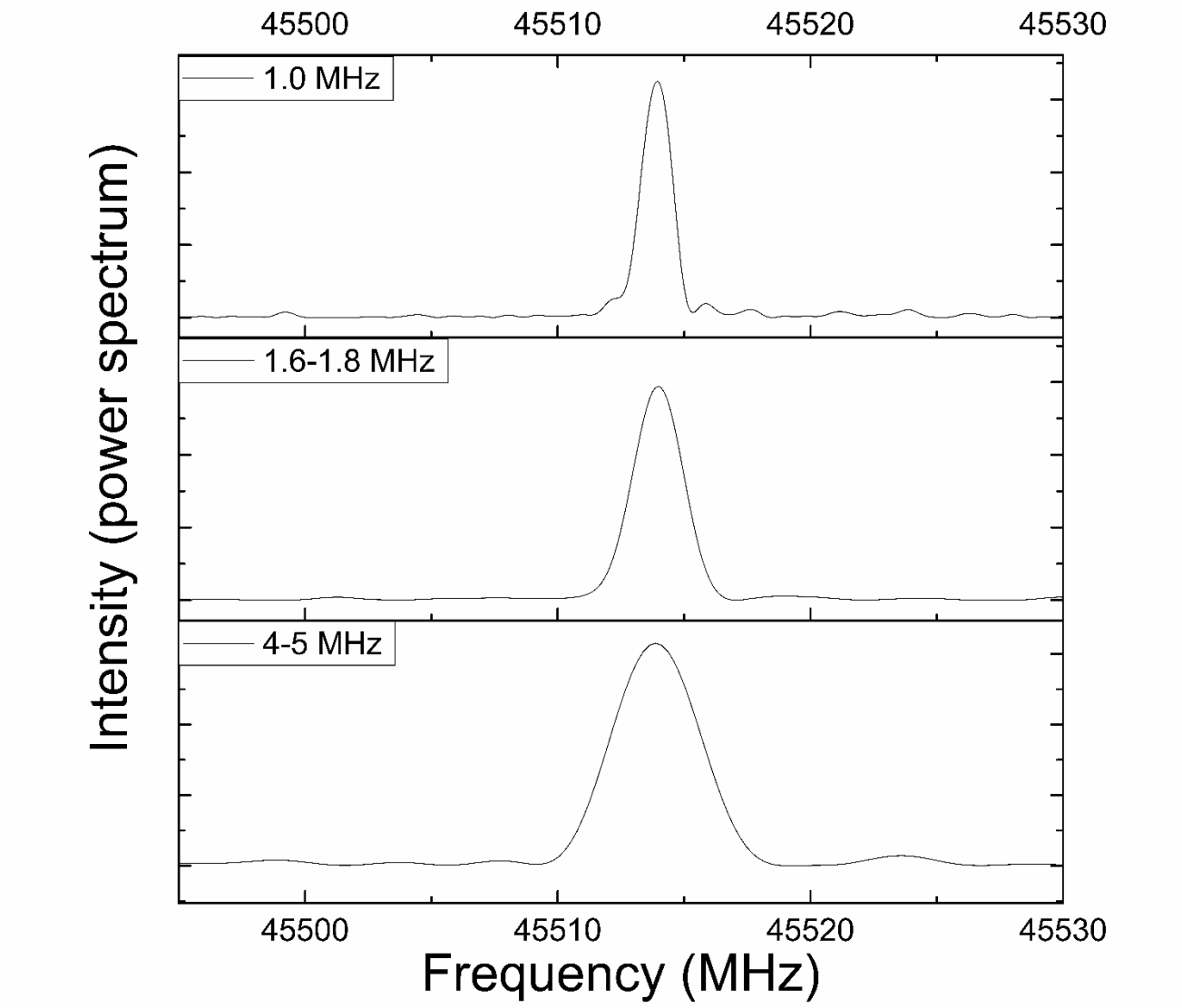

Figure.A.2.3: Experimental pure rotational Raman spectra of benzene with a different resolution are plotted. Top : the 1 MHz resolution spectrum in a range from 45495 MHz to 45530 MHz. There are only 1 transition Middle : the approximate 1.6 MHz resolution spectrum in the range. Bottom : the approximate 4-5 MHz resolution spectrum in the range. The rotational spectra are non-apodized spectra.

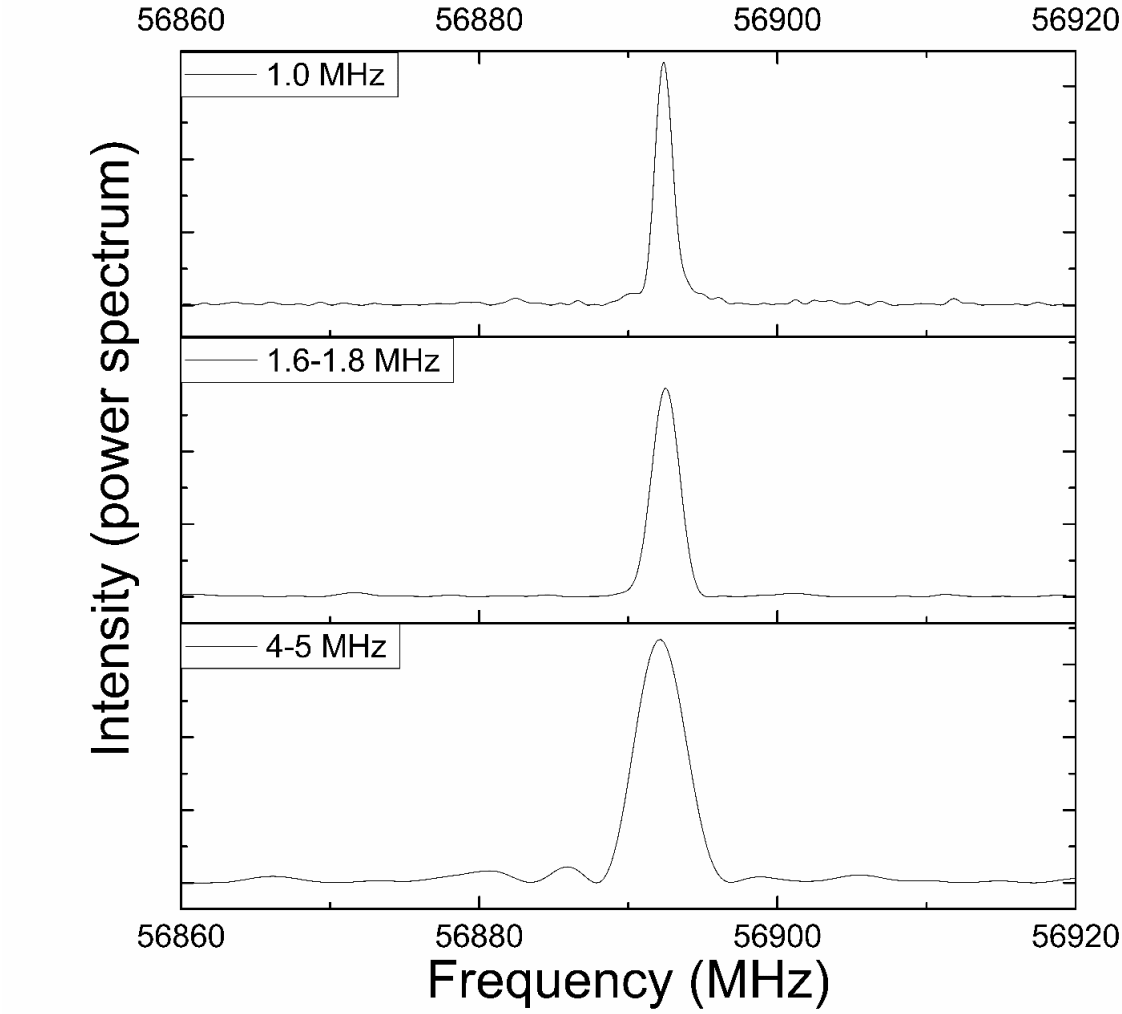

Top : the 1 MHz resolution spectrum in a range from 56860 MHz to 56920 MHz. There are only 1 transition Middle : the approximate 1.6 MHz resolution spectrum in the range. Bottom : the approximate 4-5 MHz resolution spectrum in the range. The rotational spectra are non-apodized spectra.

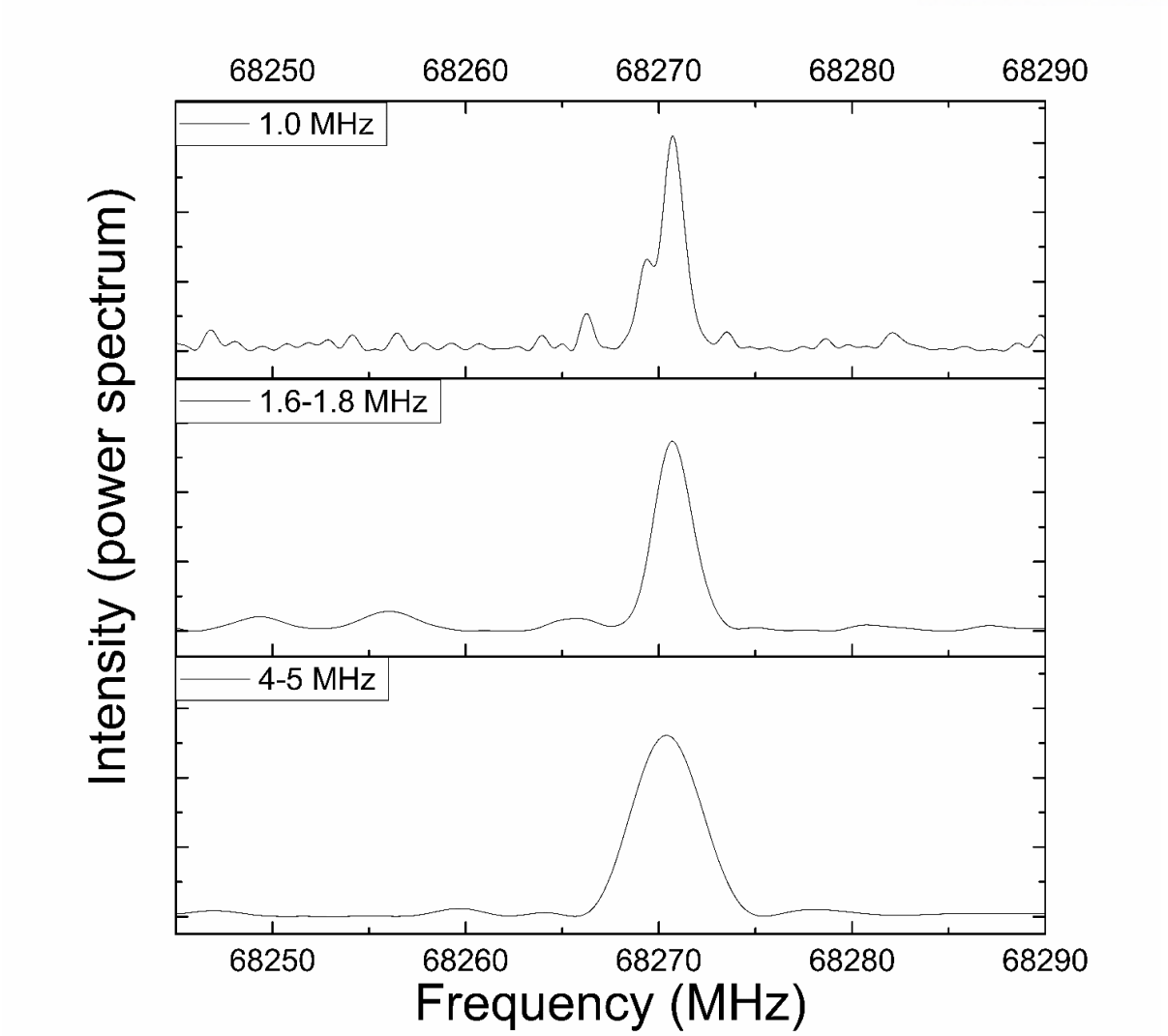

Figure A.2.5: Experimental pure rotational Raman spectra of benzene with a different resolution are plotted. Top : the 1 MHz resolution spectrum in a range from 68245 MHz to 68290 MHz. There are only 1 transition Middle : the approximate 1.6 MHz resolution spectrum in the range. Bottom : the approximate 4-5 MHz resolution spectrum in the range. The rotational spectra are non-apodized spectra.

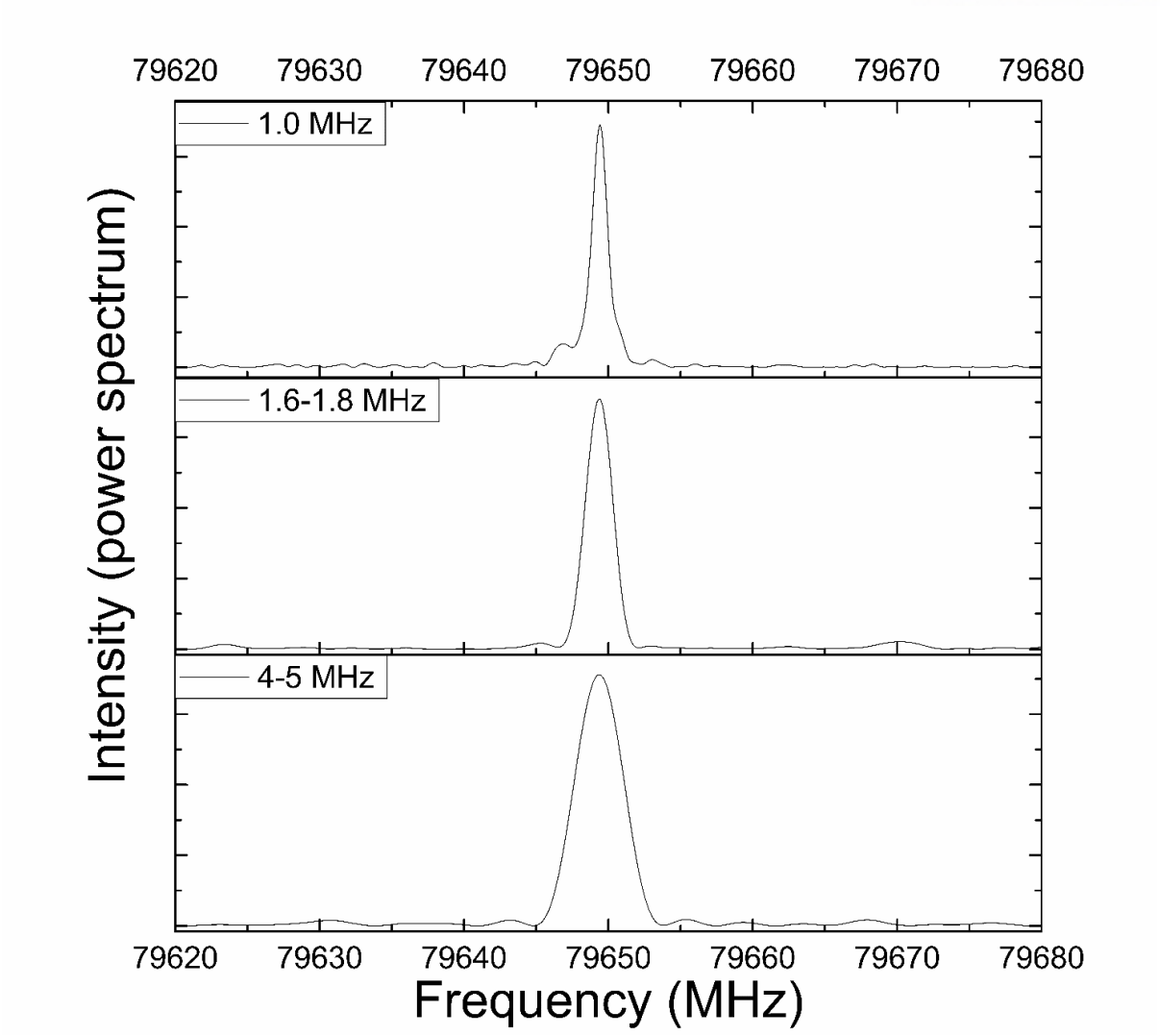

Figure A.2.6: Experimental pure rotational Raman spectra of benzene with a different resolution are plotted. Top : the 1 MHz resolution spectrum in a range from 79620 MHz to 79680 MHz. There are only 1 transition Middle : the approximate 1.6 MHz resolution spectrum in the range. Bottom : the approximate 4-5 MHz resolution spectrum in the range. The rotational spectra are non-apodized spectra.

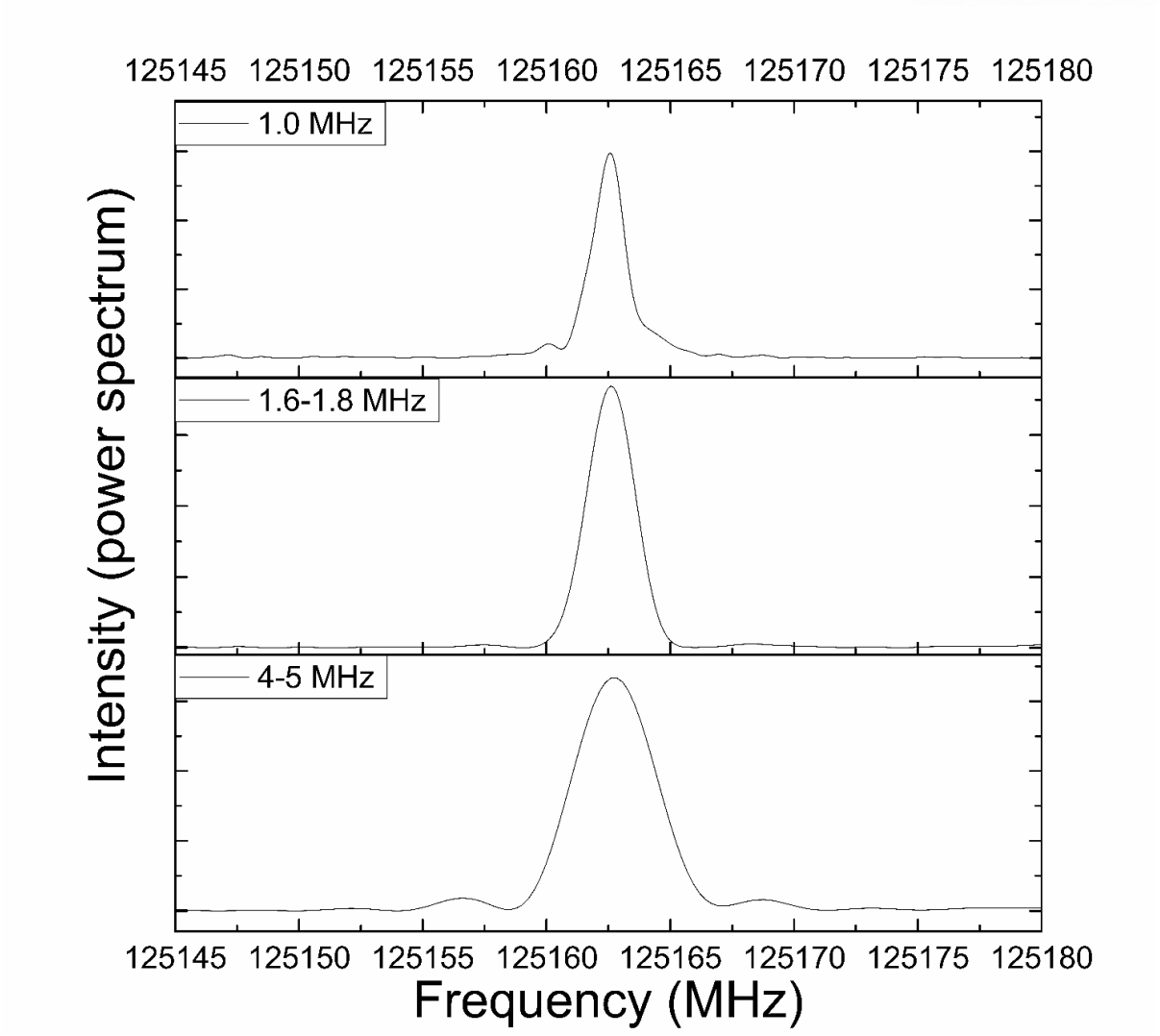

Figure A.2.7: Experimental pure rotational Raman spectra of benzene with a different resolution are plotted. Top : the 1 MHz resolution spectrum in a range from 125145 MHz to 125180 MHz. There are only 1 transition Middle : the approximate 1.6 MHz resolution spectrum in the range. Bottom : the approximate 4-5 MHz resolution spectrum in the range. The rotational spectra are non-apodized spectra.

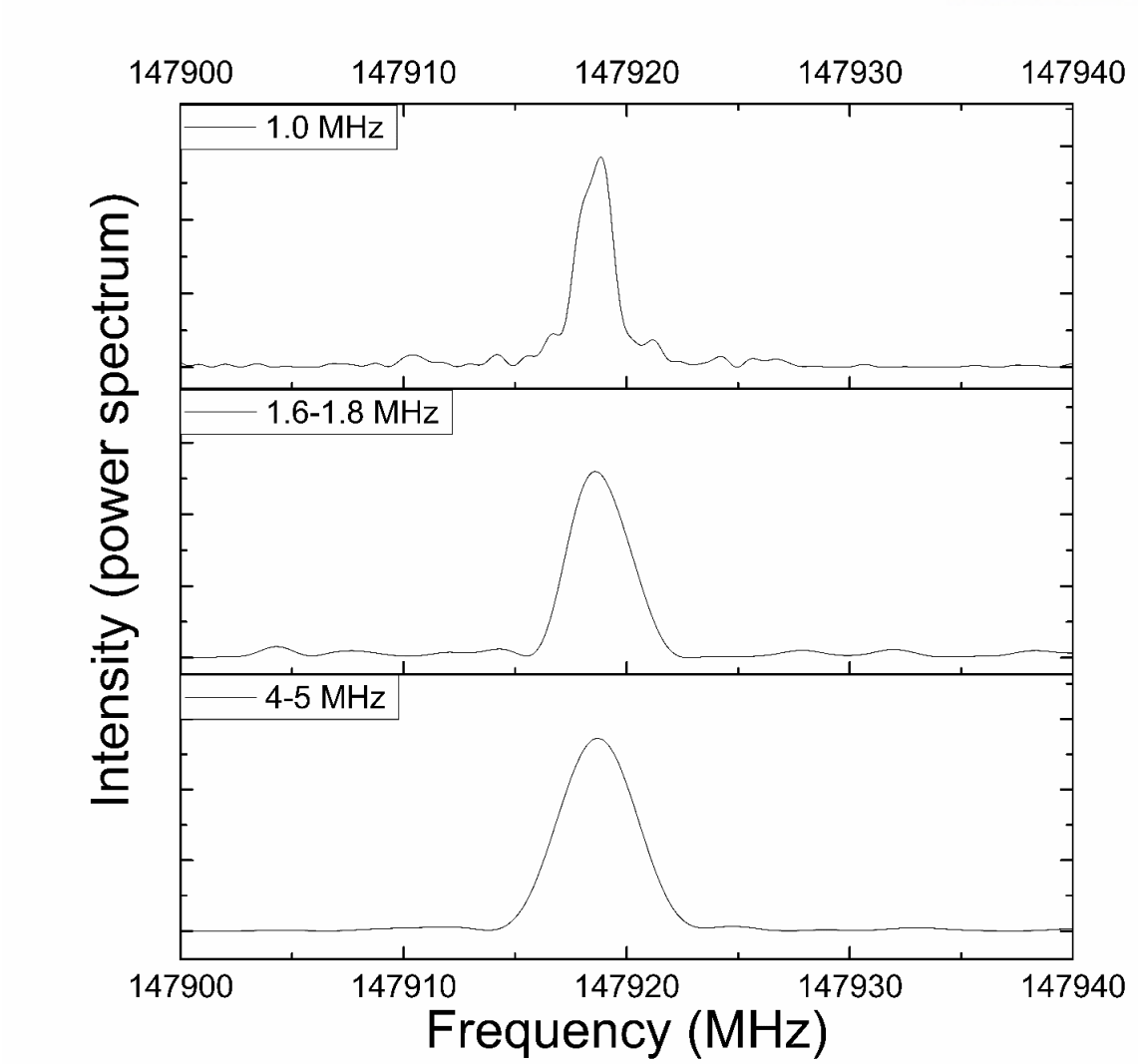

Figure A.2.8: Experimental pure rotational Raman spectra of benzene with a different resolution are plotted. Top : the 1 MHz resolution spectrum in a range from 147900 MHz to 147940 MHz. There are only 1 transition Middle : the approximate 1.6 MHz resolution spectrum in the range. Bottom : the approximate 4-5 MHz resolution spectrum in the range. The rotational spectra are non-apodized spectra.

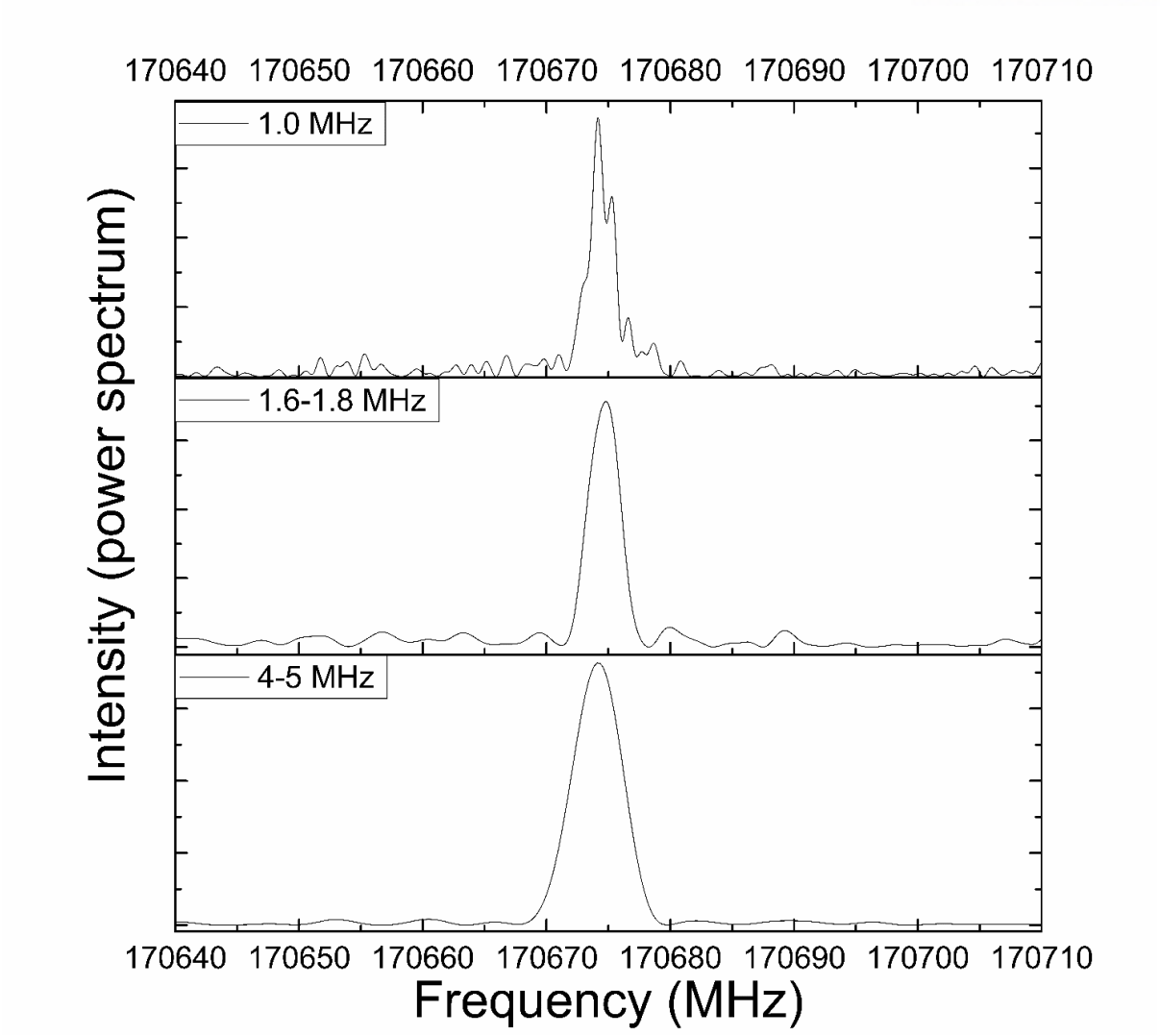

Figure A.2.9: Experimental pure rotational Raman spectra of benzene with a different resolution are plotted. Top : the 1 MHz resolution spectrum in a range from 170640 MHz to 170710 MHz. There are only 1 transition Middle : the approximate 1.6 MHz resolution spectrum in the range. Bottom : the approximate 4-5 MHz resolution spectrum in the range. The rotational spectra are non-apodized spectra.

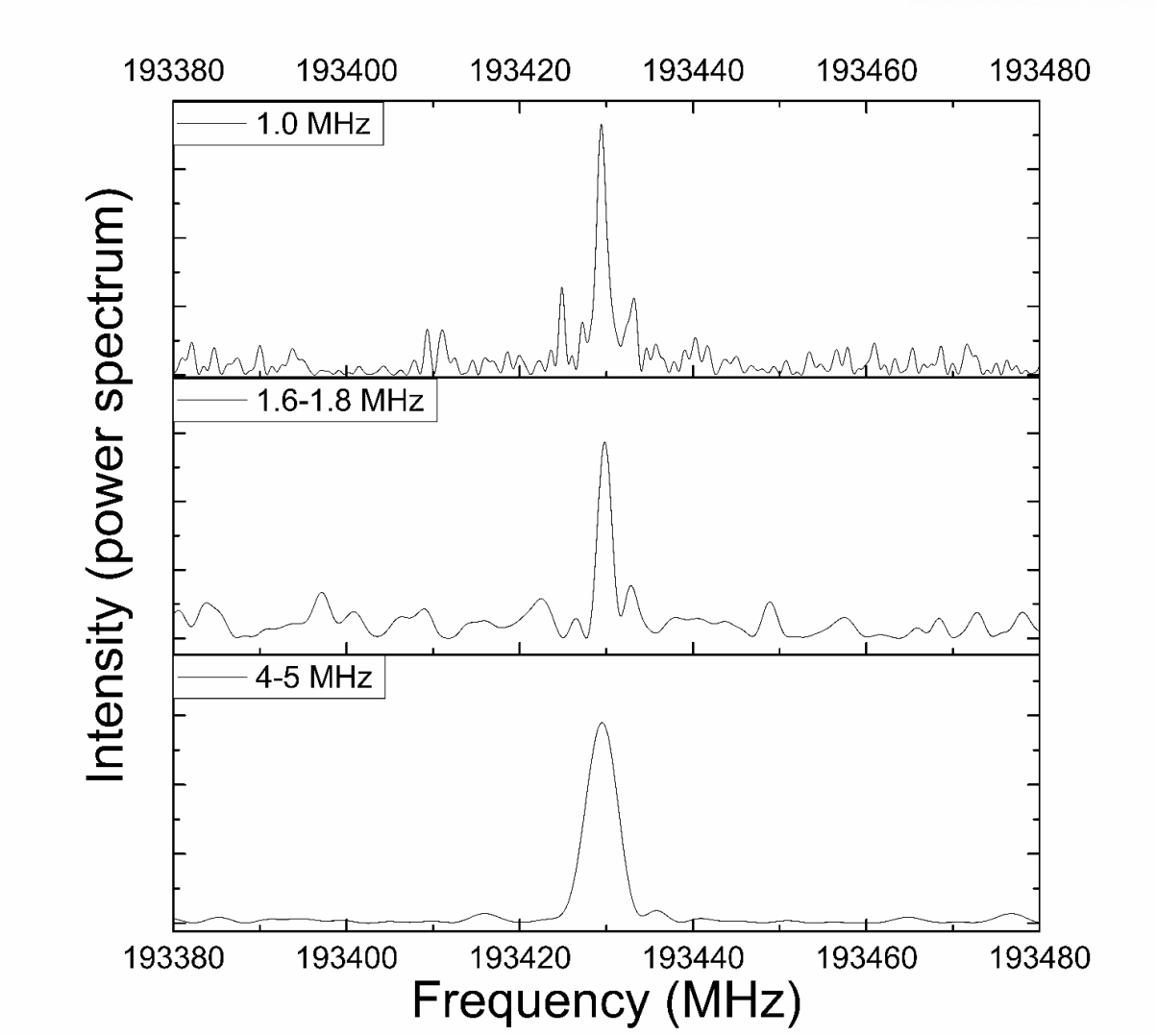

Figure A.2.10: Experimental pure rotational Raman spectra of benzene with a different resolution are plotted. Top : the 1 MHz resolution spectrum in a range from 193380 MHz to193480 MHz. There are only 1 transition Middle : the approximate 1.6 MHz resolution spectrum in the range. Bottom : the approximate 4-5 MHz resolution spectrum in the range. The rotational spectra are non-apodized spectra.

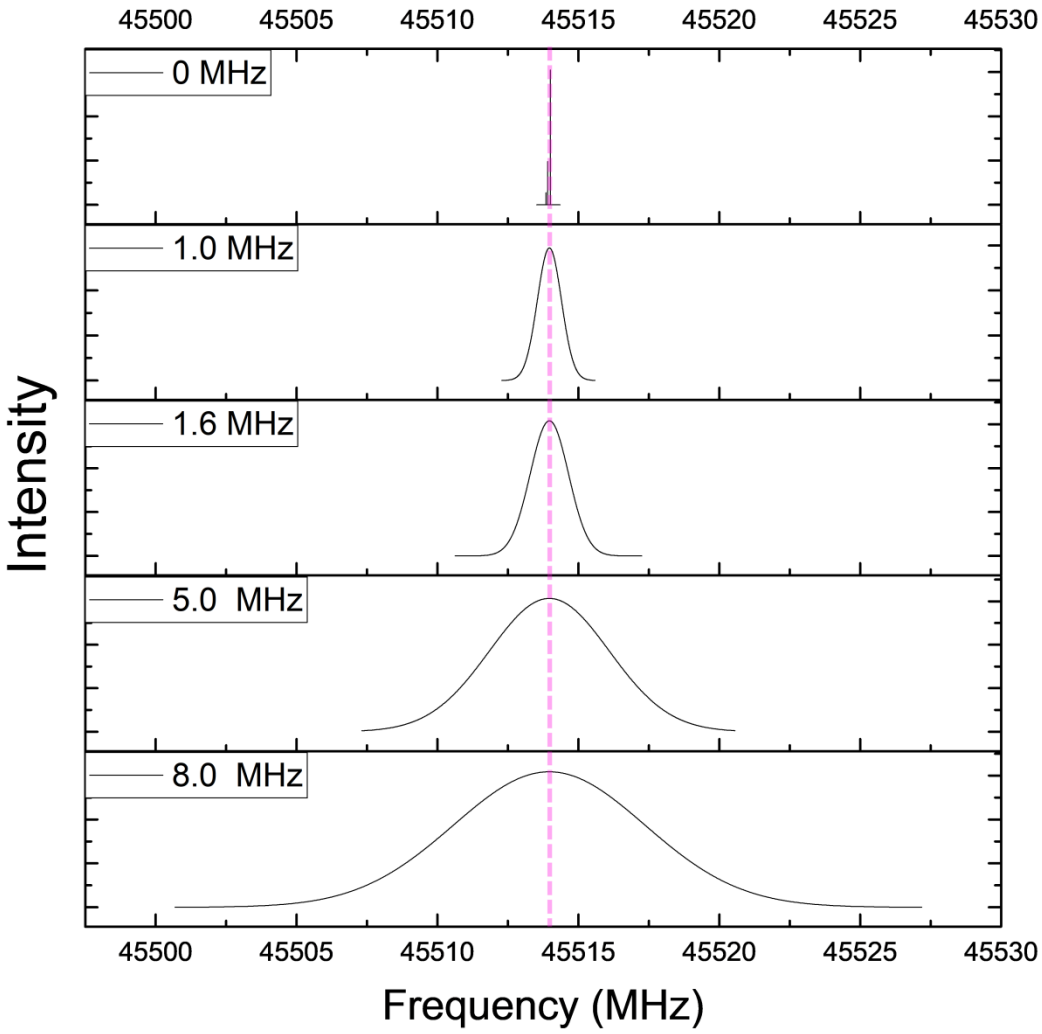

Figure A.2.11 : Resolution comparison in a range from 0 to 8.0 MHz in Pgopher simulations. The frequency range is between 45500 MHz and 45530 MHz The simulated spectra are based on B_0 (5689.2671 MHz), D_J (1178 Hz), and D_{JK} (-2300 Hz) from Pgopher fitting. The rotational temperature is 4 K.

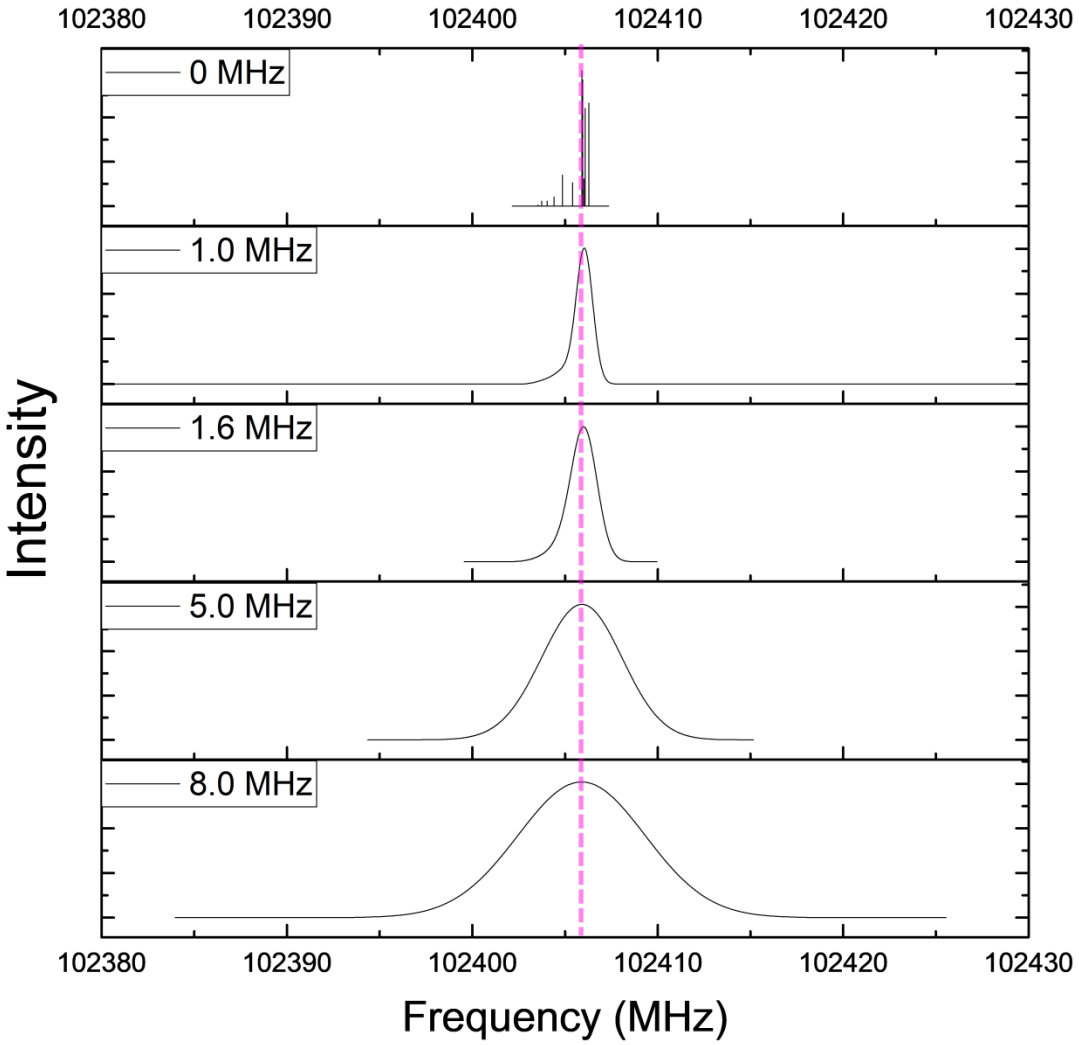

Figure A.2.12 : Resolution comparison in a range from 0 to 8.0 MHz in Pgopher simulations. The frequency range is between 102380 MHz and 102430 MHz. The simulated spectra are based on B_0 (5689.2671 MHz), D_J (1178 Hz), and D_{JK} (-2300 Hz) from Pgopher fitting. The rotational temperature is 4 K

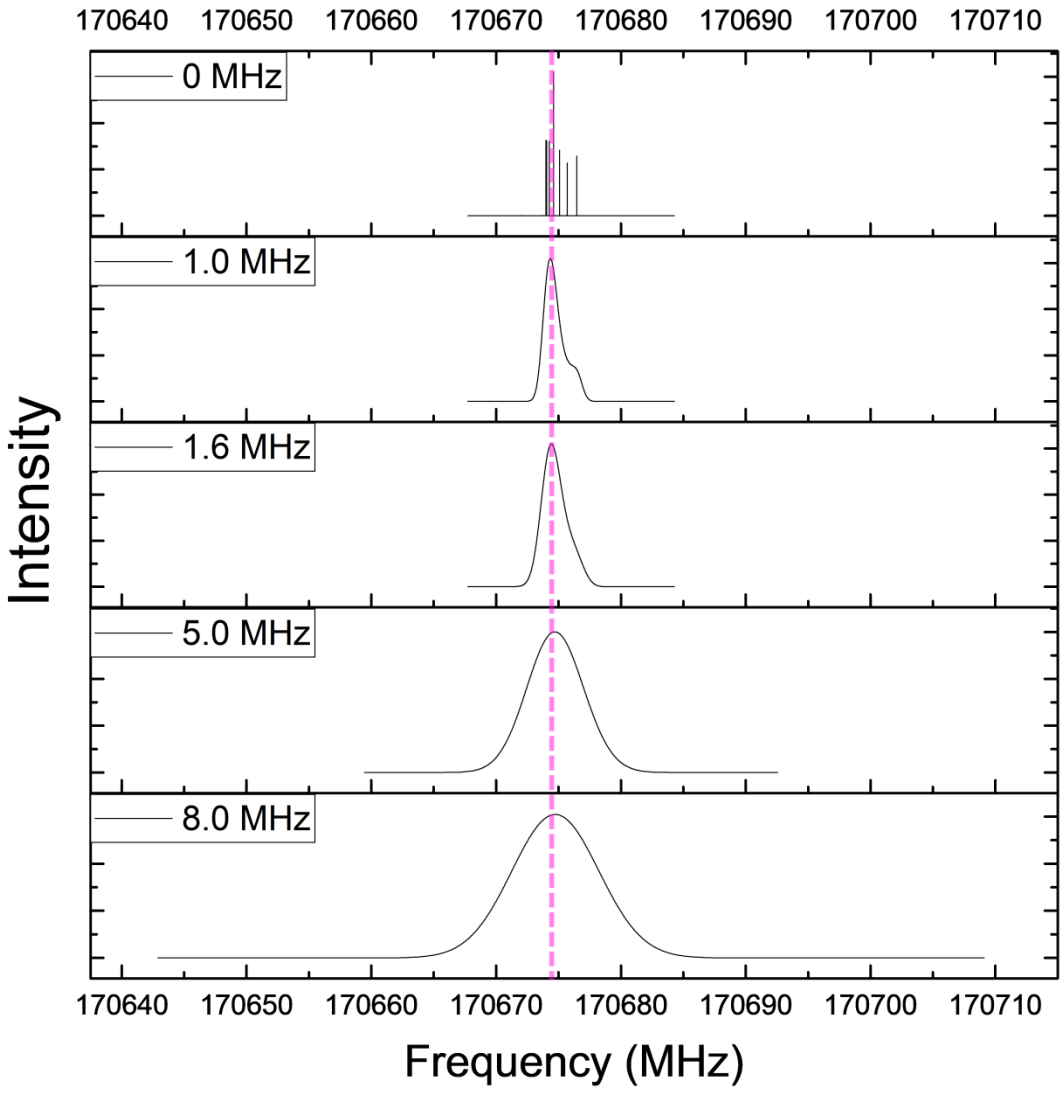

Figure A.2.13 : Resolution comparison in a range from 0 to 8.0 MHz in Pgopher simulations. The frequency range is between 170640 MHz and 170710 MHz. The simulated spectra are based on B_0 (5689.2671 MHz), D_J (1178 Hz), and D_{JK} (-2300 Hz) from Pgopher fitting. The rotational temperature is 4 K

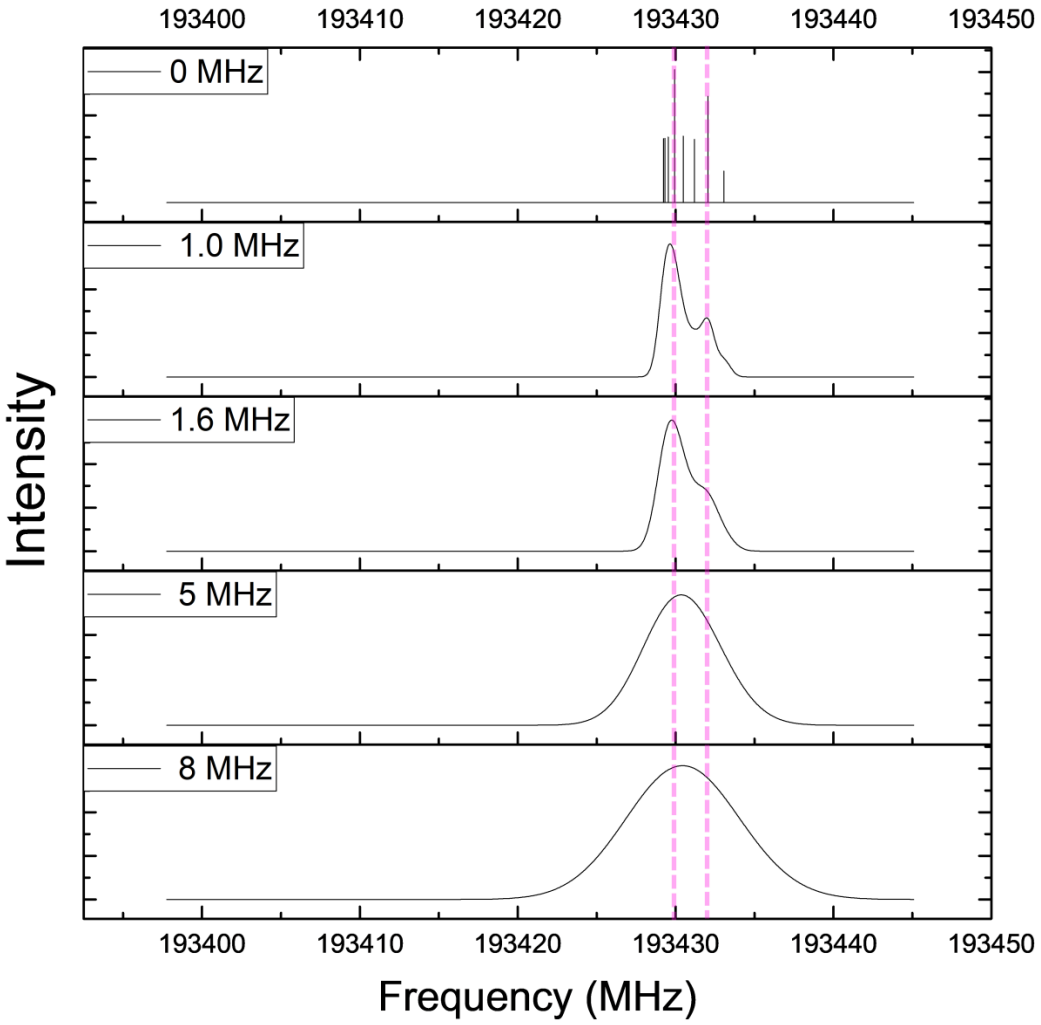

Figure A.2.14 : Resolution comparison in a range from 0 to 8.0 MHz in Pgopher simulations. The frequency range is between 193400 MHz and 193450 MHz. The simulated spectra are based on B_0 (5689.2671 MHz), D_J (1178 Hz), and D_{JK} (-2300 Hz) from Pgopher fitting. The rotational temperature is 4 K

A.3 Different centers and shapes of bands in different temperatures.

The centers and shapes of bands can be different along with different temperature due to Boltzmann distributions

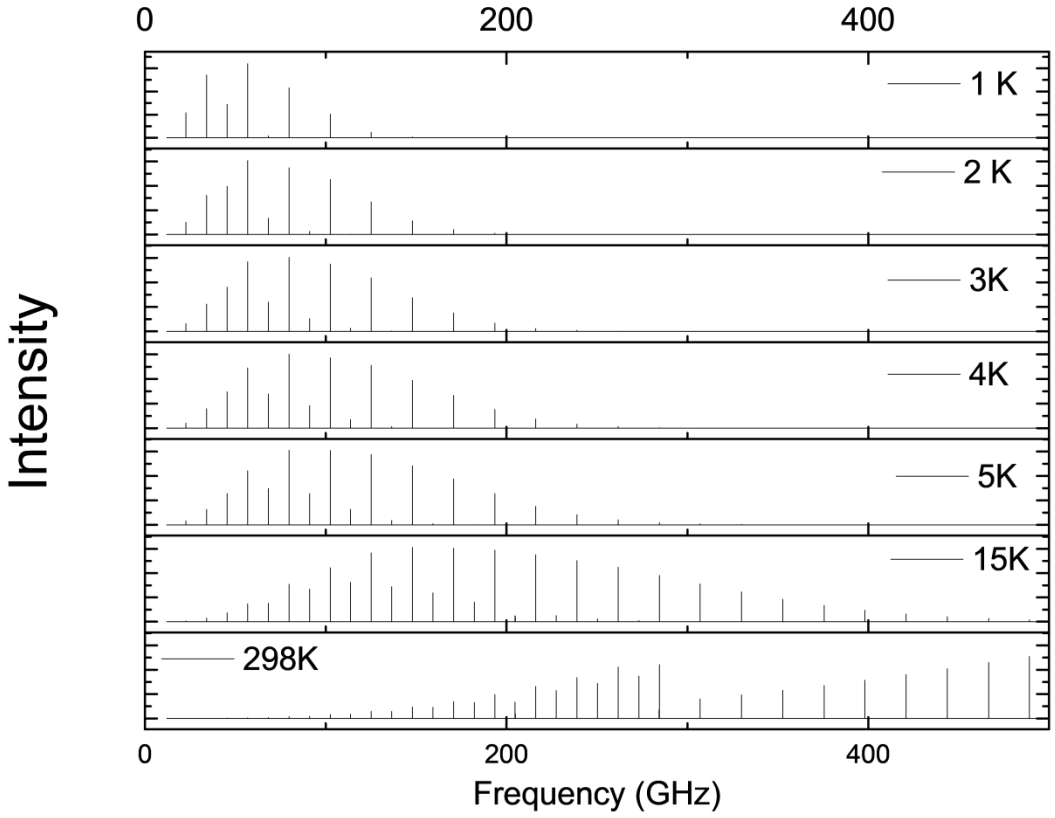

Figure A.3.1 : Pgopher simulated spectra with a different temperature from 1 K to 298 K. a simulated spectrum based on B_0 (5689.2671 MHz), D_J (1178Hz), and D_{JK} (-2300 Hz) from Pgopher fitting.

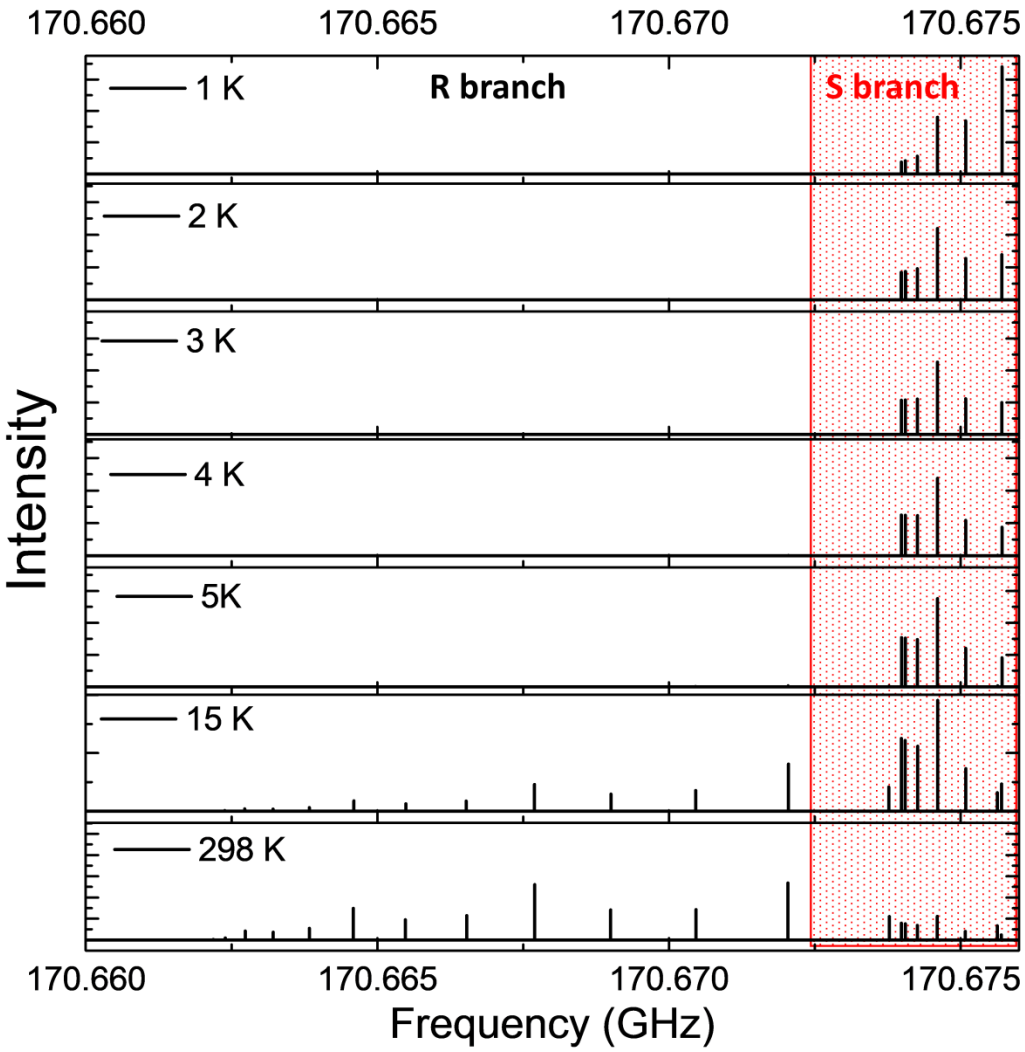

Figure A.3.2 : An enlarged simulated spectrum in a range between 170.660 GHz and 170.675 GHz. The red-shaded area shows lines in S branch. The area without any mark indicates lines in the R branch in the benzene spectra.

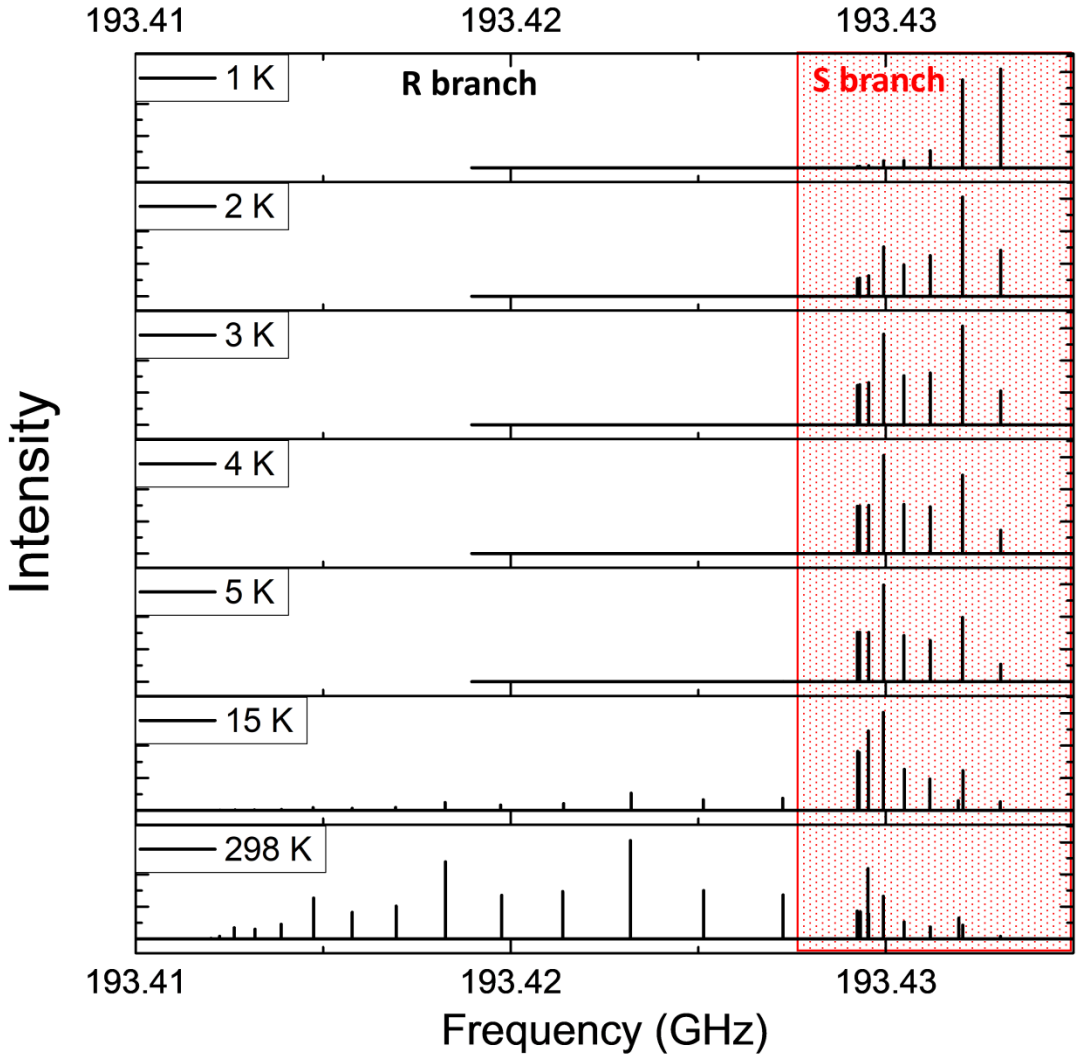

Figure A.3.3 : An enlarged simulated spectrum in a range between 193.41 GHz and 193.435 GHz. The red-shaded area shows lines in S branch. The area without any mark indicates lines in the R branch in the benzene spectra.

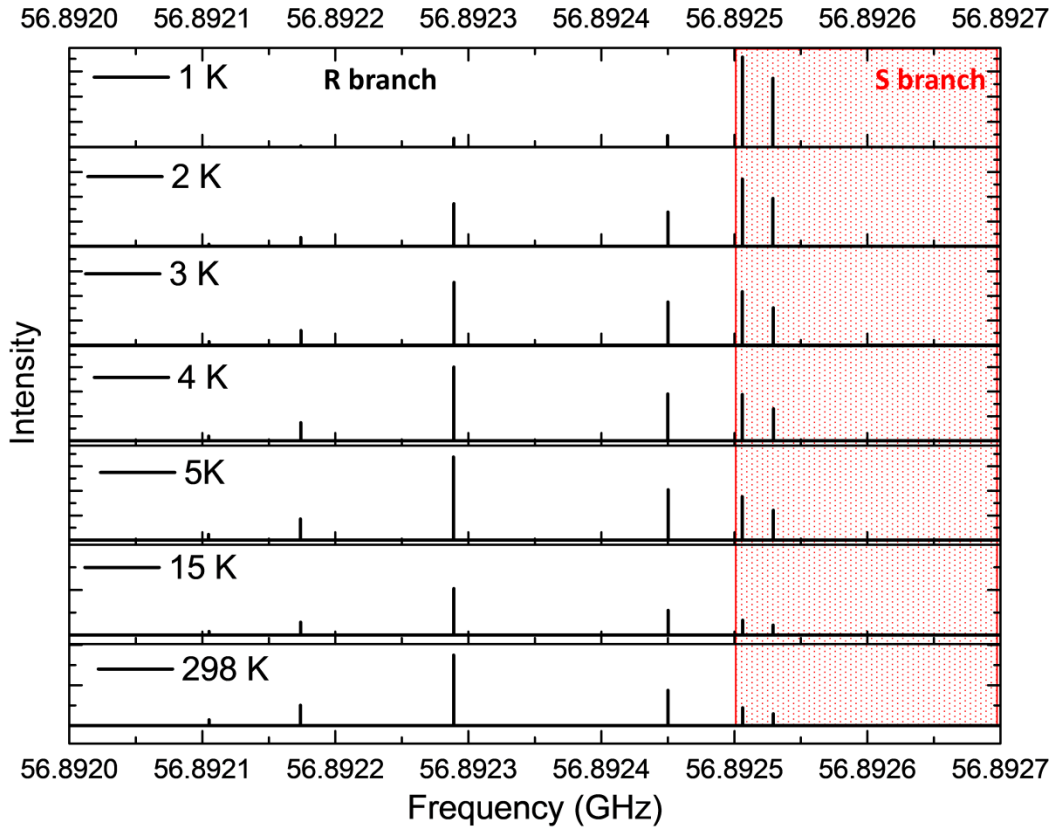

Figure A.3.4 : An enlarged simulated spectrum in a range between 56.8920 GHz and 56.8927 GHz. The red-shaded area shows lines in S branch. The area without any mark indicates lines in the R branch in the benzene spectra.

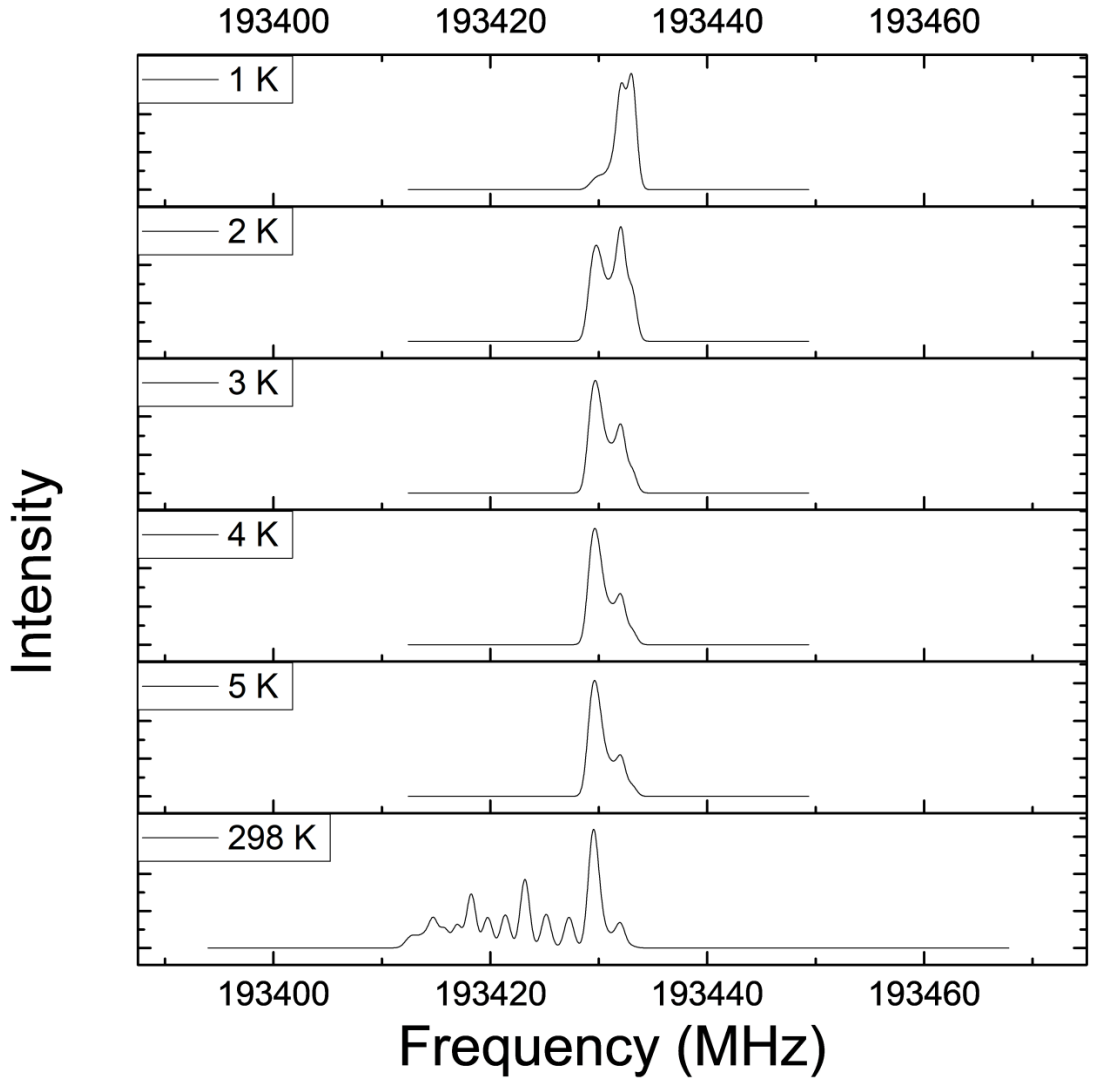

Figure A.3.5 : Calculated 1 MHz resolution bands of pure rotational Raman benzene spectra in a range between 193400 MHz (193.400 GHz) to 193460 MHz (193.460 GHz). The rotational bands have a different shape from each other. The rotational constant of B_0 is 5689.2671 MHz, D_J is 1178 Hz, and D_{JK} = -2300 Hz in the calculated rotational spectra. Pgopher simulations in a range from 193400 MHz to 193460 MHz. The band shapes are different from each other due to Boltzmann distribution on S and R branch as well as individual transitions with different J and K values. The simulated resolution is 1 MHz.

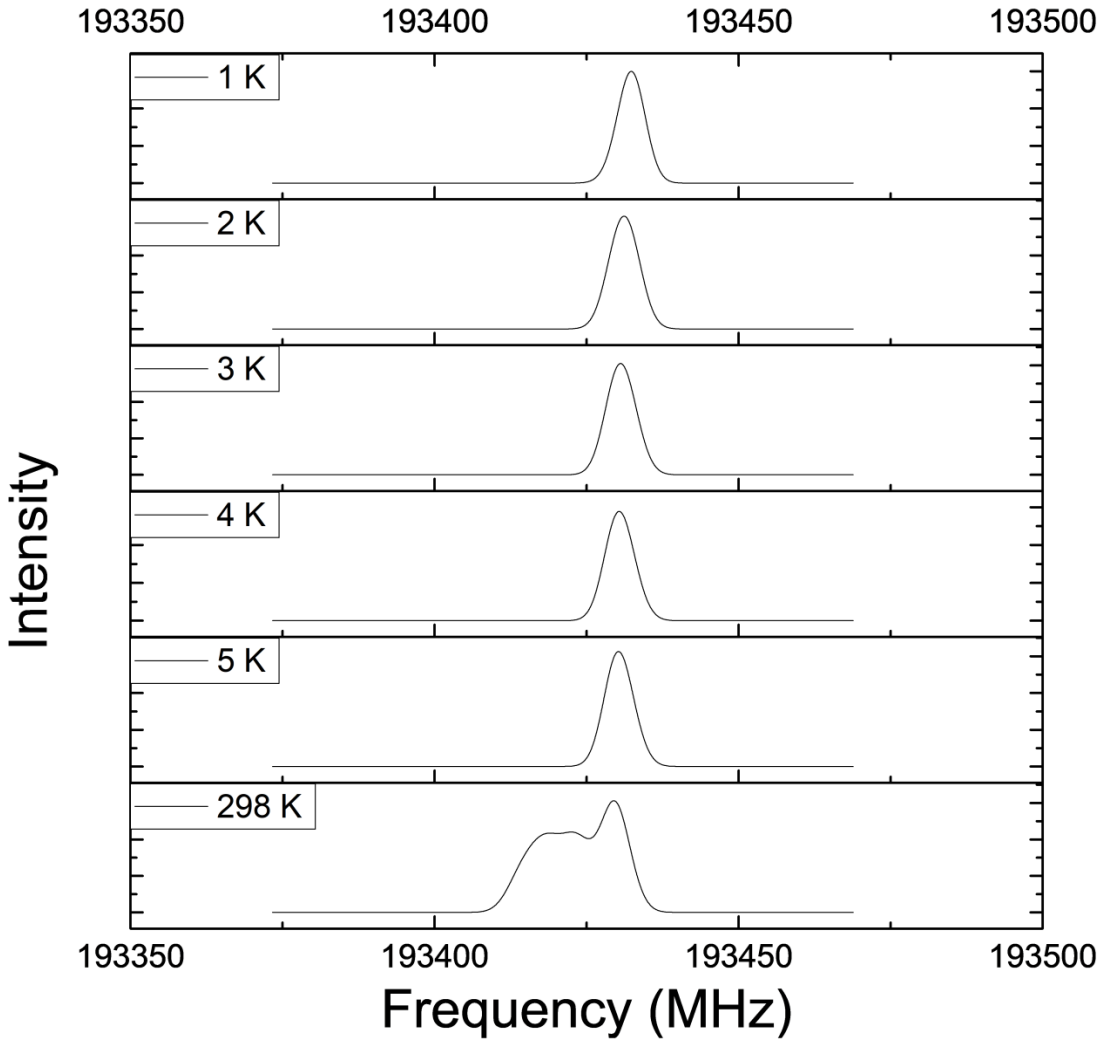

Figure. A.3.6 : Calculated 5 MHz resolution bands of pure rotational Raman benzene spectrum in a range between 193400 MHz (193.400 GHz) to 193450 MHz (193.450 GHz). The rotational bands have a different shape from each other. The rotational constant is 5689.2671 MHz, D_J is 1178 Hz, and D_{JK} = -2300 Hz in the calculated rotational spectra. Pgopher simulations in a range between 193350 MHz to 193500 MHz. The simulated resolution is 5 MHz. A band shape of 1 K, 2 K, 3 K,4 K, and 5 K is like each other, but a center of the bands is different from each other due to different intensities of each transition in the different rotational temperature spectra.

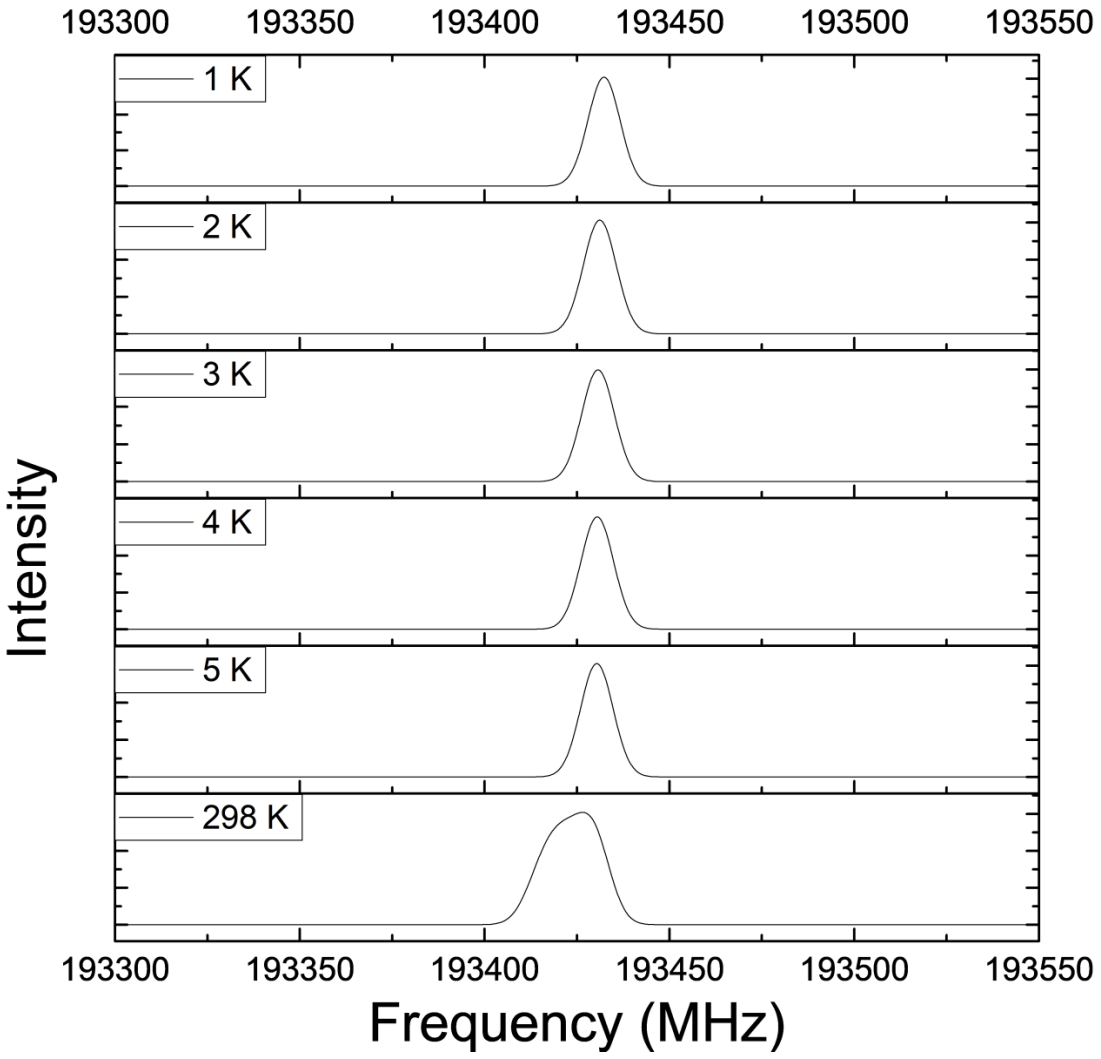

Figure. A.3.7: Calculated 10 MHz resolution bands of pure rotational Raman benzene spectrum in a range between 193400 MHz (193.400 GHz) to 1934500 MHz (193.450 GHz). The rotational bands have a different shape from each other. The rotational constant is 5689.2671 MHz, D_J is 1178 Hz, and D_{JK} = -2300 Hz in the calculated rotational spectra. The simulated rotational spectra in a range between 193300 MHz (193.300 GHz) and 193550 MHz (193.550 GHz). The simulated resolution is 10 MHz. A rotational band of 1 K, 2 K, 3 K, 4 K, and 5 K is like each other, but a center of bands differs from each other. A band of 298 K is broader than other bands as an intensity of lines in R branch is high enough and the lines are merged into one band in 10 MHz resolution.

A.4 Rotational constants and centrifugal distortion constants on oblate top molecules

A.4.1 Relationship between the three rotational constants in oblate top molecules

The three rotational constants A,B, and C for benzene are related to each other as benzene is an oblate top $A = \frac{h^2}{8\pi^2 I_A}$, $B = \frac{h^2}{8\pi^2 I_B}$, and $C = \frac{h^2}{8\pi^2 I_C}$ as the relationship between three momentum of inertia was assumed to be $2\ I_A = 2\ I_B = I_C$ in the benzene . A=B=2C is valid from the assumption.

A.4.2 Selection rules on pure rotational Raman spectrum of symmetric molecules

(1) $E(J,K) = B_0(J+1)J - D_J\,(J(J+1))^2 + (A-B)K^2 - D_K K^4 - D_{JK}J(J+1)K^2$ [42]

There are three centrifugal distortion constants D_J, D_{JK}, and D_K. A molecule distorts because of centrifugal distortion force when it rotates. The selection rules for benzene is two in here as the obtained spectra showed only Stokes bands and lines. One is $\Delta J = 1, \Delta K = 0$ for R branch, and the other is $\Delta J = 2, \Delta K = 0$ for S branch.

(2) $\mathrm{v} = E_{J+1,K} - E_{J,K} = 2B_0(J+1) - 4D_J(J+1)^3 - 4D_{JK}(J+1)K^2$ for R branch ($\Delta \mathrm{J} = 1, \Delta \mathrm{K} = 0$ J,K=0,1,2,3⋯) [42]

(3) $\nu = E_{J+2,K} - E_{J,K} = (4B_0 - 6D_J)(J+\frac{3}{2}) - 4D_{JK}(J+\frac{3}{2})K^2$ for S branch ($\Delta J = 2, \Delta K = 0$ J,K=0,1,2,3⋯) [42]

The rotational constant A and C can be calculated from the value of B and D_K can not be obtained in a pure rotational Raman spectrum of benzene in the ground state. The bands from two branches seem to be overlapped in pure rotational Raman spectra. However, bands are not overlapped but there is a distance between two bands due to centrifugal distortion constants.

A.4.3. Relationship between/among three centrifugal distortion constants D_J, D_{JK}, and D_K

Ideally planar molecules with D_{3h} and D_{6h} symmetry have solid relationships among the three centrifugal distortion constants. These relationships were used to validate the value of obtained centrifugal distortion constants in the planar molecules whose K substructures have not been resolved yet.

(1) $D_{JK} = -\frac{15}{8} D_J = -1.875\, D_J$, and $D_J > 0$ for all oblate top [38]

(2) $2D_J + 3D_{JK} + 4D_K = 0$ [39]

(3) $D_J + D_{JK} + D_K > 0$ [38]

(4) $D_K = \frac{29}{32} D_J$ from (1), (2) [38, 39]

(5) $D_J + D_{JK} + D_K = \frac{1}{32} D_J > 0$ from (1),(2),(3), and (4) [38,39]

A.4.4 Quadratic centrifugal distortion constants in planar molecules with

D_{3h} and D_{6h} symmetry

(1) H_J, H_{JK}, H_{KJ}, and H_K are zero in the D_{3h} and D_{6h} symmetry or higher symmetry in oblate top molecules when the rotational constant A=B=2C in the ground state.

Quadratic centrifugal distortion constants (H_J, H_{JK}, H_{KJ}, and H_K) are determined by internal defects ($\Delta = I_C - I_B - I_A$). These constants of the ground state are zero in the assumption of rotational momentum of inertia for planar molecules ($I_C = I_B + I_A$, and A=B=1/2 C). Therefore, the quadratic centrifugal distortion constants are hardly determined in the assumption. They were not calculated to obtain rotational constants of B and two centrifugal distortion constants of D_J and D_{JK} in the benzene.

A.4.5 Unresolved K structures of oblate top molecules and additional assumptions to determine the rotational constants and centrifugal distortion constants.

It is hard to accurately determine a value of D_{JK} for a pure rotational Raman spectrum of symmetric oblate top molecules even in rovibronic spectroscopic methods. As the two centrifugal distortion constants are small and have an opposite sign to each other. Therefore, a low-resolution spectrum hardly observes split lines due to D_J and D_{JK}. Therefore, previous studies on rotational constants and centrifugal distortion constants of benzene needed additional assumptions to calculate centrifugal distortions in the low-resolution spectra. – (1) The higher intensity is corresponding to a transition of $(J_f = n, K_f = 0) \leftarrow (J_f = n, K_f = 0)$. (2) There are no centrifugal distortion constants at all as the molecules are too rigid. (3) There are no D_{jk} and D_K, but is H_K in oblate top molecules. (4)

Discrepancies between R and S branch can give opportunities to calculate centrifugal distortion constants. (5) There are certain relationships among centrifugal distortions. However, these four assumptions are problematic for oblate top molecules with a high symmetry, and yield discrepancies between literatures.

The researchers did set the highest intensity have a K=0 transition in a given quantum number J [11]. It is only valid in prolate top molecules but inappropriate for oblate top molecules due to the negative centrifugal distortion term. In the symmetric top, there are two models. One is a prolate top, and the other is oblate top. However, properties of prolate tops and oblate top are totally different from each other. If the K components have not been resolved in the rotational spectra, intensity analyses could be helpful for prolate top molecules but not for oblate top molecules. [43] For the prolate top. The intensity of lines of a given J falls when K number increases. Even if K splitting is not observed in a low-resolution spectrum, the position of the maximum intensity is corresponding to K=0 in the given J value. In the other hands, Boltzmann factors and rotational line intensities with a given J values can be high or low. The energy of E(J,K) does not always increase because the terms of D_{JK} ($-4D_{JK}(J+1)K^2\ for\ R\ branch,\ -4D_{JK}(J+3/2)K^2\ for\ S\ branch$) cancel out the terms of D_J ($-6D_J(J+1)\ for\ R\ branch\ -6D_J(J+\frac{3}{2})$ for S branch) degeneracy also affects an intensity of each individual transitions in a certain number of K. Therefore, it is hard to predict exact J, K transitions in the oblate top.

(2) Two centrifugal distortions of D_{JK}, and D_K have been ignored. Some researchers set the centrifugal distortions to be zero in the fitting as a resolution of spectra could no resolve them. They attempted to calculated both D_{JK} and D_K in the oblate top molecules but they gained different sets of rotational constant and centrifugal distortion constants in individual S and R branch. According to Cloppenburg, the unresolved K-splitting made displacements of the S and R branches. The

displacements cause difficulties when we determine the rotational constant centrifugal distortion constants D_J and D_{JK}. However, the difficulties can be theoretically solved with properly estimated values of D_{JK}. [42] However, When we neglect effects of D_{JK} and the K-structures of the given J transitions, the assumption leads to an error in the values of the B and D_J. [33]

(3) The quadratic terms of centrifugal distortion constants, H_J, H_{JK}, H_{KJ}, and H_K hardly contribute to an intensity and a position of bands in pure rotational Raman spectra in the ground state. For pure rotational Raman spectra in the cold temperature, there are a few bands, and it is not enough to resolve D_{JK}. One of quadratic term can be plugged into energy equations in order to explain discrepancy between S and R branch in a low-resolution spectrum due to possible effects of line shifts from unresolved K structure. They did set the constants D_{JK}, H_{JK}, and H_{KJ} equal to zero as the K-structure of the Raman transition of s-tetrazine was not resolved and bands seem to be symmetric enough to ignore them. [51] However, according to Aliev [38] and Dowling [39], the term of D_{JK} can not be ignored in the pure rotational Raman spectra for planar molecules with D_{3h} and D_{6h} molecules.

(4) The differences between R and S branch have been discussed in not only pure rotational Raman spectra but also rovibronic spectra and rotationally resolved spectra for molecular structure investigations. [51] [52]

(5) There are certain relationships among three distortion constants in section. Relationship between three centrifugal distortion constants $D_J, D_{JK},$ and D_K. These theoretical relationships were used to check determined constants in the experimental spectra and compare them with distortion constants of literature. The relationships between the centrifugal distortion constants would manage to validate their values of obtained D_J and D_{JK} in low resolution spectra with the unresolved K structure, but not assign the transition lines. Hence, the relationships do not give by themselves a single exact value

of rotational constant, and centrifugal distortion constants in the low-resolution spectrum.

Unresolved K structures irritate researchers when they investigate molecular structures with a planar structure and their harmonicity with a low-resolution rotational spectra or rotationally resolved rovibronic spectra. Owing to unresolved K structures in the oblate top, a lot of assumptions and calculation methods have been applied. Even if there were reasonable assumptions in assignment of bands and lines of rotational spectra or rotationally resolved spectra for benzene, these different assumptions merely showed numerical discrepancies of the rotational constant and centrifugal distortion constants. [33]

A.5 . Cold pure rotational Raman spectra

A temperature of rotational spectra with unresolved K substructures could be determined by an envelope of a rotational spectrum, however, the spectrum temperature would have effects on an intensity of individual transition lines. Therefore, the center of a band as a set of unresolved transition lines would different when the temperature of the spectrum changed. As a result, inappropriate temperature estimation would cause wrong band assignment to determine wrong rotational constants and centrifugal distortion constants in the unresolved pure rotational Raman spectra of non-equilibrium state benzene.

The non-equilibrium state molecules cause a non-Boltzmann distribution to difficult temperature interpretation and other factors. For medium size molecule including benzene, the colder temperature supersonic jet experiment (From 1 K to 15 K) can obtain even simpler pure rotational spectra of benzene in the ground state than the hotter temperature. [53] For reducing analysis cost and properly assigning bands, the colder spectra were preferred. However, The coupling of rotational and

translational level of simple molecules would occur below 1 K [49] The extremely low rotational temperature (< 1 K) can cause coupling between rotational and translational degree of freedoms to non-equilibrium states. Molecular collision of supersonic jet also contributes to the non-equilibrium states.

Appendix. B Fragmentation and fragments rotational spectrum

As fragments were generated in the ionic state after the rotational wave packet was probed by the ionization pulse, the rotational spectra of molecular fragments are corresponding to their parental molecule. Therefore, the rotational spectrum and constants of the fragments were emanated from their own parental molecules. Mass-CRASY can keep tracking molecular fragmentation pathway with comparing rotational spectra of parental molecules to rotational spectrum of fragments.

B.1 Rotational constants of fragments and parental molecules in uncalibrated mass-correlated frequency domain spectrum

Fig.B.1.1 is mass spectrum obtained in uncalibrated frequency domain rotational spectra in 16 ns continuous measurement. There are 32 u, 34 u, 44 u, 46 u, 52 u, 76 u, 77 u, 78 u, 79 u, and 80 u mass peak. Their rotational spectrum was obtained at the same time. Fig.B.1.1, B1.2,B1.3, B.1.4,B.1.5,B.1.6,B.1.7,B.1.8,B.1.9,B.1.10,and B.1.11 are mass-correlated pure rotational Raman spectrum. The frequency domain spectra were not calibrated. The rotational spectra were plotted to compare their parental spectrum or fragment spectra rather than obtain a highly accurate rotational constant and centrifugal distortion constants in the ground state. The obtained rotational constants and centrifugal distortion constant in the ground state were from transition bands in the ground state. The transition bands were marked in fig B.1.1, B.1.2, B.1.3, B.1.4, B.1.5, B.1.6, B.1.7, B.1.8, B.1.9, B.1.10, B.1.11, B.1.12, and B.1.13. Fig.B.1.11, Fig.B.1.12, and Fig.B.1.13 shows paired rotational spectrum of parental molecules and their fragments. The rotational constants were fitted by Pgopher. Centrifugal distortion constant in literatures were used and fixed to fit the rotational constants in the fitting program. The used literature values are tabulated in table 5. The rotational constants were not

obtained in calibrated spectrum, and their value is far from literature values. Rotational spectra of fragments have low a signal to noise ratio than rotational spectra of their parental molecules. For the determination of rotational constant and centrifugal distortion constants, the literature values were used. Table B.1.1,B.1.2, B.1.3, and B.1.4 showed that literature values of Junttila et al. [13] were used to fit the rotational constant of benzene , as well as, literature values of rotational constants carbon disulfide isotopologues were used.

Fig. B.1.2 shows a mass-correlated rotational spectrum of 32S of a fragment from main carbon disulfide isotope in the frequency domain, the rotational spectrum of 32S12C32S, 32S13C32S, and 34S12C32S could have been observed in the rotational spectrum of 32S. However, Fig.B.1.11 shows that the rotational spectrum of the fragment of 32 u is corresponding to 32S12C32S. The rotational constant of 32 u is 3272.303 MHz, which is like the rotational constant of 76 u (5272.2910(61) MHz). Fig. B.1.3 shows a mass-correlated rotational spectrum of 34S of a fragment of rare isotopomers of CS2. The rotational spectrum of 34S12C34S, 34S12C32S could have been observed in the 34 u spectrum. Fig.B.1.12 shows rotational spectrum of 34 u is identical to the rotational spectrum of 34S12C32S in 78 u. The rotational constant of the 34 u spectrum is 3175.746(43) MHz, which is like the rotational constant of 32S12C34S (5175.611(42) MHz)

Fig B.1.4 represents a mass-correlated rotational spectrum of 44 u, which is a mass of a fragment of 32S12C32S. Fig B.1.11 shows the rotational spectrum of 44 u is responded to 32S12C32S. The mass fragment of 44 u originated from the main isotope of carbon disulfide. The rotational constant of 44 u is 3272.2935(94) MHz, which is similar to the rotational constant of CS2 at 76 u (3272.2910(61) MHz).

Fig.B.1.5. Represent a mass-correlated rotational spectrum of 46u, which is one of mass fragments from 32S12C34S. Fig B.1.12 shows the rotational spectrum of 46 u is corresponding to the rotational

spectrum of the carbon disulfide isotopomer in 78 u. The rotational constant of 46 u is 3175.819(75) MHz, which is like the rotational constant of 32S12C34S (3175.611(42) MHz). Fig.B.1.6 indicates a benzene fragment rotational spectrum in 52 u. The fragment mass is corresponding to C4H4. Fig B.1.13 shows that a position of rotational bands in 52 u is corresponding bands in 78 u. The rotational constant of benzene fragment is 5690.432(27) MHz, which is similar to its parental molecule. (5690.433(15) MHz).

Fig B.1.7 describes the main isotope of carbon disulfide at 76 u. The rotational constant is 3272.2910(61) MHz, which is obtained in the uncalibrated rotational spectrum as the measurement was performed without any external calibration during the experiment. The rotational constant of 76 u is far from other literature values and the rotational constants obtained in CRASY spectra with the external GPS calibration.

Fig.B.1.8 shows that there are two isotopes of carbon disulfide at 77 u. One is 32S13S32S. The other is 33S12C32S. The rotational constant of 32S13C32S is 3272.368(19) MHz the rotational constant of 33S12S32S is 3222.510(28) MHz. The rotational constant.

Fig. B.1.9 shows that there are two different molecules in 78 u. It describes the rotational spectrum of benzene at 78 u and 32S12S34S. The rotational constant of benzene is 5690.433(15) MHz the rotational constant of the CS2 isotopomer is 3175.611(42) MHz. Fig.19 shows one of carbon disulfide isotopologues in 80 u. it represents a rotational spectrum of 34S12c34S. The rotational constant of 34S12C34S is 3080.167(54) MHz

B.2 Rotational constant of benzene, CS2 and fragments of benzene in 8 MHz resolution spectrum

Fig. B.2.1 shows the mass-correlated spectra for benzene, benzene fragment and carbon disulfide from 8 MHz resolution spectrum measured over the 100 ns randomly sparse sampling measurement. The three rotational spectra including benzene, benzene fragment, and CS2 seems to have same band positions. However, lines in the spectrum of benzene fragment are respectively corresponding to these of benzene. However, lines in the CS2 spectrum are out of joint in lines in the benzene spectrum at 78 u. The mass-correlated rotational constant of CS_2 at 76 u is 3271.517(11), as well as, a distortion constant is 338(29). As carbon disulfide is a linear molecule, there is no D_{JK} due to absence of another molecular axis of K axis. We resolved the rotational spectrum of a fragment of benzene. As the rotational constant of 52 u (C_4H_4), The ground state rotational constant is 5689.322(63) MHz and distortion constant $D_J$is 1660(400) Hz. D_{JK} is -2100(610) Hz. The rotational constant of benzene in the spectrum is 5689.302(14) MHz, and the centrifugal distortion constant of D_J is 1604(62) Hz. The literature value of D_{JK} (-2059.1[13]) was fixed in fitting the constants. .

B.3 Rotational constant of benzene, CS2 and fragments of benzene of the single MHz resolution spectrum

Fig.B.3.1 shows the mass correlated spectra of benzene, CS2 and a fragment of CS2 from the single MHz resolution spectrum measured over the 1 μs random sparse sampling with the external GPS calibration. The rotational constant of benzene in the spectrum is 5689.2671(52) MHz, D_J is 1178(50) Hz, and D_{JK} is -2300 (120) Hz. 7 transition lines were resolved in the carbon disulfide

rotational Raman spectrum in Fig. 24. The rotational constant of CS_2 is 3271.51789(98) MHz when the literature centrifugal distortion constant of 359.72 Hz [32] was fixed in the fitting program. The rotational constant of a fragment at 44 u is one of fragments emanated from the main isotope of carbon disulfide. 4 transition lines were resolved in the fragment rotational Raman spectrum in Fig. B.3.1. The rotational constant of the fragment is 3271.5210(31) MHz and the centrifugal distortion constant of 359.72 Hz was used to determine the rotational constant for fragment.

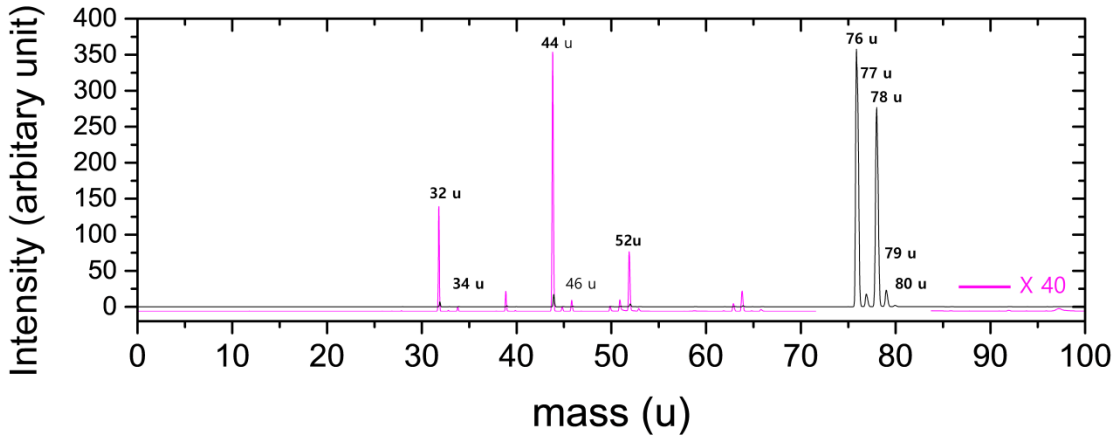

Figure B.1.1 : The mass spectrum was obtained in the uncalibrated frequency domain rotational spectra in 16 ns continuous measurement

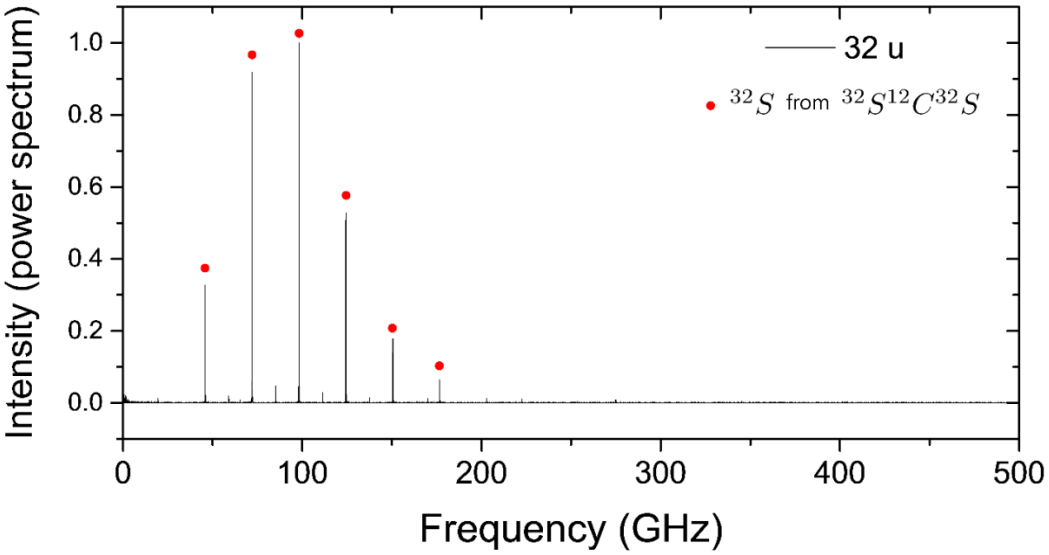

Figure B.1.2 : Rotational spectrum of 32S of a fragment from 32S12C32S in the frequency domain. The frequency domain was not calibrated. Red dots indicate transition lines of 32S, which is a fragment of 32S12C32S and 32S12C.

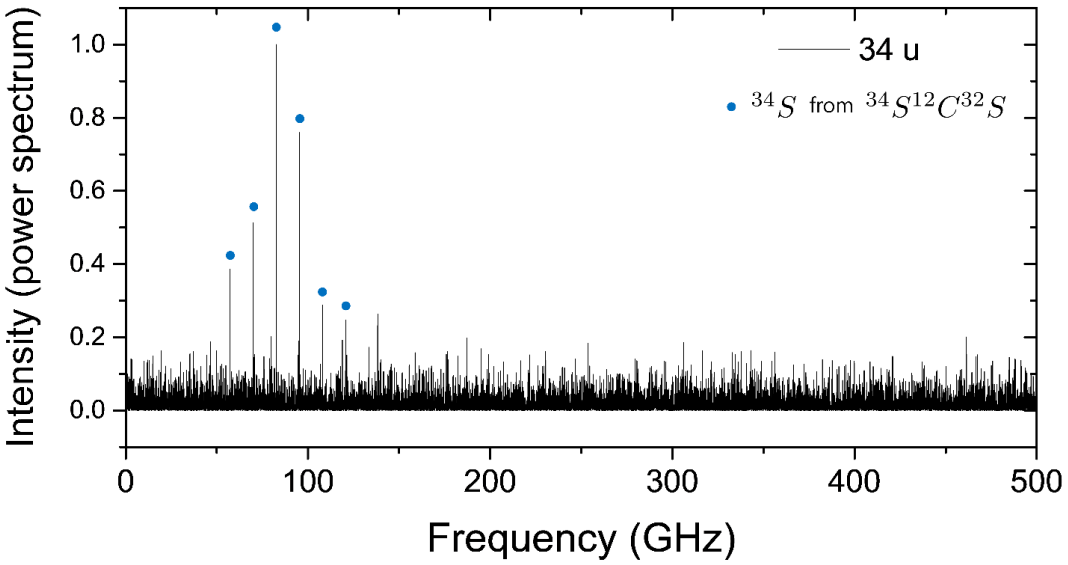

Figure B.1.3 : Rotational spectrum of 34S of a fragment from 34S12C32S in the frequency domain. The frequency domain was not calibrated. Blue dots indicate transition lines of 34S, which is fragment of 34S12C32S and 34S12C.

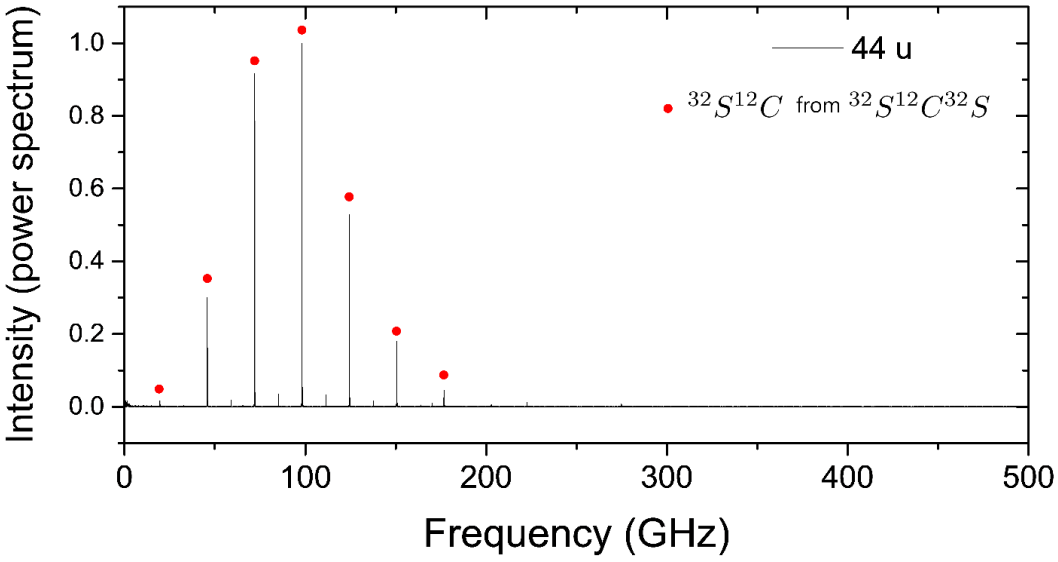

Figure B.1.4 : Rotational spectrum of 32S12C from 32S12C32S in the frequency domain. The frequency domain was not calibrated. Red dots indicate transition lines of 32S12C, which is a fragment of 32S12C32S.

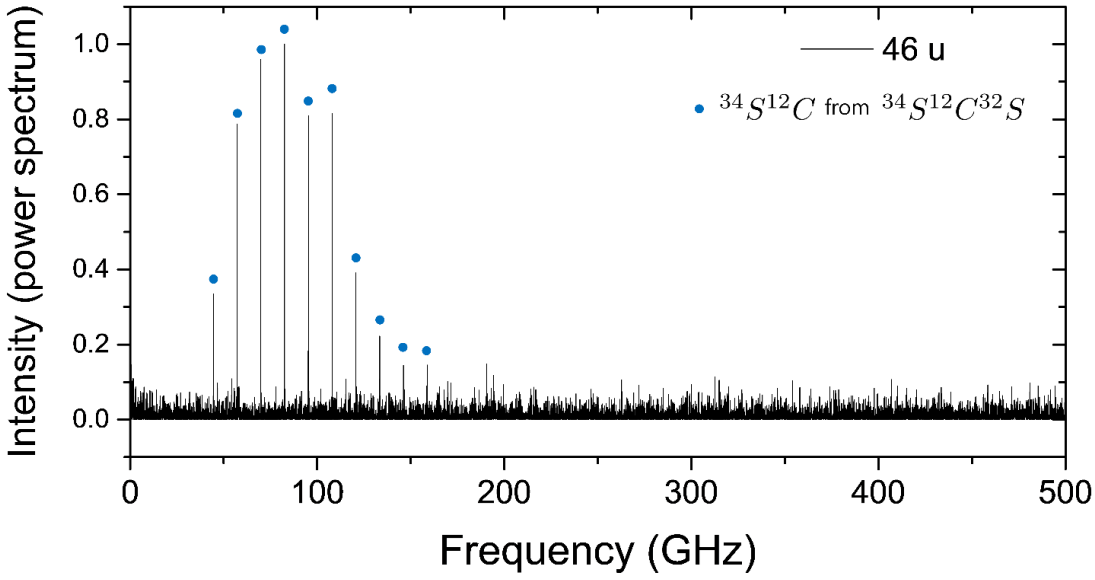

Figure B.1.5 : Rotational spectrum of 34S12C from 34S12C32S in the frequency domain. The frequency domain was not calibrated. Blue dots indicate transition lines of 34S12C, which is a fragment of 3S12C34S.

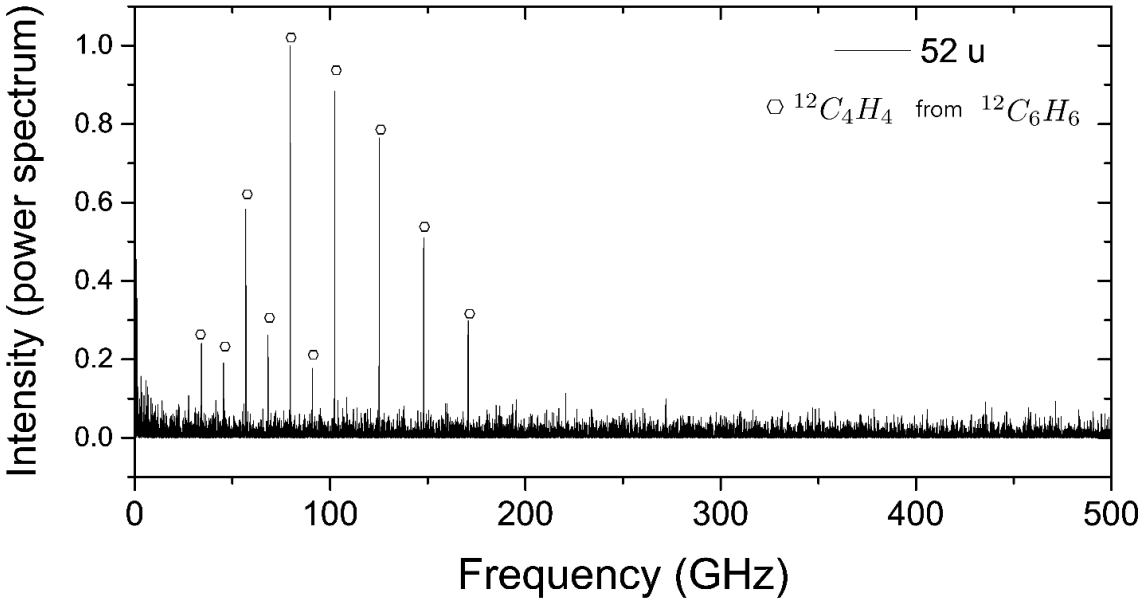

Figure B.1.6 : Rotational spectrum of C4H4 from C6H6 (benzene) in the frequency domain. The frequency domain was not calibrated. White hexagons indicate transition bands of the fragment of benzene in 52 u.

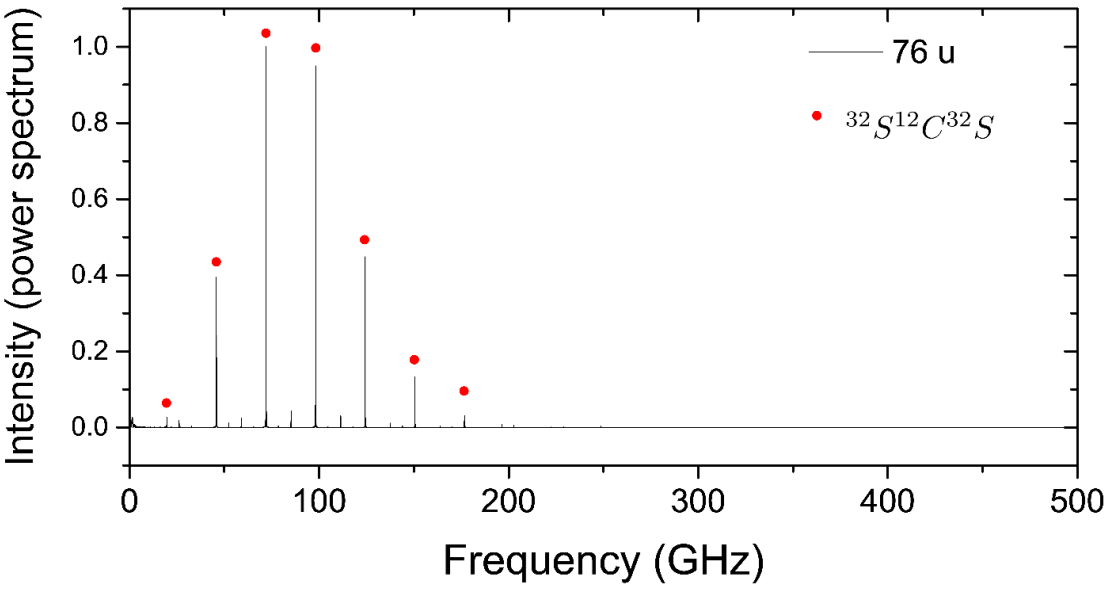

Figure B.1.7 : Rotational spectrum of 32S12C32S (main carbon disulfide isotope) in the frequency domain. The frequency domain was not calibrated. Red dots indicate transition lines of 32S12C32S.

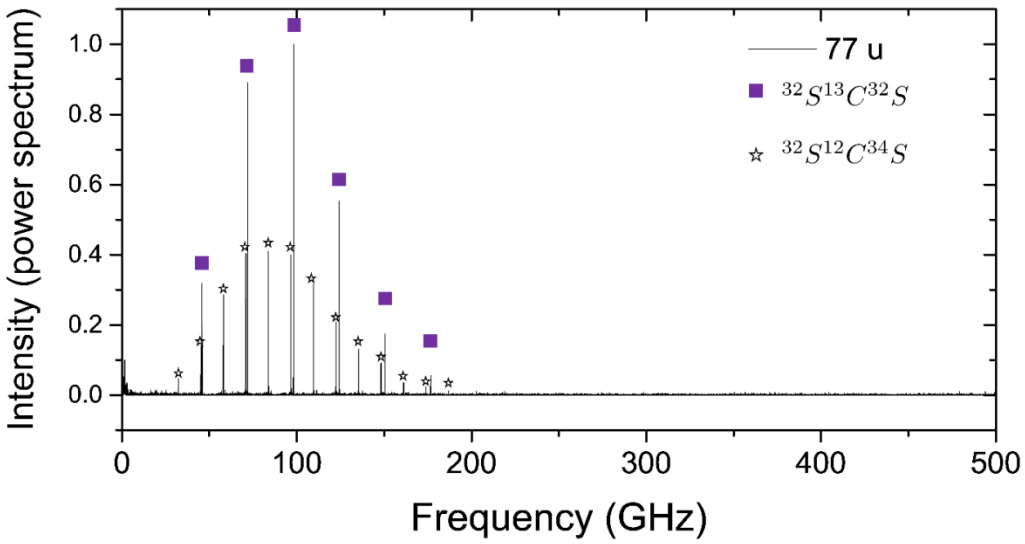

Figure B.1.8 : Rotational spectrum of 32S13C32S and 33S12C32S in the frequency domain. The frequency domain was not calibrated. Purple dots indicate transition lines of 32S13C32S in 77 u. White starts indicate transition lines of 32S12C33S in 77 u.

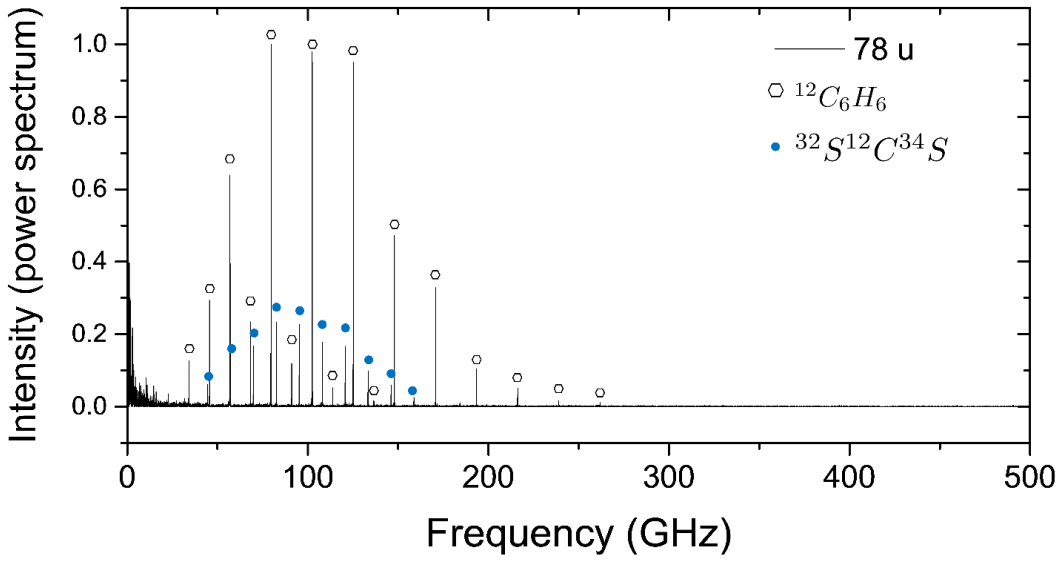

Figure B.1.9 : Rotational spectrum of C6H6 (benzene) and 34S12C32S in the frequency domain. The frequency domain was not calibrated. Blue dots indicate rotational transition lines of 32S12C34S. White hexagons indicate rotational transition bands of benzene in 78 u.

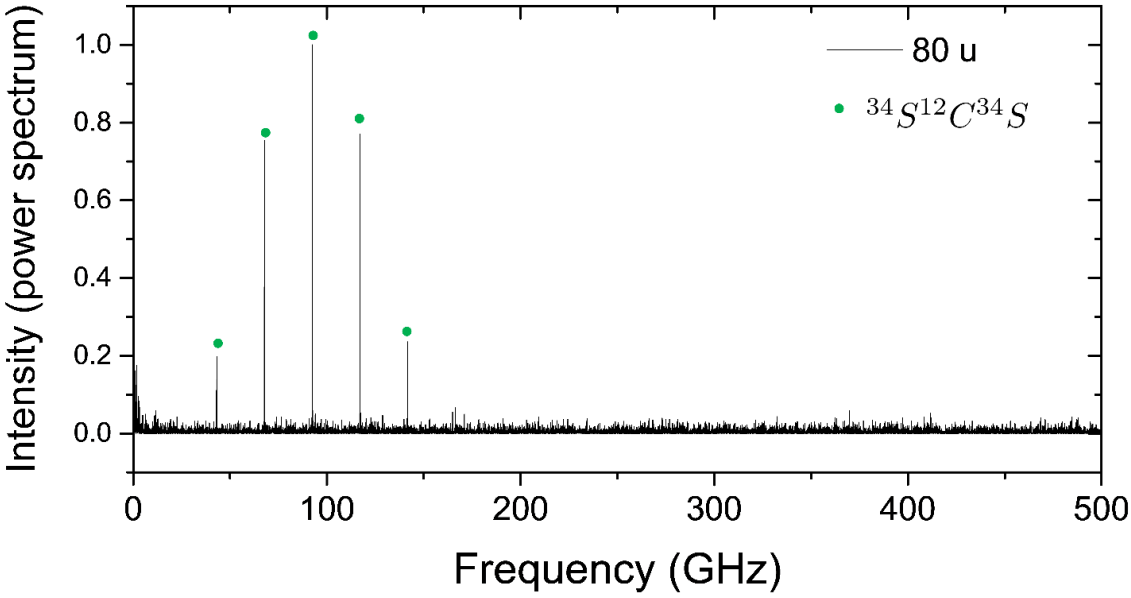

Figure B.1.10 : Rotational spectrum of 34S12C34S in the frequency domain. The frequency domain was not calibrated. Green dots indicate the rotational transition lines of 34S12C34S.

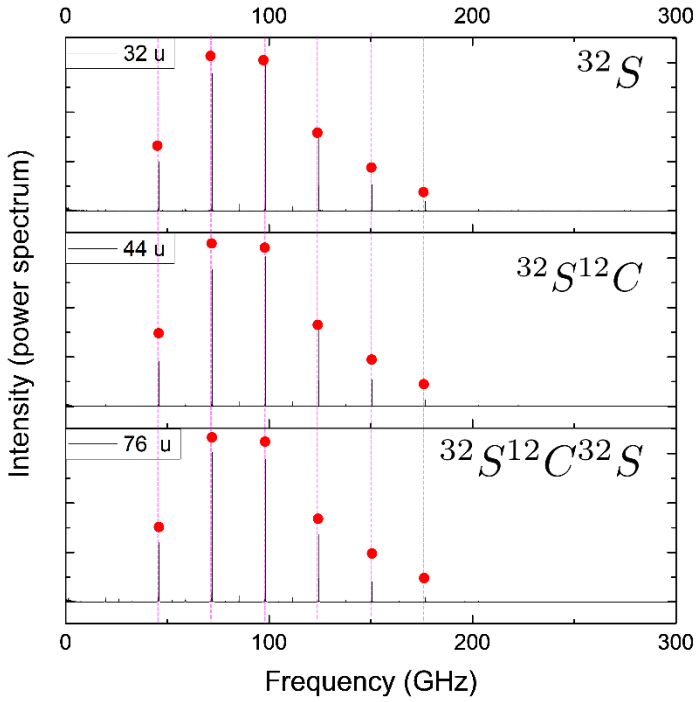

Figure B.1.11: Rotational spectrum of fragments of 32S12C32S and 32S12C32S in the frequency domain. The frequency domain was not calibrated. Top is the rotational spectrum of 32 S. Middle is the rotational spectrum of 32S12C. Bottom is the rotational spectrum of parental molecule (main isotope of carbon disulfide)

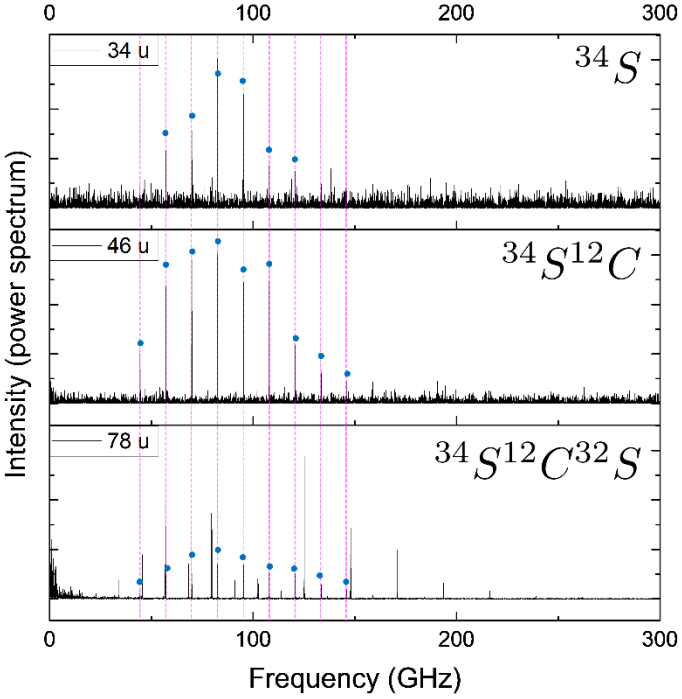

Figure B.1.12 : Rotational spectrum of fragments of 34S12C32S and 32S12C32S in the frequency domain. The frequency domain was not calibrated. Top is the rotational spectrum of 34 S. Middle is the rotational spectrum of 34S12C. Bottom is the rotational spectrum of parental molecule of 34S12C32S

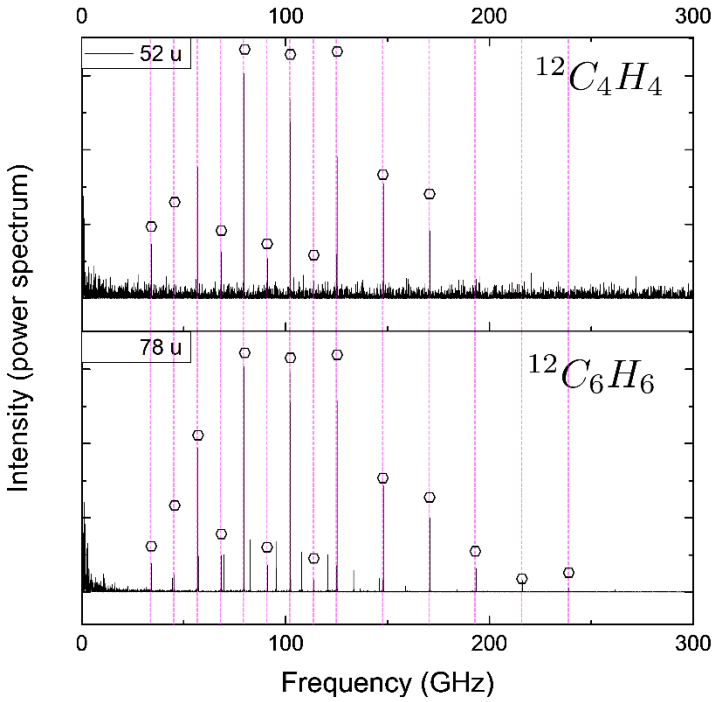

Figure B.1.13 : Rotational spectrum main isotope of benzene and the fragment in the frequency domain. The frequency domain was not calibrated. Top is the rotational spectrum of C4H4. Bottom is the rotational spectrum of parental molecule of benzene.

Mass	Molecule	Rotational constant	Distortion constant	Parental molecule
32 u	32S	3272.303(13) MHz^a	D = 352.79 Hz^b	32S12C32S
34 u	34S	3175.746(43) MHz^a	D = 332.6 Hz^c	32S12C34S
44 u	32S12C	3272.2935(94) MHz^a	D = 352.79 Hz^b	32S12C32S
46 u	34S12C	3175.819(75) MHz^a	D = 332.6 Hz^c	32S12C34S
52 u	C_4H_4	5690.432(27) MHz^a	D_J =1242.8 Hz^d D_{JK} = -2059.1 Hz^d	C_6H_6
76 u	32S12C32S	3272.2910(61) MHz^a	D = 352.79 Hz^b	Parental molecule
77 u	32S13C32S	3272.368(19) MHz^a	D = 350.76 Hz^c	Parental molecule
77 u	33S12C32S	3222.510(28) MHz^a	D = 341.3 Hz^e	Parental molecule
78 u	32S12C34S	3175.611(42) MHz^a	D =332.6 Hz^c	Parental molecule
78 u	C_6H_6	5690.433(15) MHz^a	D_J =1242.8 Hz^d D_{JK} = -2059.1 Hz^d	Parental molecule
80 u	34S12C34S	3080.167(54) MHz^a	D = 312 Hz^f	Parental molecule

Table B.1.1 : Rotational constant of fragments of carbon disulfide isotopomers and benzene. The rotational constants were obtained in uncalibrated frequency domain rotational spectra in 16 ns continuous measurement. (a) : Single sigma uncertainty (b) : Anhonen et al. [32] (c) Winther et al. [54] (d) Juntilla et al.[13] (e) : Horneman et al. [55] (f) : Cheng et al.[56]

Mass	Molecule	Rotational constant	Distortion constant	Parental molecule
32 u	32S	3272.303(13) MHz^a	D = 352.79 Hz^b	32S12C32S
44 u	32S12C	3272.2935(94) MHz^a	D = 352.79 Hz^b	32S12C32S
76 u	32S12C32S	3272.2910(61) MHz^a	D = 352.79 Hz^b	Parental molecule

Table B.1.2 : Rotational constant of fragments of carbon disulfide isotopomers and benzene. The rotational constants were obtained in uncalibrated frequency domain rotational spectra in 16 ns continuous measurement. (a) : Single sigma uncertainty (b) : Anhonen et al. [32]

Mass	Molecule	Rotational constant	Distortion constant	Parental molecule
34 u	34S	3175.746(43) MHz^a	D = 332.6 Hz^b	32S12C34S
46 u	34S12C	3175.819(75) MHz^a	D = 332.6 Hz^b	32S12C34S
78 u	32S12C34S	3175.611(42) MHz^a	D =332.6 Hz^b	Parental molecule

Table B.1.3 : Rotational constant of fragments of carbon disulfide isotopomers and benzene. The rotational constants were obtained in uncalibrated frequency domain rotational spectra in 16 ns continuous measurement. (a) : Single sigma uncertainty (b) Winther et al. [54]

Mass	Molecule	Rotational constant	Distortion constant	Parental molecule
52 u	C_4H_4	5690.432(27) MHz^a	D_J =1242.8 Hz^b D_{JK} = -2059.1 Hz^b	C_6H_6
78 u	C_6H_6	5690.433(15) MHz^a	D_J =1242.8 Hz^b D_{JK} = -2059.1 Hz^b	Parental molecule

Table B.1.4 : Rotational constant of fragments of carbon disulfide isotopomers and benzene. The rotational constants were obtained in uncalibrated frequency domain rotational spectra in 16 ns continuous measurement. (a) : Single sigma uncertainty (b) Juntilla et al.[13]

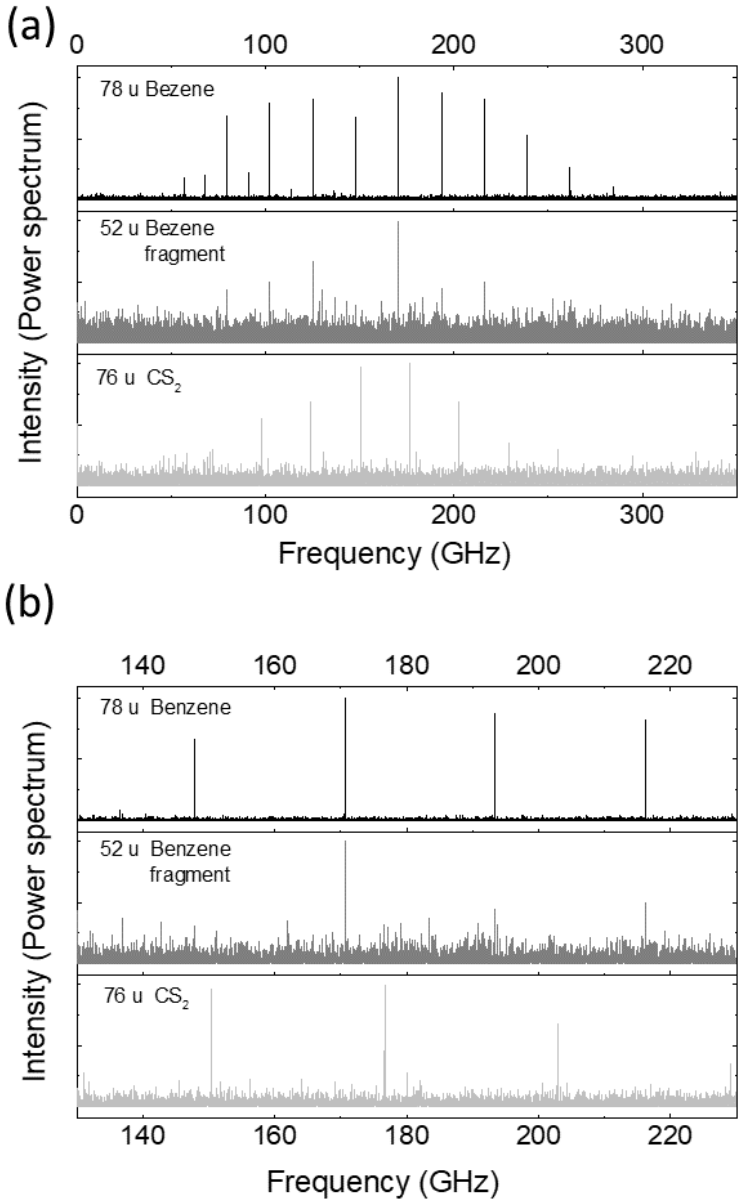

Figure B.2.1 : Three rotational spectra, rotational spectrum of mass 52 u (One of fragments from Benzene) , 76 u (Main isotoplogue of carbon disulfide) and 78 u (Benzene (12C6H6)) spectrum . These 8 MHz resolution spectra were obtained by measurement of random sparse sampling over 100 ns time delay with GPS calibration (a) : 500 GHz range of 12C32S2, the fragment of benzene 12C4H4, benzene(12C6H6). (b) : The enlarged rotational spectra in the range between 130 to 230 GHz. The order of assigned spectrum is identical in (a) and (b). The rotational spectra were from 100 ns random sparse sampling measurement.

Mass	Molecule	Rotational constant	Distortion constant	Parental molecule
52 u	C_4H_4	5689.322(63) MHz^a	D_J = 1660(400) Hz^a D_{JK} = -2059.1 Hz^b	C_6H_6
76 u	32S12C32S	3271.517(11),	D = 338(29) Hz^a	Parental molecule
78 u	C_6H_6	5689.302(14)) MHz^a	D_J = 1604(62) Hz^a D_{JK} = -2059.1Hz^b	Parental molecule

Table B.2.1 : Rotational constant of fragments of benzene and carbon disulfide. The rotational constants were obtained in frequency domain rotational spectra in 100 ns random sparse sampling measurement with GPS clock calibration. (a) : Single sigma uncertainty (b) Juntilla et al. [13]

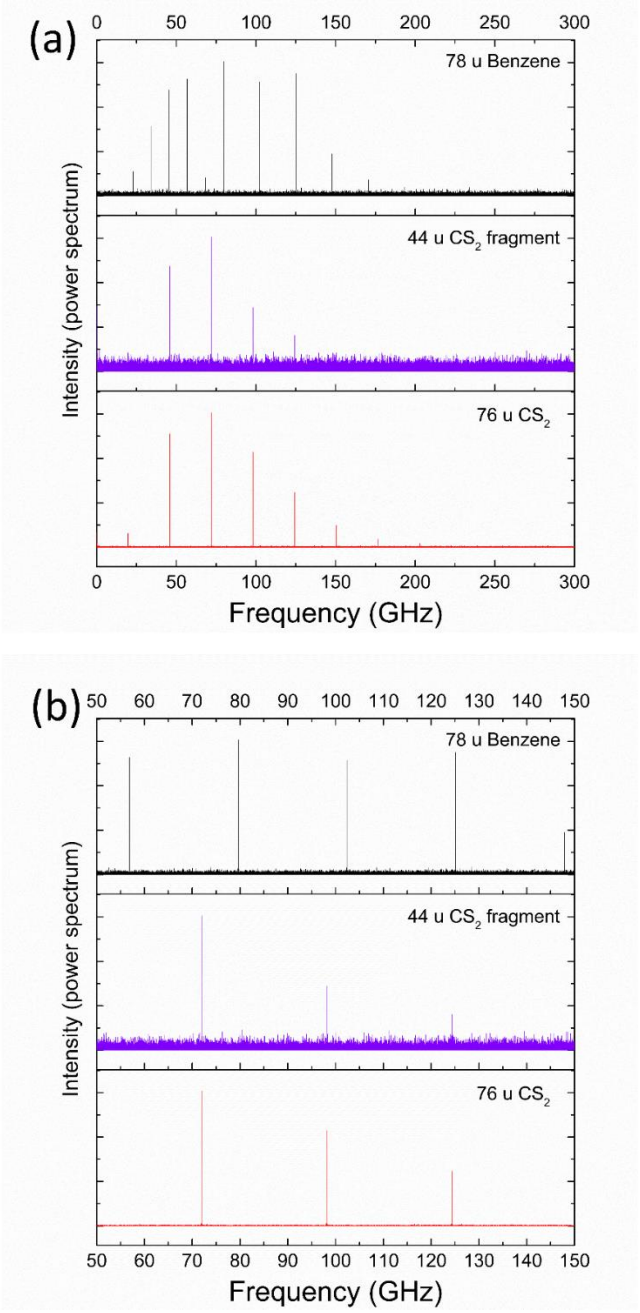

Figure B.3.1 : Three rotational spectra, rotational spectrum of mass 44 u (one of fragments from carbon disulfide (32S12C32S)), 76u(32S12C32S), and benzene (12C6H6) spectrum. The single MHz resolution spectra were obtained by measurement of random sparse sampling over 1μs random sparse sampling measurement with GPS calibration (a) : pure rotational spectrum of 76 u of 12C32S, the fragment of carbon disulfide (32S12C), and benzene(12C6H6) in the frequency domain between 0 and 300 GHZ. (b) : Zoomed up three rotational spectra in the range between 50 to 150 GHz.

Mass	Molecule	Rotational constant	Distortion constant	Parental molecule
44 u	32S12C	3271.5210(31)MHz^a	D = 352.79 Hz^b	32S12C32S
76 u	32S12C32S	3271.51789(98) MHz	D = 352.79 Hz^b	Parental molecule
78 u	C_6H_6	5689.2671(52) MHz^a	D_J = 1178(50) Hz^a D_{JK} = -2300(120) Hz^a	Parental molecule

Table B.3.1 : Rotational constant of fragments of carbon disulfide isotopomers and benzene. The rotational constants were obtained in 1 μs. (a) : Single sigma uncertainty (b) : Anhonen et al. [32]

REFERENCES

1. B. P. Stoicheff, The Journal of Chemical Physics **21** (8), 1410-1411 (1953).

2. B. P. Stoicheff, Canadian Journal of Physics **32** (5), 339-346 (1954).

3. H. B. Jensen and S. Brodersen, Journal of Raman Spectroscopy **8** (2), 103-110 (1979).

4. R. C. Lord and T. K. McCubbin, J. Opt. Soc. Am. **47** (8), 689-697 (1957).

5. A. Danti and R. C. Lord, Spectrochimica Acta **13** (3), 180-191 (1958).

6. R. Anttila, Zeitschrift für Naturforschung A **23** (7), 1089-1089 (1968).

7. A. Cabana, J. Bachand and J. Giguère, Canadian Journal of Physics **52** (20), 1949-1955 (1974).

8. J. Kauppinen, P. Jensen and S. Brodersen, Journal of Molecular Spectroscopy **83** (1), 161-174 (1980).

9. J. Plíva, J. W. C. Johns and L. Goodman, Journal of Molecular Spectroscopy **140**, 214-225 (1990).

10. J. Lindenmayer, U. Magg and H. Jones, Journal of Molecular Spectroscopy **128** (1), 172 - 175 (1988).

11. H. Hollenstein, S. Piccirillo, M. Quack and M. Snels, Molecular Physics **71** (4), 759-768 (1990).

12. J. Plíva and A. S. Pine, Journal of Molecular Spectroscopy **126** (1), 82-98 (1987).

13. M. L. Junttila, J. L. Domenech, G. T. Fraser and A. S. Pine, Journal of Molecular Spectroscopy **147** (2), 513-520 (1991).

14. J. L. Domenech, M. L. Junttila and A. S. Pine, Journal of Molecular Spectroscopy **149** (2), 391-398 (1991).

15. W. Demtröder, in *Laser Spectroscopy 2: Experimental Techniques* (Springer Berlin Heidelberg, Berlin, Heidelberg, 2015), pp. 1-82.

16. E. Riedle, T. Knittel, T. Weber and H. J. Neusser, The Journal of Chemical Physics **91** (8), 4555-4563 (1989).

17. M. Okruss, R. Müller and A. Hese, Journal of molecular spectroscopy **193** (2), 293-305 (1999).

18. A. Doi, M. Baba, S. Kasahara and H. Katô, Journal of Molecular Spectroscopy **227** (2), 180 - 186 (2004).

19. M. Baba, Y. Kowaka, U. Nagashima, T. Ishimoto, H. Goto and N. Nakayama, The Journal of Chemical Physics **135** (5), 054305 (2011).

20. C. Riehn, A. Weichert and B. Brutschy, The Journal of Physical Chemistry A **105** (23), 5618-5621 (2001).

21. W. Jarzęba, V. V. Matylitsky, A. Weichert and C. Riehn, Phys. Chem. Chem. Phys. **4**, 451-454 (2002).

22. V. V. Matylitsky, W. Jarzęba, C. Riehn and B. Brutschy, Journal of Raman Spectroscopy **33** (11-12), 877-883 (2002).

23. J. Demaison, Journal of Molecular Structure **31** (2), 233-236 (1976).

24. C. Schröter, K. Kosma and T. Schultz, Science **333** (6045), 1011-1015 (2011).

25. C. Schröter, C. M. Choi and T. Schultz, The Journal of Physical Chemistry A **119** (8), 1309-1314 (2015).

26. C. Schröter, J. C. Lee and T. Schultz, Proceedings of the National Academy of Sciences, 201721756 (2018).

27. U. Even, J. Jortner, D. Noy, N. Lavie and C. Cossart-Magos, The Journal of Chemical Physics **112** (18), 8068-8071 (2000).

28. W. C. Wiley and I. H. McLaren, Review of scientific instruments **26** (12), 1150-1157 (1955).

29. C. M. Western, Journal of Quantitative Spectroscopy and Radiative Transfer **186**, 221 - 242 (2017).

30. J. Plíva and A. S. Pine, Journal of Molecular Spectroscopy **93** (1), 209-236 (1982).

31. J. Plíva and J. W. C. Johns, Canadian Journal of Physics **61** (2), 269-277 (1983).

32. T. Ahonen, S. Alanko, V.-M. Horneman, M. Koivusaari, R. Paso, A.-M. Tolonen and R. Anttila, Journal of Molecular Spectroscopy **181** (2), 279-286 (1997).

33. A. Weber, Handbook of High-resolution Spectroscopy (2011).

34. K. K. A. Sieghard Albert, Hans Hollenstein, Carine Manca Tanner ,Martin Quack, in *Handbook of High-resolution Spectroscopy*, edited by a. F. M. M. Quack (2011).

35. E. B. Wilson, The Journal of Chemical Physics **3** (5), 276-285 (1935).

36. C. M. Western and B. E. Billinghurst, Physical Chemistry Chemical Physics **19** (16), 10222-10226 (2017).

37. M. R. Aliev and J. K. G. Watson, Journal of Molecular Spectroscopy **74** (2), 282-293 (1979).

38. M. R. Aliev, S. I. Subbotin and V. I. Tyulin, Opics and Spectroscopy-USSR **{24}** ({1}), 93-99 (1968).

39. J. M. Dowling, Journal of Molecular Spectroscopy **6**, 550 - 553 (1961).

40. J. A. Stone Jr and J. H. Zimmerman, Website 2001.

41. A. B. Hollinger and H. L. Welsh, Canadian Journal of Physics **56** (7), 974-982 (1978).

42. B. Cloppenburg, K. Manczak, H. Prockl, H. W. Schrötter and G. Strey, Zeitschrift für Naturforschung A **34** (10), 1160-1163 (1979).

43. G. W. Chantry, H. A. Gebbie, R. J. L. Popplewell, H. W. Thompson and others, Proc. R. Soc. Lond. A **304** (1476), 45-51 (1968).

44. W. F. Guthrie, https://www.itl.nist.gov/div898/handbook/index.htm (Chapter 4.6.3.2. Initial Non-Linear Fit, Determining Appropriate Starting Values) (2013).

45. R. J. Butcher, Optical and Quantum Electronics **25** (2), 79-95 (1993).

46. H. Mori, T. Niimi, I. Akiyama and T. Tsuzuki, **17** (11), 117103 (2005).

47. R. L. LeRoy and T. R. Govers, Canadian Journal of Chemistry **48** (11), 1743-1747 (1970).

48. H. Hulsman, in *Atomic and Molecular Beams: The State of the Art 2000*, edited by R. Campargue (Springer Berlin Heidelberg, Berlin, Heidelberg, 2001), pp. 273-282.

49. A. Amrein, M. Quack and U. Schmitt, The Journal of Physical Chemistry

92 (19), 5455-5466 (1988).

50. S. Kunishige, T. Katori, M. Baba, M. Nakajima and Y. Endo, The Journal of Chemical Physics **143** (24), 244302 (2015).

51. J. Schlupf and A. Weber, Journal of Molecular Spectroscopy **54** (1), 10-19 (1975).

52. J. Schlupf and A. Weber, Journal of Raman Spectroscopy

1 (1), 3-15 (1973).

53. D. H. Levy, Annual Review of Physical Chemistry **31** (1), 197-225 (1980).

54. F. Winther, Zeitschrift für Naturforschung A **44** (6), 594-594 (1989).

55. V.-M. Horneman, R. Anttila, S. Alanko and J. Pietilä, Journal of Molecular Spectroscopy

234 (2), 238-254 (2005).

56. C.-L. C. Cheng, J. L. Hardwick and T. R. Dyke, Journal of Molecular Spectroscopy **179** (2), 205-218 (1996).

Acknowledgement

This research was supported by UNIST grant UNIST-1.180058 and the National Research Foundation of Korea (NRF- 2018R1D1A1A02042720).

I firstly would like to thank Jong Chan Lee, who worked together on the high-resolution Benzene spectra in the ground state research, for his expert experimental helps and fruitful discussions in this research. I would like to thank Dr. Christian Schröter for his professional knowledge of physics on Mass-CRASY experiments. I would also like to thank Prof. Oh-Hoon Kwon and Prof. Yung Sam Kim for productive comments on me. Above all, my adviser, Prof. Thomas Schultz, He taught me how to start a scientific research and how to properly finish it. I thank Prof. Schultz for his support and advice in each steps of this research. This paper is dedicated to my CRASY laboratory colleagues with gratitude.